NASA Technical Memorandum 78560

Low-Speed Wind-Tunnel Investigation of a Large-Scale VTOL Lift-Fan Transport Model

Kiyoshi Aoyagi

April 1979

National Aeronautics and
Space Administration

NASA Technical Memorandum 78560

Low-Speed Wind-Tunnel Investigation of a Large-Scale VTOL Lift-Fan Transport Model

Kiyoshi Aoyagi, Ames Research Center, Moffett Field, California

NASA
National Aeronautics and
Space Administration

Ames Research Center
Moffett Field, California 94035

NOMENCLATURE

b	wing span, m (ft)
c	wing chord measured parallel to the plane of symmetry, m (ft)
$\bar{c}$	mean aerodynamic chord of the wing, $\frac{2}{S}\int_0^{b/2} c^2 dy$, m (ft)
C_D	drag coefficient about the wind axis, $\frac{\text{drag}}{q_\infty S}$
C_L	lift coefficient about the wind axis, $\frac{\text{lift}}{q_\infty S}$
C_ℓ	rolling-moment coefficient about the wind axis, $\frac{\text{rolling moment}}{q_\infty Sb}$
C_m	pitching-moment coefficient about the wind axis, $\frac{\text{pitching moment}}{q_\infty S\bar{c}}$
C_n	yawing-moment coefficient about the wind axis, $\frac{\text{yawing moment}}{q_\infty Sb}$
C_y	side-force coefficient about the wind axis, $\frac{\text{side force}}{q_\infty S}$
F_A	static (wind off) axial force, N (lb)
F_N	static (wind off) normal force, N (lb)
F_R	resultant force, $\sqrt{F_A^2 + F_N^2}$, N (lb)
N	lift fan rotational speed, RPM
P_o	standard atmospheric pressure, N/m^2 (lb/ft^2)
P_s	free-stream static pressure, N/m^2 (lb/ft^2)
q_∞	free-stream dynamic pressure, N/m^2 (lb/ft^2)
R	lift fan radius, 0.457 m (1.50 ft)
S	wing area, m^2 $(ft)^2$
T	free-stream absolute temperature, K
T_o	standard absolute temperature, 288.16 K
T_s	static (wind off) normal force resulting from lift fan operating at $\sigma_v = 0°$, $\beta_v = 0°$, N (lb)
V_j	fan exit isentropic velocity, m/sec (ft/sec)

V_∞ free-stream air velocity, m/sec (ft/sec)

α angle of attack, deg

β angle of sideslip, deg

β_v lift fan exit louver geometric deflection angle; 0° in the direction to produce maximum thrust in the lift direction with $\alpha = 0°$, $\sigma_v = 0°$

δ static pressure ratio, $\frac{P_s}{P_o}$

δ_{cn} lift/cruise fan thrust deflector geometric angle; 90° in the direction to produce maximum thrust in the lift direction

δ_f trailing-edge flap deflection measured normal to the hinge line, deg

δ_j static turning angle, $\tan^{-1} \frac{F_N}{F_A}$, deg

$\bar{\varepsilon}$ average downwash angle, deg

η static turning effectiveness

θ absolute temperature ratio, $\frac{T}{T_o}$

μ fan-tip speed ratio, $\frac{V_\infty}{\omega R}$

σ_v lift fan exit lower cascade rotation geometric angle; 0° in the direction to produce maximum thrust in the lift direction

τ ratio of ideal thrust with forward speed to static ideal thrust assuming isentropic expansion to ambient pressure

ω fan rotational speed, rad/s

Subscript

u uncorrected

LOW-SPEED WIND-TUNNEL INVESTIGATION OF A LARGE-SCALE VTOL LIFT-FAN TRANSPORT MODEL

Kiyoshi Aoyagi

Ames Research Center

SUMMARY

An investigation was conducted in the NASA-Ames 40- by 80-Foot Wind Tunnel, to determine the aerodynamic characteristics of a large-scale, VTOL, lift-fan, jet-transport model. The model had two lift fans at the forward portion of the fuselage, a lift fan at each wing tip, and two lift/cruise fans at the aft portion of the fuselage. All fans were driven by tip turbines using T-58 gas generators. Results were obtained for several lift-fan, exit-vane deflections and lift/cruise fan-thrust deflections at zero sideslip. Three-component longitudinal data are presented at several fan-tip speed ratios. A limited amount of six-component data were obtained with asymmetric vane settings. All of the data were obtained without a horizontal tail. Downwash angles at a typical tail location are also presented.

INTRODUCTION

The low-speed aerodynamic characteristics of large scale V/STOL models with the lift-fan and lift/cruise-fan propulsive systems is being studied at NASA Ames Research Center. Previous large-scale studies conducted in the Ames 40- by 80-Foot Wind Tunnel have investigated the aerodynamic characteristics and propulsion-system performance of fan-in-fuselage, fan-in-wing, and podded fan configurations. These studies are reported in references 1-13. Studies with lift/cruise fan configurations are reported in references 14-16. Reference 16 reported on a large scale STOL transport model with two lift fans located side-by-side at the forward section of the fuselage and two lift/cruise fans located at the rear section of the fuselage. The thrust vectoring control of the front lift fans on this model was different from those previously investigated. The exit louvers were canted and mounted to a rotatable ring to provide a greater thrust vectoring capability in both the longitudinal and lateral directions. The model for this study had two lift fans at the forward portion of the fuselage, a lift fan at each wing tip, and two lift/cruise fans at the aft portion of the fuselage. All of the fans were driven by tip turbines using T-58 gas generators. This model was derived from the four-fan model of reference 16 by reducing the wing span and by adding podded lift fans at the wing tips. An investigation in the Ames 40- by 80-Foot Wind Tunnel was undertaken to determine the low-speed aerodynamic characteristics and propulsion-system performance of this model. The longitudinal characteristics of the model are shown for several fan-tip speed ratios from 0.06 to 0.27.

The test data in this report are presented without analysis.

METHODS

Model Description

Photographs of the model mounted in the Ames 40- by 80-Foot Wind Tunnel are shown in figures 1(a) and (b). Geometric details and pertinent dimensions of the model are shown in figure 2(a).

Fuselage

The fuselage used in reference 16 was modified. This modification consisted of increasing the length of the fuselage nose section from 2.23 m (7.31 ft) to 2.87 m (9.41 ft) forward of the forward lift-fan centerline and adding an additional fuselage section 0.70 m (92.30 ft) in length between the wing and the lift/cruise fans. The fuselage had circular cross sections with a maximum diameter of 1.75 m (5.75 ft). The forward section of the fuselage contained two 0.91-m (3.00-ft) lift fans. This required a bulbous fairing around each fan inlet that tapered along the fuselage side to the wing leading edge.

Wing

The wing that was used in reference 16 was modified for this investigation, and a pod housing a lift fan was installed on the tip. The resulting span measured to the pod centerline was 10.24 m (33.62 ft) compared with the original 13.65 m (44.80 ft). This modification reduced the aspect ratio from 8.14 to 5.25 and increased the taper ratio from 0.233 to 0.420. The wing had a quarter-chord sweep of 22.6°, a dihedral of 3°, an incidence of 0°, and a NACA 65-412 airfoil section.

A 0.22 C single-slotted trailing-edge flap extended from the fuselage to 0.63 of the wing semispan and was deflected 30° throughout the investigation as shown in figure 2(b). Also shown in figure 2(b) is the 0.07 C chord leading-edge slat, which extended from the fuselage to the wing tip and was deflected 20° during the entire investigation. Both of these high-lift devices were the same ones used in reference 16.

Propulsion System

The propulsion system consisted of four lift fans and two lift/cruise fans driven by six T58-8B gas generators as shown in figure 2(a). The lift fans were General Electric X-376 lift fans with a fan diameter of 0.91 m (3.00 ft) and a design pressure ratio of 1.1. Two lift fans each were located at the forward fuselage section and at the wing tips. Two lift/cruise fans were located at the rear fuselage section behind the wing. Location and arrangement of the forward lift fans were the same as reference 16. Gas generator inlets for these fans were relocated from the top of the fuselage

location of reference 16 to each side of the fuselage behind the fans. The arrangement and vertical location from the moment center of the lift/cruise fans and gas generators were also the same as reference 16. The longitudinal location from the moment center increased an additional 0.70 m (2.30 ft) because of the fuselage length increase. All lift fans, including the wing-tip fans, rotated in a clockwise direction as viewed from the inlet.

Four total-pressure rakes, consisting of six probes, were equally spaced downstream of the fan exit at each fan located on the right side of the model. A typical installation is shown in figure 2(c) with the probes spaced to provide equal areas. Rake measurements were used to compute ideal velocities and thrusts assuming an isentropic expansion to ambient pressure.

Forward-lift fans- Installation of these fans is shown in figures 2(c) and (d). The fans were mounted with the thrust axis canted 10° with respect to the horizontal plane. Thrust vectoring control was provided by a cascade of 14 0.114 m (0.37 ft) chord highly cambered exit vanes, which spanned the fan duct exit. The vane details are shown in figure 2(e). These vanes were mounted to a manually rotatable ring in the 40° canted plane. The cascade ring rotation angle of 0° (σ_v = 0°) was defined when the vane spans were parallel to the model plane of symmetry. Rotation of the ring in the direction giving positive thrust vectoring was defined as positive σ_v. The cascade ring-rotation angles ranged 0° to 90°. The exit vanes deflection (β_v) was changed remotely and varied -16° to +16°, about the maximum direct-lift position. The fan exit louver angle of 0° (β_v = 0°) was established with one fan operating and by trimming the side force to zero with the fan speed 3600 RPM at α = 0°, σ_v = 0°, and forward speed = 0. The fan inlets were the same as the modified inlets described in reference 16.

Wing-tip lift fans- A lift fan was installed in a pod located at each wing tip. The fan inlet was bellmouth-shaped, and the pod details are shown in figure 2(f). The fans were mounted with the thrust axis canted 10° with respect to the horizontal plane. Thrust vectoring control was the same as described for the forward lift fans using the same exit vane design as shown in figure 2(e). The vanes were mounted to a manually rotatable ring in the 31.2°-canted plane. The definitions of σ_v = 0° and β_v = 0° were the same as the forward lift fans.

Lift/cruise fans- The two aft fans were mounted in cruise pods as shown in figure 2(g). The fan exhaust was deflected through ducts for thrust vectoring. The duct angles used during the investigation were 23°, 56°, and 90°, with 90° in a direction to provide maximum direct lift. The exhaust nozzle area was sized to accommodate both fan and tip turbine flows.

Corrections

The model meets the geometric criteria of reference 17 for small corrections resulting from wind tunnel walls. The results are therefore presented uncorrected and may be corrected as the user desires.

Because the tail strut fairing was off throughout the investigation, drag and moment tares resulting from the exposed tail strut and the main strut tips have been applied to the data.

Data obtained without the lift fans operating (power off) were corrected as follows:

$$\alpha = \alpha_u + 0.467\ C_{L_u}$$

$$C_D = C_{D_u} + 0.0081\ C_{L_u}^2$$

$$C_m = C_{m_u}$$

Testing and Procedure

The installed static fan thrust data were obtained at $\alpha = 0°$ with forward speed = 0. The variations of thrust with fan speed were obtained for the forward lift fans and the wing-tip fans at $\beta_v = 0°$ and $\sigma_v = 0°$. The fans were operated in pairs and individually. When β_v was varied at a constant σ_v value, thrust measurements were taken with two fans operating together at a constant minimum fan speed of 3600 RPM. Thrust measurements for the lift/cruise fans were obtained with both fans operating at $\delta_{cn} = 23°$, 56°, and 90° at several fan speeds. Data were also obtained with each of the lift/cruise fans operating alone at $\delta_{cn} = 90°$.

In most cases, longitudinal force and moment data were obtained at several forward speeds and angle of attacks with all fans operating at a minimum speed of 3600 RPM. Several σ_v and β_v settings were tested at $\delta_{cn} = 23°$, 56° and 90° by using the same settings at both the forward and the wing-tip fans. The β_v settings were varied from -16 to 16° when $\alpha = 0°$ and were set to 0° when α was varied -4 to 20°. The trailing-edge flap was deflected 30°, and the horizontal tail was off throughout the investigation.

RESULTS

The relationship between velocity ratio (V_∞/V_J) and fan-tip speed ratio is shown in figure 3. The fan static thrusts and the basic aerodynamic data are presented in figures 4-19. An index to these data is given in table 1. The variations of measured fan thrust with fan RPM at forward speed = 0 are shown in figures 4(a), (b), and (c) for the forward-lift fans, wing-tip lift fans, and the lift/cruise fans, respectively. Figure 5 presents the ratio of the measured static resultant fan thrust to the maximum fan vertical lift as a function of fan exit louver deflection angle (β_v) for the front and wing-tip lift fans. The variations of the fan exhaust static turning angle with the lift fan exit louver deflection and with the lift/cruise fan deflector are shown in figures 6 and 7, respectively. The turning efficiency of the lift/cruise fan deflector is also shown in figure 7. The lift/cruise fan thrust

value at $\delta_{cn} = 0°$ was obtained from reference 16. The variations of ideal thrust with forward speed to static ideal thrust ratio with fan-tip speed ratio are shown in figures 8(a)-(c) for the forward lift fan, wing-tip fan, and the lift/cruise fan. These fans were located on the right side of the model.

Figures 9-15 show the variation of the longitudinal characteristics of the model with fan tip-speed ratio at $\alpha = 0°$. The variation of the longitudinal and the lateral characteristics of the model with fan-tip speed ratio is shown in figure 16 with asymmetrical deflections of β_v between the left and right wing-tip fans. The longitudinal characteristics of the model with variable angle-of-attack are shown in figures 17-20. Figure 17 shows the longitudinal characteristics of the model with the lift/cruise fans windmilling and with the forward and wing-tip lift fans inoperative. Figures 18-20 show the longitudinal characteristics of the model at several fan-tip speed ratios with all fans operating.

The variations of the averaged downwash angle with angle of attack are shown in figures 21, 22, and 23 with $\delta_{cn} = 90°$, 56°, and 23°, respectively. Figure 24 shows the variation of the averaged downwash angle with β_v at $\alpha = 0°$. The downwash angles were obtained from the measurements of the directional pressure probes that were located near the top of the vertical tail as shown in figure 2(a).

REFERENCES

1. Aoyagi, Kiyoshi; Hickey, David H.; and deSavigny, Richard, A.: Aerodynamic Characteristics of a Large-Scale Model with a High Disk-Loading Lifting Fan Mounted in the Fuselage. NASA TN D-755, 1961.

2. deSavigny, Richard A.; and Hickey, David H.: Aerodynamic Characteristics in Ground Effect of a Large-Scale Model with a High Disk-Loading Lifting Fan Mounted in the Fuselage. NASA TN D-1557, 1962.

3. Hickey, David H.; and Hall, Leo P.: Aerodynamic Characteristics of a Large-Scale Model with Two High Disk-Loading Fans Mounted in the Wing. NASA TN D-1650, 1963.

4. Kirk, Jerry V.; Hickey, David H.; and Hall, Leo P.: Aerodynamic Characteristics of a Full-Scale Fan-in-Wing Model Including Results in Ground Effect with Nose-Fan Pitch Control. NASA TN D-2368, 1964.

5. Hall, Leo P.; Hickey, David H.; and Kirk, Jerry V.: Aerodynamic Characteristics of a Large-Scale V/STOL Transport Model with Lift and Lift-Cruise Fans. NASA TN D-4092, 1967.

6. Hickey, David H.; Kirk, Jerry V.; and Hall, Leo P.: Aerodynamic Characteristics of a V/STOL Transport Model with Lift and Lift/Cruise Fan Power Plants. NASA SP-116, Paper 15, 1966.

7. Hickey, David H.; and Cook, Woodrow L.: Aerodynamic of V/STOL Aircraft Powered by Lift Fans. AGARD CP 22, Paper 15, 1967.

8. Kirk, Jerry V.; Hodder, Brent K.; and Hall, Leo P.: Large-Scale Wind Tunnel Investigation of a V/STOL Transport Model with Wing-Mounted Lift Fans and Fuselage-Mounted Lift-Cruise Engines for Propulsion. NASA TN D-4233, 1967.

9. Hodder, Brent K.; Kirk, Jerry V.; and Hall, Leo P.: Aerodynamic Characteristics of a Large-Scale Model with a Lift Fan Mounted in a 5-percent Thick Triangular Wing, Including the Effects of BLC on the Lift-Fan Inlet. NASA TN D-7031, 1970.

10. Dickinson, Stanley O.; Hall, Leo P.; and Hodder, Brent K.: Aerodynamic Characteristics of a Large-Scale V/STOL Transport Model with Tandem Lift Fans Mounted at Mid-Semispan of the Wing. NASA TN D-6234, 1971.

11. Kirk, Jerry V.; Hall, Leo P.; and Hodder, Brent K.: Aerodynamics of Lift Fan V/STOL Aircraft. NASA TM X-62,086, 1971.

12. Hall, Leo P.; and Kirk, Jerry V.: Large-Scale Wind Tunnel Investigation of a V/STOL Transport Model with Podded Lift Fans Forward and Aft of a Low Mounted Wing. NASA TM X-62,102, 1971.

13. Kirk, Jerry V.; Dickinson, Stanley O.; Hall, Leo P.; and Coffman, Mary G.: Aerodynamic Characteristics of a Large-Scale Lift Fan Transport Model with Podded Fans Forward and Lift Cruise Fans Mounted Above the Wing. NASA TM X-62,151, 1972.

14. Gambucci, Bruno J.; Aoyagi, Kiyoshi; and Rolls, Stewart L.: Wind Tunnel Investigation of a Large-Scale Model of a Lift/cruise Fan V/STOL Aircraft. NASA TM X-73,139, 1976.

15. Gambucci, Bruno J.; Aoyagi, Kiyoshi; and Rolls, Stewart L.: Wind Tunnel Investigation of a Large-Scale Model of a Lift/cruise Fan V/STOL Aircraft with Extended Lift/Cruise Nacelles. NASA TM X-73,164, 1976.

16. Atencio, Adolph Jr.; Hall, Leo P.; and Kirk, Jerry V.: Low Speed Wind Tunnel Investigation of a Large-Scale Lift Fan STOL Transport Model. NASA TM X-62,231, 1973.

17. Cook, Woodrow L.; and Hickey, David H.: Comparison of Wind-Tunnel and Flight-Test Aerodynamic Data in the Transition Flight Speed Range for Five V/STOL Aircraft. NASA SP-116, Paper 26, 1966.

TABLE 1.- INDEX OF FIGURES

Figure	α_u, deg	μ	Forward-lift fan		Wing-tip lift fan		Lift/cruise fan	Remarks
			β_v, deg	σ_v, deg	β_v, deg	σ_v, deg	δ_{cn}, deg	
Fan characteristics								
4(a)	0	---	0	0	---	---	---	Forward lift fan static thrust calibration
4(b)			---	---	0	0	---	Wing-tip lift fan static thrust calibration
4(c)			---	---	---	---	90	Lift/cruise fan static thrust calibration
5			-16 to 16	0,40,60,80	-16 to 16	0,40,60,80	---	Forward lift fan and wing-tip lift fan static resultant fan thrust to maximum static fan lift ($\sigma_v = 0°$, $\beta_v = 0°$) ratio with fan exit louver deflection angle; fan RPM = 3600

TABLE 1.- Continued.

Figure	α_u, deg	μ	Forward-lift fan		Wing-tip lift fan		Lift/cruise fan	Remarks
			β_v, deg	σ_v, deg	β_v, deg	σ_v, deg	δ_{cn}, deg	
6	0	---	-16 to 16	0,40,60,80	-16 to 16	0,40,60,80	---	Forward lift fan and wing-tip lift fan efflux static turning angle with fan exit louver deflection angle; fan RPM = 3600
7		---	---	---	---	---	23,56,90	Lift/cruise fan static turning angle and static turning efficiency; fan RPM = 3600
8(a)		0.06-0.27	-16,0,16	0,40,60,80	---		---	Variation of ideal thrust with forward speed to ideal static thrust ratio with fan-tip speed ratio
8(b)		0.06-0.27	-16,0,16	0,40,60,80	-16,0,16	0,40,60,80	---	
8(c)		0.06-0.27	---	---	---	---	23,56,90	

TABLE 1.- Continued.

Figure	α_u, deg	μ	Forward-lift fan		Wing-tip lift fan		Lift-cruise fan	Remarks
			β_v, deg	σ_v, deg	β_v, deg	σ_v, deg	δ_{cn}, deg	
Longitudinal characteristics at α = 0°								
9(a)&(b)	0	0.06-0.18	0	0	-16 to 16	0	90	β_v varied on wing-tip lift fans only with forward lift fan inlets covered. Lift/cruise fans: windmilling
10(a)&(b)	↓	.06- .08	0	0	-16 to 16	0	↓	β_v varied on wing-tip lift fans only with forward lift fan β_v = 0°; all fans operating
11(a)&(b)	↓	.06- .18	-16 to 16	0	0	0	↓	β_v varied on forward lift fan only with wing-tip lift fan β_v = 0°; all fans operating
12(a)&(b)	↓	.06- .18	0	0,40	↓	0,40	↓	All fans operating

TABLE 1.- Continued.

Figure	α_u, deg	μ	Forward-lift fan		Wing-tip lift fan		Lift/cruise fan	Remarks
			β_v, deg	σ_v, deg	β_v, deg	σ_v, deg	δ_{cn}, deg	
13(a)&(b)	0	0.08-0.27	Closed	40,60	0	40,60	56	Wing-tip lift fan operating alone. Forward lift-fan inlets covered; lift/cruise fans windmilling
14(a)&(b)			0	40,60,80		40,60,80		All fans operating
14(c)&(d)			-8	40,60,80	-8	40,60,80		
14(e)&(f)			-16		-16			
14(g)&(h)			8		8			
14(i)&(j)			16		16			
15(a)&(b)		0.12-0.27	0		0		23	
Longitudinal and lateral characteristics at $\alpha = 0°$								
16(a)&(b)	0	0.08-0.19	0	0	-16 to 16	0	90	All fans operating. Right side wing-tip lift fan β_v varied with left wing-tip lift fan $\beta_\ell = 0°$

TABLE 1.- Concluded.

Figure	α_u, deg	μ	Forward-lift fan		Wing-tip lift fan		Lift/cruise fan	Remarks
			β_v, deg	σ_v, deg	β_v, deg	σ_v, deg	δ_{cn}, deg	
Longitudinal characteristics with variable angle of attack								
17	-4 - 20	---	Closed	90	Closed	90	23	Power off; forward lift fan and wing-tip lift fan inlets covered; lift/cruise fans windmilling
18(a)	-4 - 12	0.08	0	0,40	0	0,40	90	All fans operating
18(b)	-4 - 18	.12		0,40		0.40	90	
18(c)	-4 - 16	.18		0,40		0,40	90	
19(a)	-4 - 18	.12		40,60,80		40,60,80	56	
19(b)	-4 - 20	.18					56	
19(c)	-4 - 20	.26					56	
20(a)	-4 - 22	.12					23	
20(b)	-4 - 22	.18						
20(c)	-4 - 22	.26						

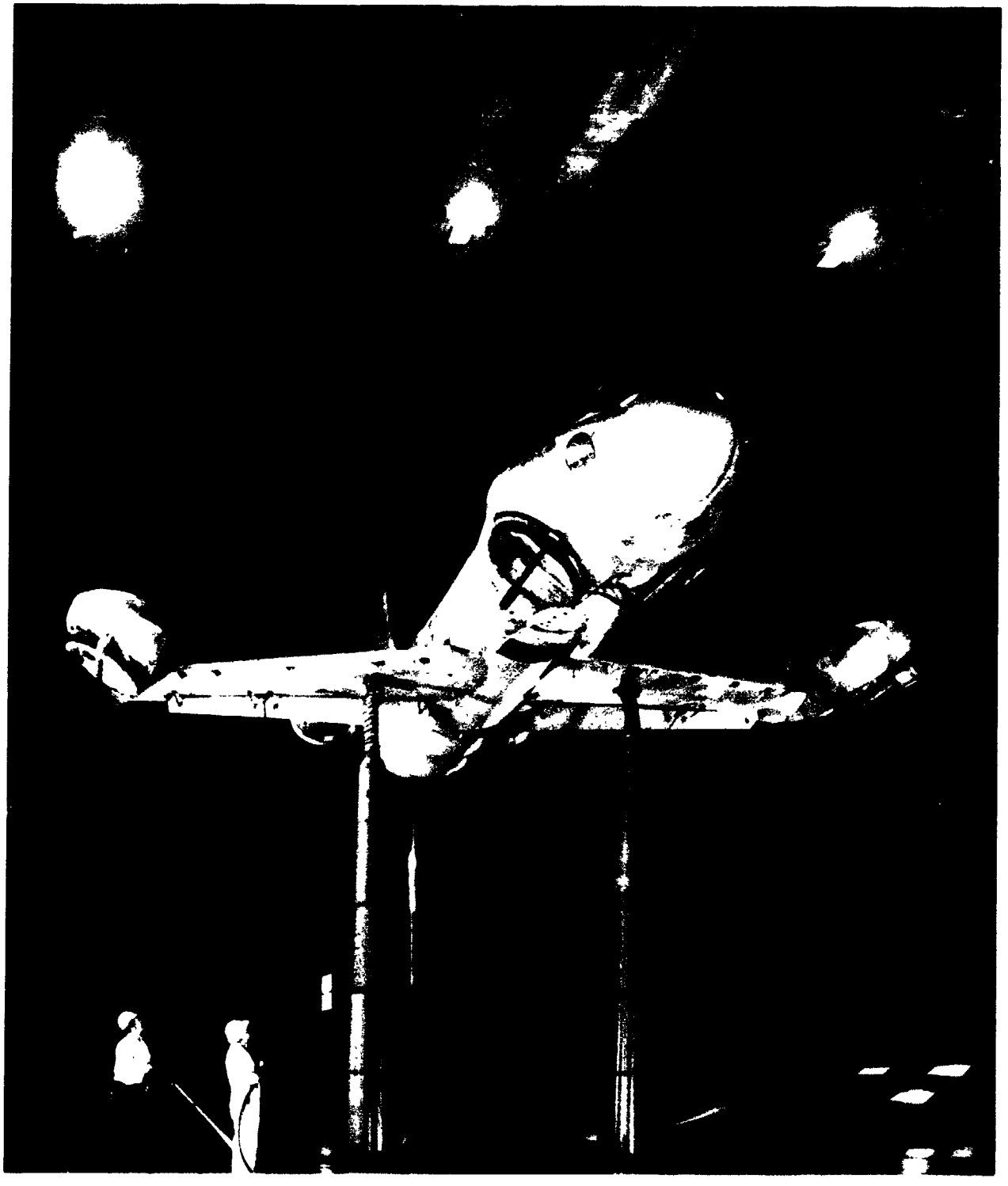

(a) Three-fourth front view.

Figure 1.- Photographs of the model mounted in the Ames 40- by 80-Foot Wind Tunnel.

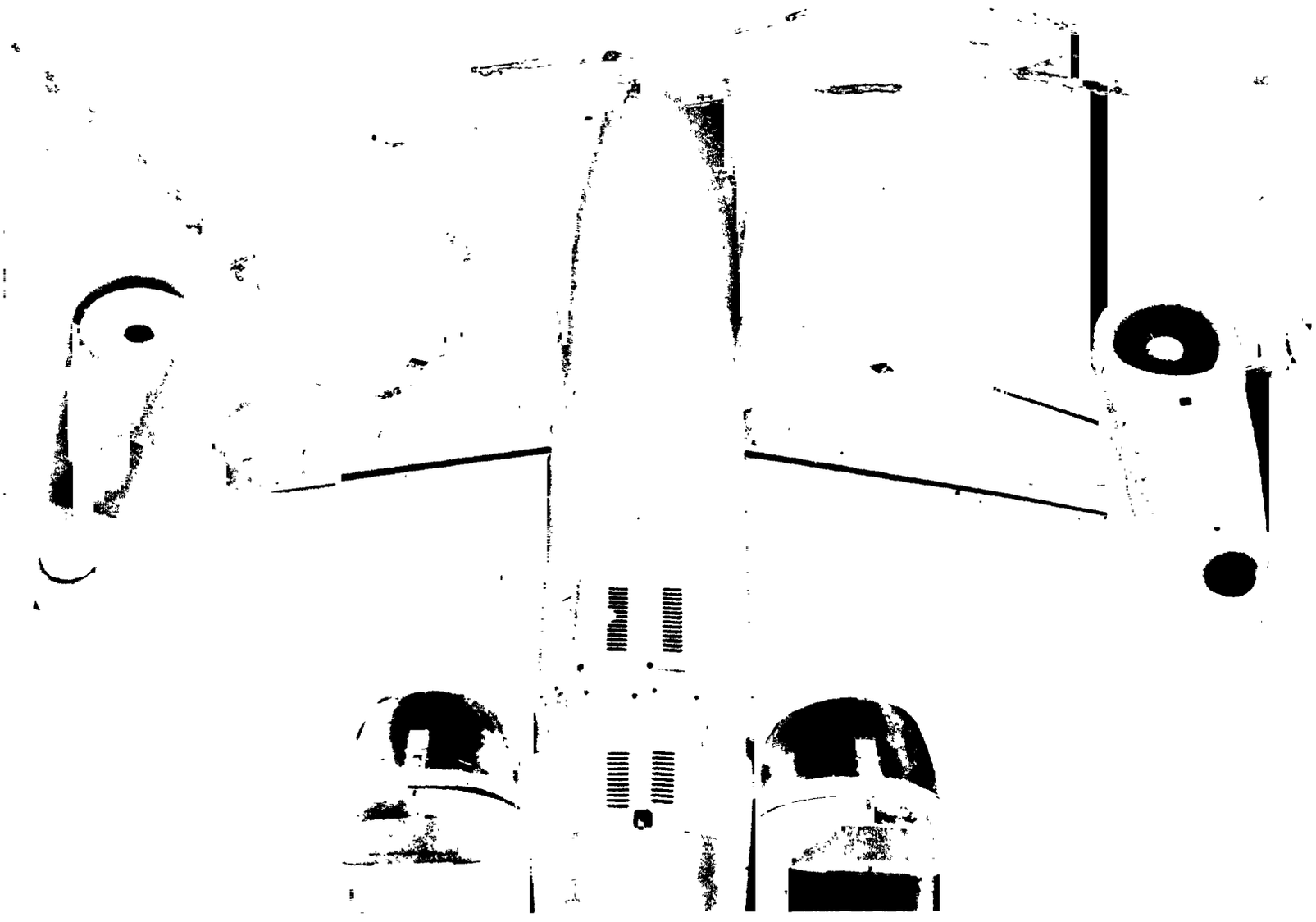

(b) Overhead view.

Figure 1.- Concluded.

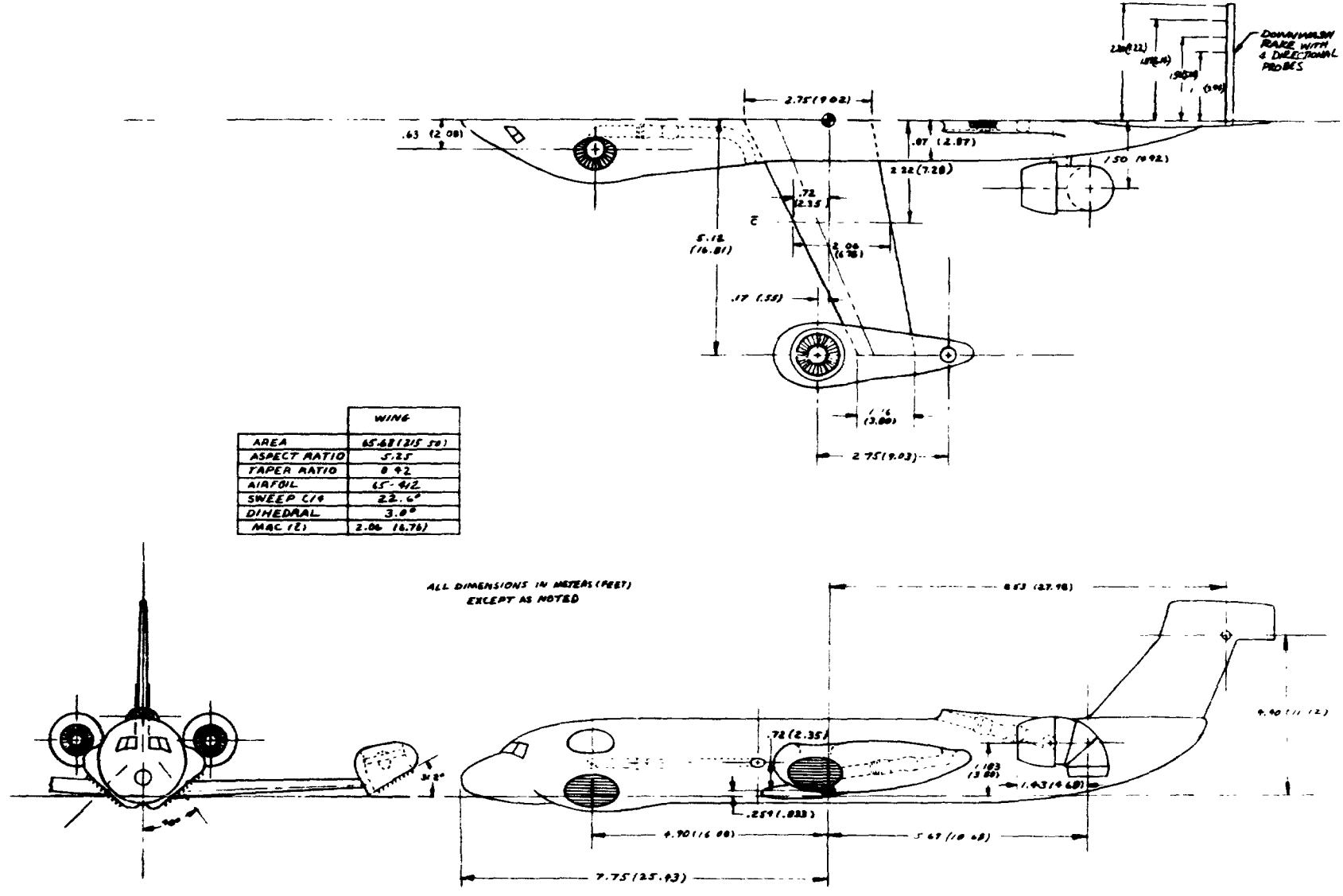

	WING
AREA	65.68 (215.50)
ASPECT RATIO	5.25
TAPER RATIO	0.42
AIRFOIL	65-412
SWEEP C/4	22.6°
DIHEDRAL	3.0°
MAC (ℓ)	2.06 (6.76)

(a) General arrangement of the model.

Figure 2.- Geometric details of the model.

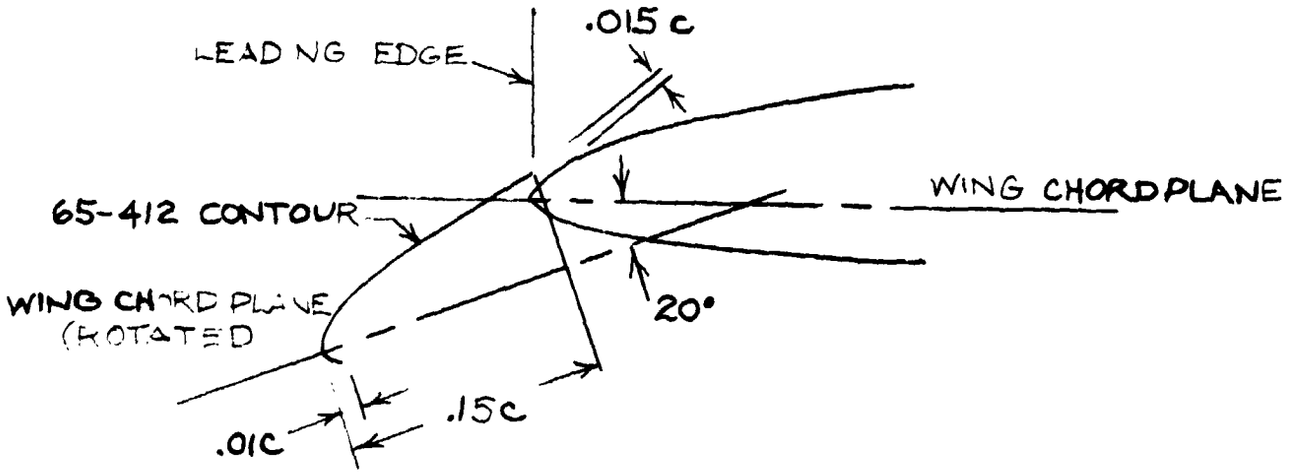

LEADING EDGE SLAT

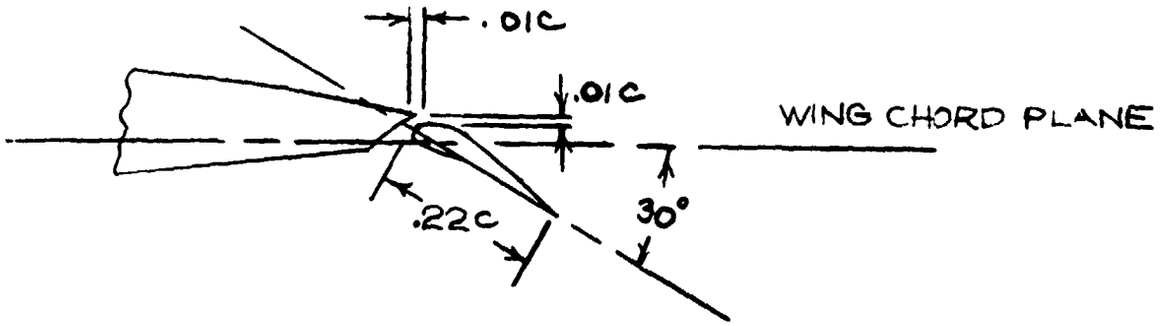

TRAILING EDGE FLAP

(b) Leading- and trailing-edge high-lift devices.

Figure 2.- Continued.

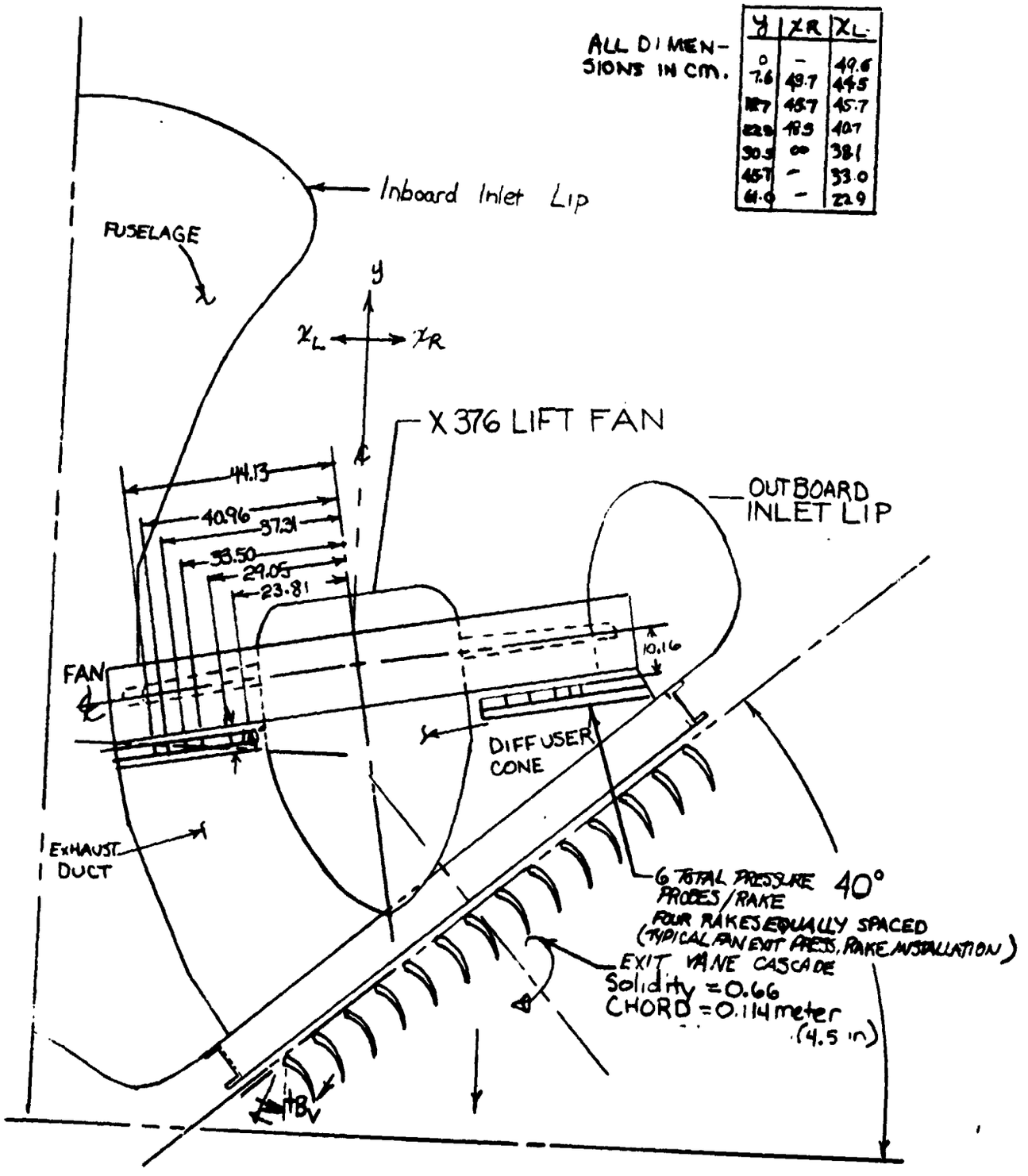

(c) Forward lift fan and exit lower installation.

Figure 2.- Continued.

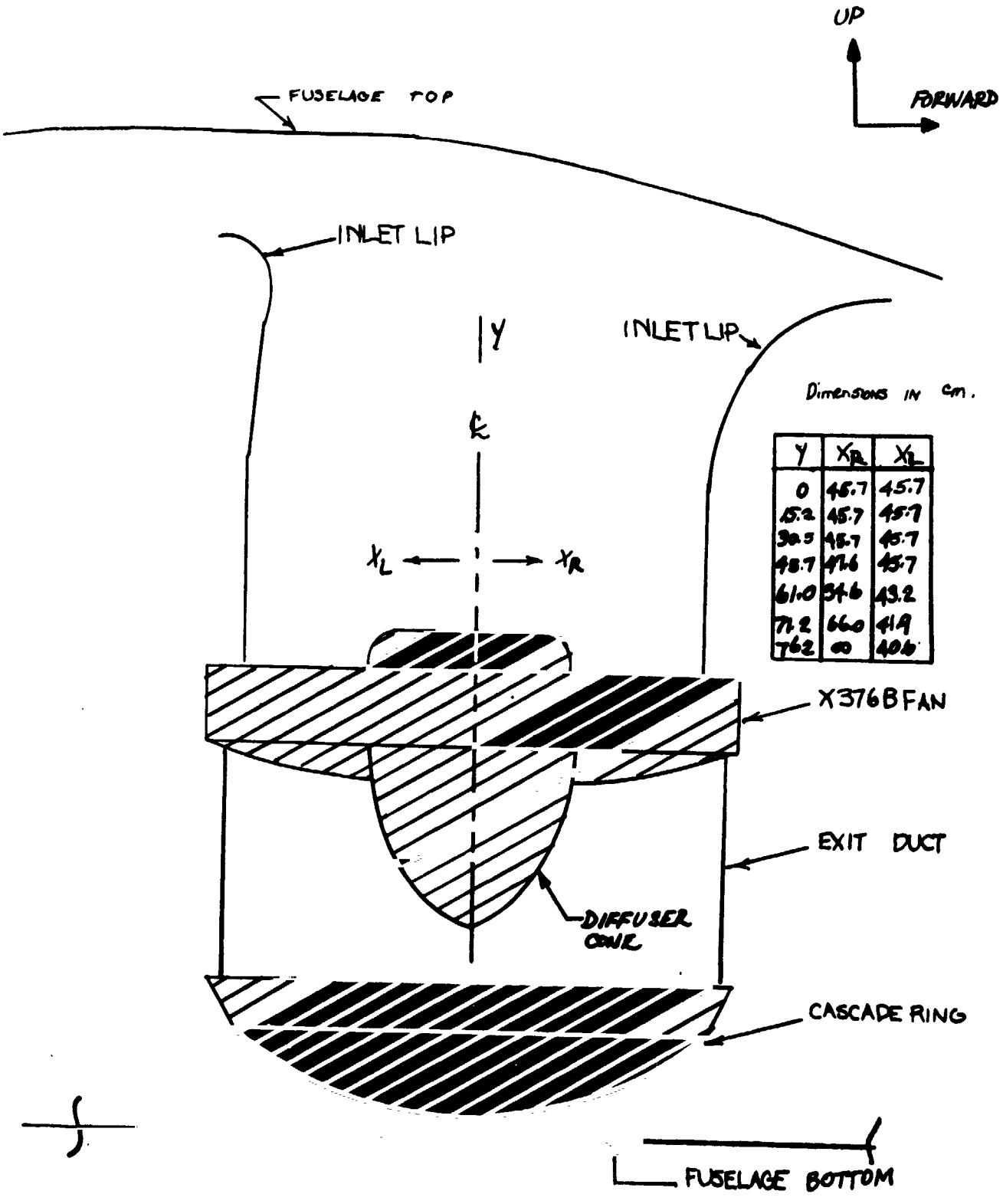

y	X_R	X_L
0	45.7	45.7
15.2	45.7	45.7
30.5	45.7	45.7
45.7	47.6	45.7
61.0	54.6	43.2
71.2	66.0	41.9
76.2	∞	40.6

(d) Forward lift-fan inlet cross section along free stream.

Figure 2.- Continued.

NACA 65A010 BASIC THICKNESS

X%	X-CM	Y%	Y-CM
0	0	0	0
0.50	.06	.765	1.94
0.75	.86	.928	2.35
1.25	.143	1.183	3.00
2.50	.286	1.623	4.12
5.00	.571	2.182	5.54
7.50	.859	2.650	6.73
10	1.14	3.040	7.72
15	1.71	3.658	9.29
20	2.29	4.127	10.48
25	2.86	4.483	11.39
30	3.43	4.742	2.04
35	4.00	4.912	12.48
40	4.57	4.995	12.69
45	5.14	4.989	2.66
50	5.71	4.863	12.35
55	6.29	4.632	11.77
60	6.86	4.304	10.93
65	7.43	3.899	9.90
70	8.00	3.432	8.72
75	8.57	2.912	7.40
80	9.14	2.352	7.40
85	9.72	1.771	5.97
90	10.29	1.188	4.50
95	10.86	0.604	3.02
100	11.43	0.021	.05

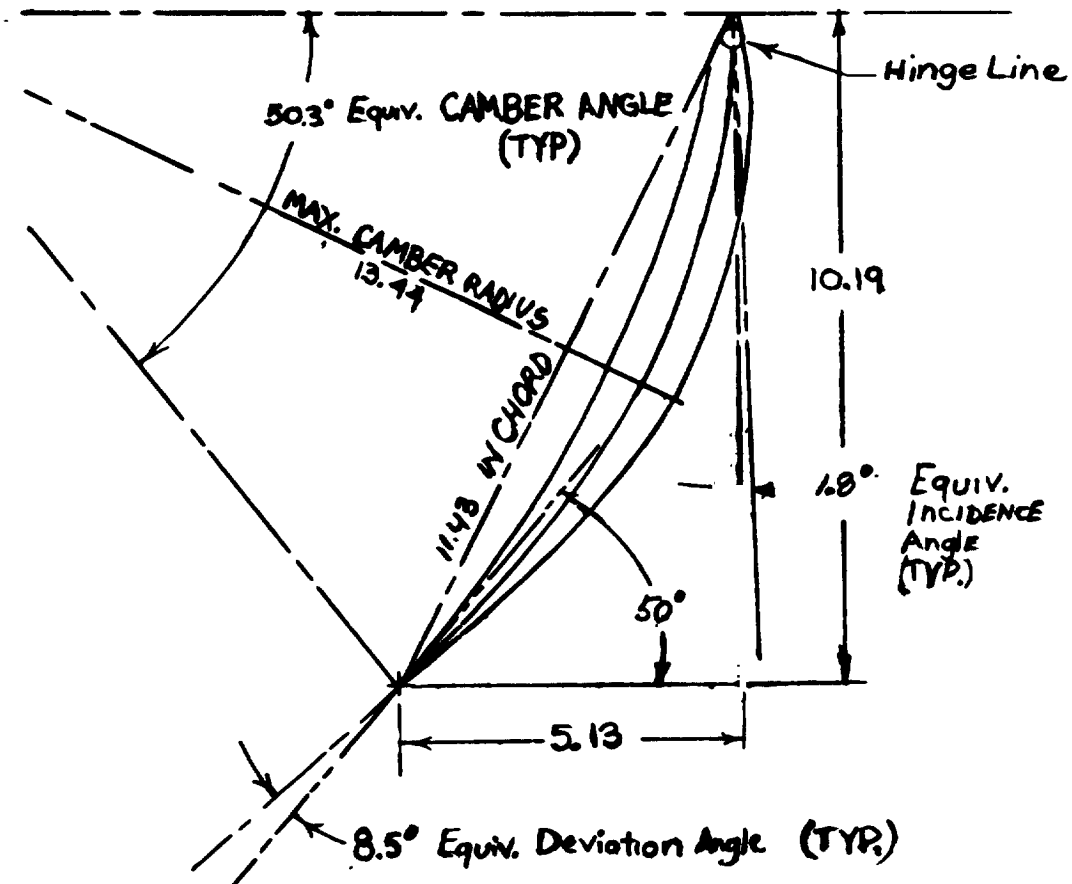

NOTE: ALL DIMENSIONS IN CM. EXCEPT AS NOTED.

(e) Lift-fan exit lower details.

Figure 2.- Continued.

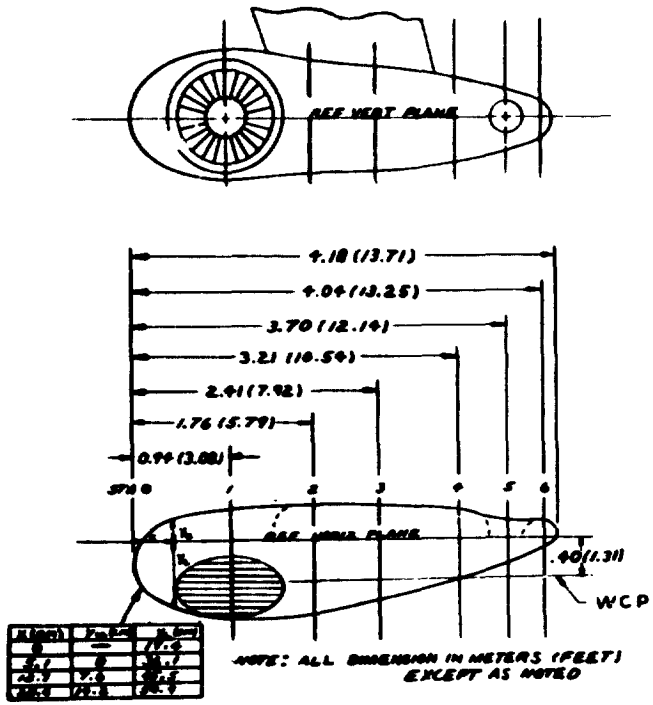

STA 1

SECTION A-A

Y_U, cm	Z_{L_1}, cm	Z_{L_2}, cm
0	70.5	43.7
0	70.5	64 0
5.1	71.5	46 1
5.1	71.5	63 0
10.2	71.1	49.1
10.2	71.1	60.9
13 0	70.1	56.3
20.3	69.8	—
20.3	66.5	—
25.9	45.5	—
25.9	63.0	—
31.9	58.1	—
Y_L, cm	Z_{L_1}, cm	Z_{L_2}, cm
7.4	68.0	69.5
25.4	41.1	61.9
59.3	0	49.2
78.2	—	34.6

STA 2

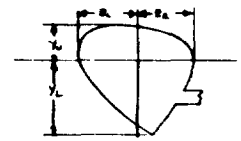

Y_U, cm	Z_{L_1}, cm	Z_{L_2}, cm
0	56.7	55.3
7.6	58.1	52.0
18.2	57.0	44.0
22.9	52.0	28.9
31.4	37.7	0
33.2	20.8	—
Y_L, cm	Z_{L_1}, cm	Z_{L_2}, cm
7.6	53.9	59.6
15.2	49.8	52.2
22.9	45.0	49.0
39.3	36.2	62.8
35.2	35.6	44.3
46.5	24.5	40.8
48.4	22.7	40.1
65.2	0	26.2
75.7	—	16.5

STA 3

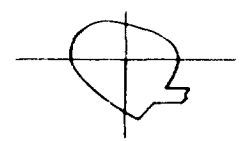

Y_U, cm	Z_{L_1}, cm	Z_{L_2}, cm
0	49.5	52 9
7 6	50.8	51.0
15 2	50.0	43.8
22.9	47.3	27.6
32.1	37 9	0
35.1	26.4	—
Y_L, cm	Z_{L_1}, cm	Z_{L_2}, cm
7.6	47.1	51.1
15.2	42 9	48.6
22.9	36.3	44.7
31.1	27.3	40.6
32.1	25.7	39.7
43 8	9 4	56 6
45.3	7.4	25.4
49.8	0	21 4
59.1	—	19.2

STA 4

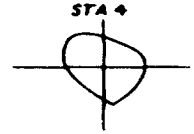

Y_U, cm	Z_{L_1}, cm	Z_{L_2}, cm
0	35.4	41.6
2.5	36.4	42.0
8.9	37.8	40.8
15.2	38.2	36.4
21.6	37.1	27.3
27.9	33.7	12.5
31.9	28.4	0
35.1	15.2	—
Y_L, cm	Z_{L_1}, cm	Z_{L_2}, cm
3.8	39.5	40.2
10.2	28.5	36.6
16.6	22.1	31.8
22.9	13.9	27.4
31.5	0	16.2
37.1	—	10.0

STA 5

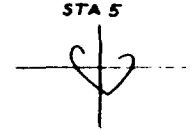

Y_U, cm	Z_{L_1}, cm	Z_{L_2}, cm
0	23.1	29.0
7.6	27.5	17.7
7.6	27.5	30.9
13.3	28.4	24 4
16.8	18.7	—
16.8	27.5	—
21.4	22.0	—
Y_L, cm	Z_{L_1}, cm	Z_{L_2}, cm
7 6	16.8	24.1
15.2	7.5	17.0
20.1	0	11.3
24.0	—	6 6

STA 6

Y_U, cm	Z_{L_1}, cm	Z_{L_2}, cm
0	6.6	17.0
5.1	10.8	21.6
15 2	14.1	13.1
19.5	5.6	0
20.0	5.3	—
Y_L, cm	Z_{L_1}, cm	Z_{L_2}, cm
4.8	12	8.6
8.1	—	1 8

(f) Wing-tip lift-fan pod details.

Figure 2.- Continued.

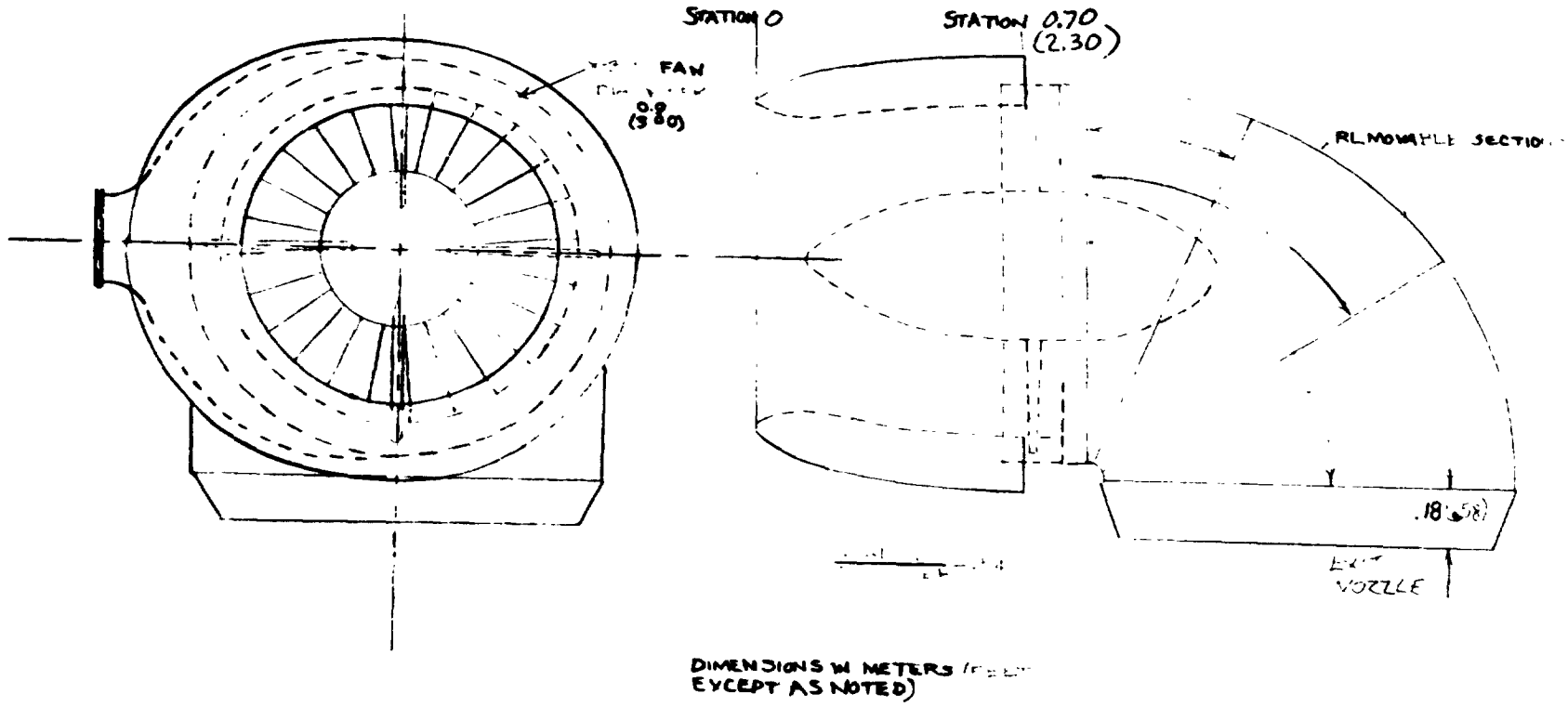

(g) Lift cruise fan details.

Figure 2.- Concluded.

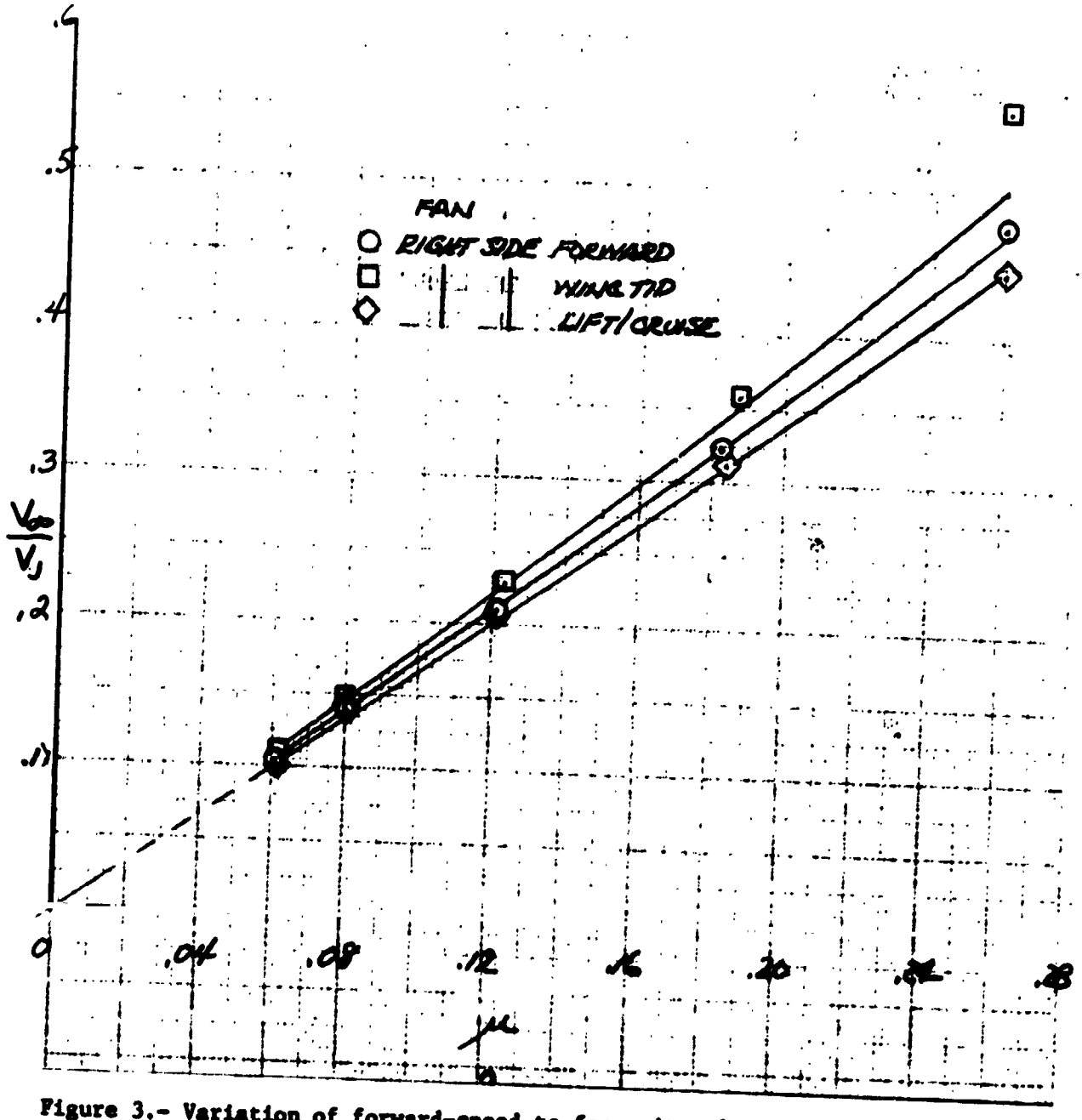

Figure 3.- Variation of forward-speed-to-fan-exit-velocity ratio with fan-tip speed ratio.

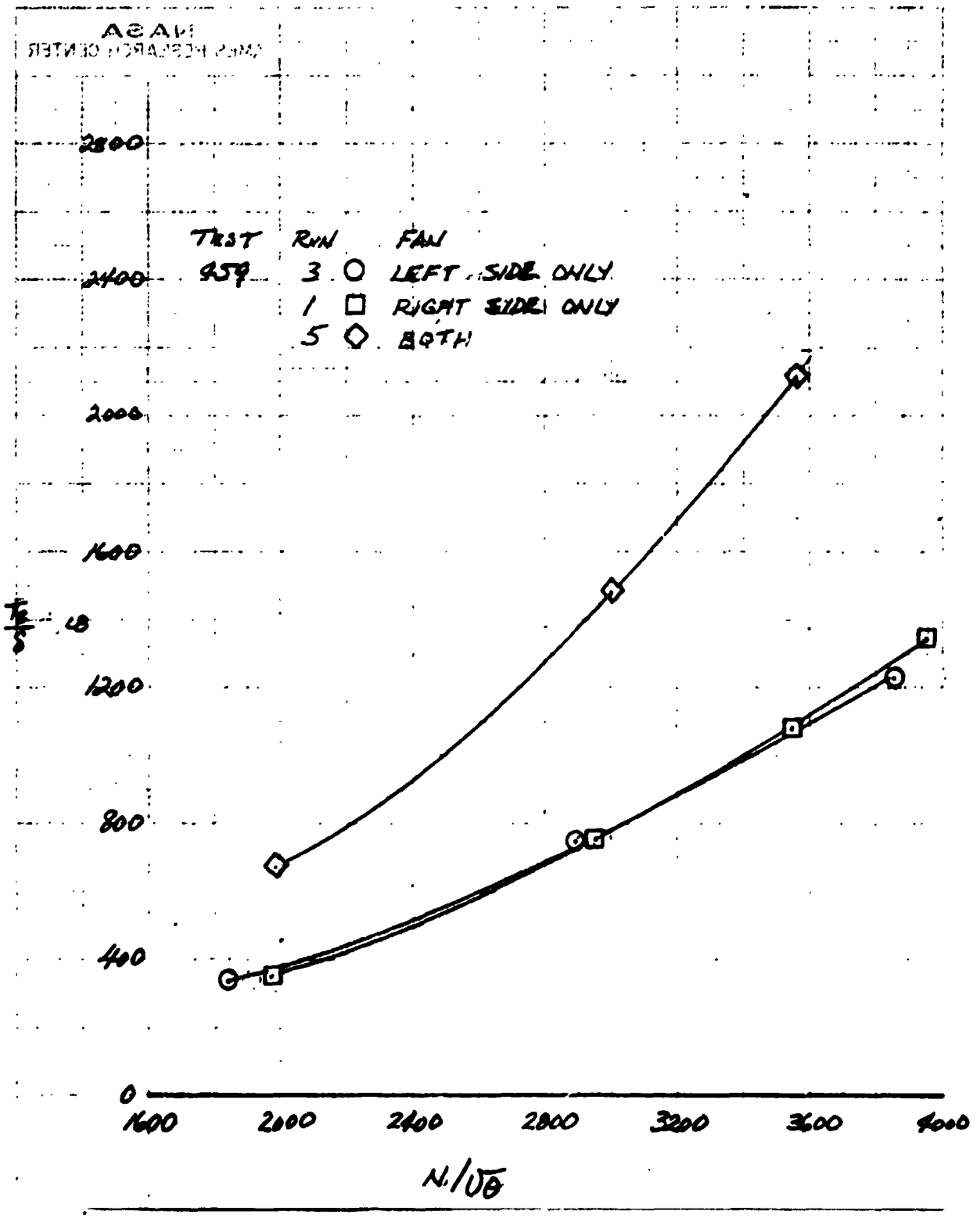

(a) Forward fan, $\sigma_v = 0°$, $\beta_v = 0°$.

Figure 4.- Variation of fan thrust with fan RPM; $\alpha = 0°$, $q = 0$ psf.

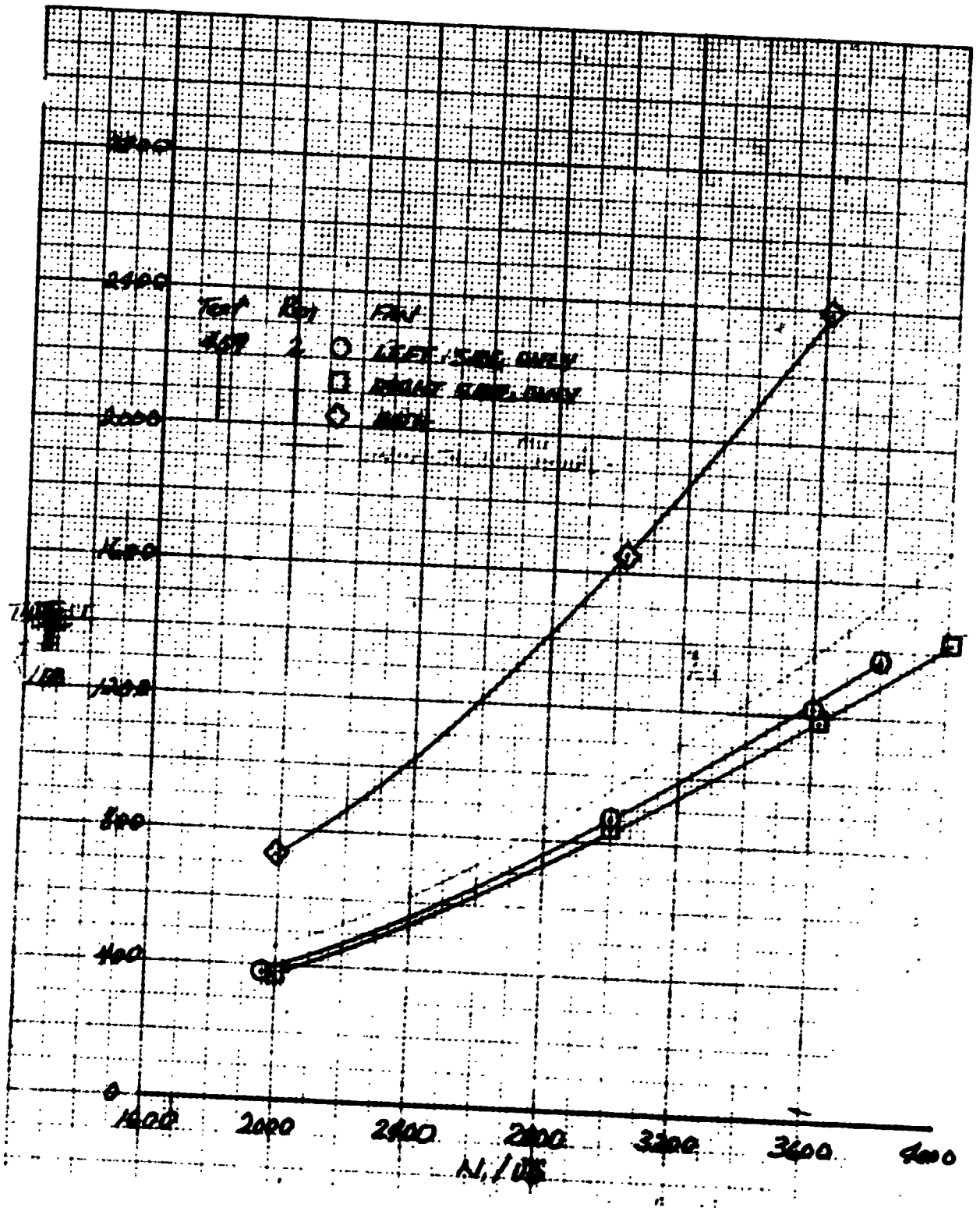

(b) Wing-tip fan, $\sigma_v = 0°$, $\beta_v = 0°$.

Figure 4.- Continued.

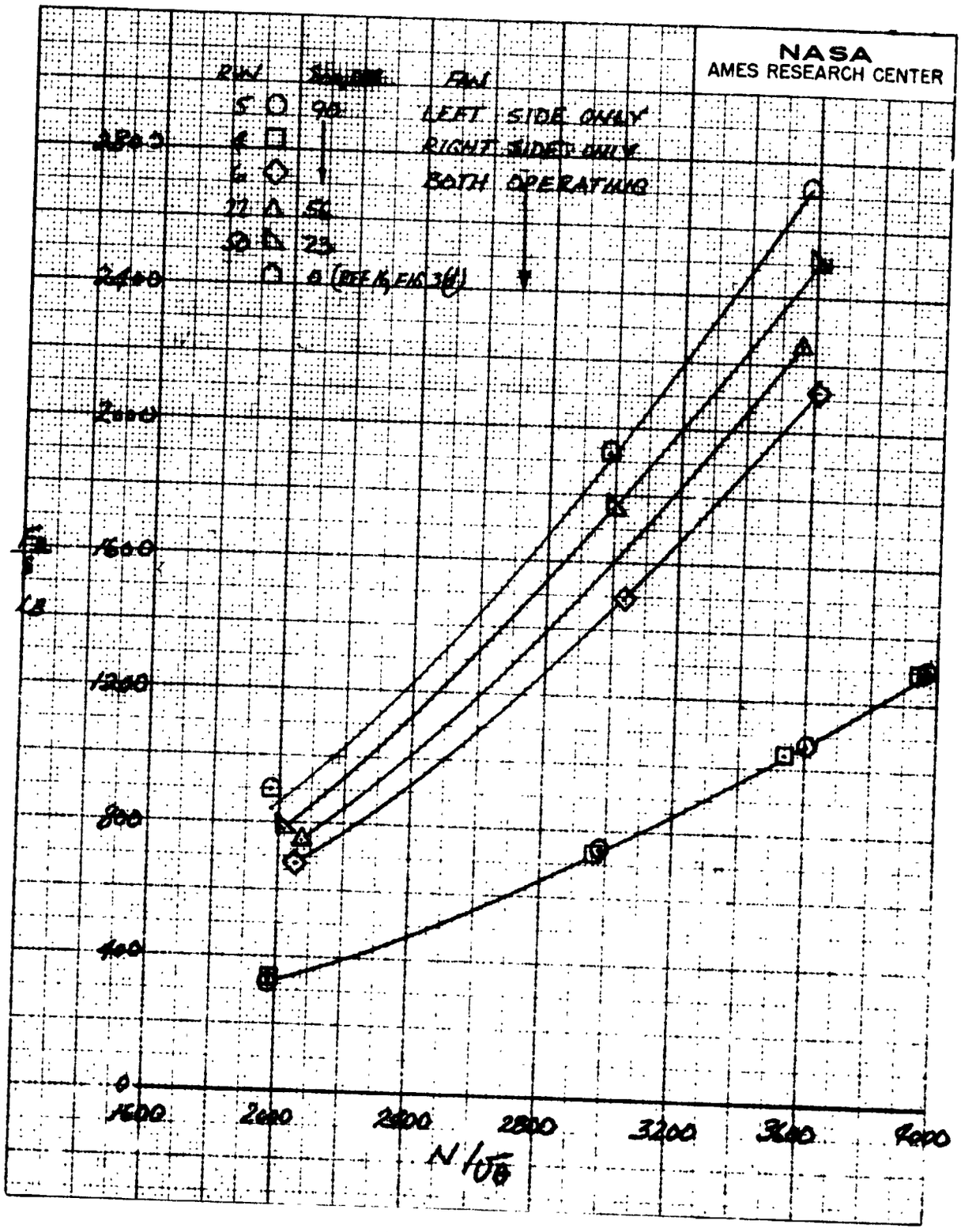

(c) Lift/cruise fan.

Figure 4.- Concluded.

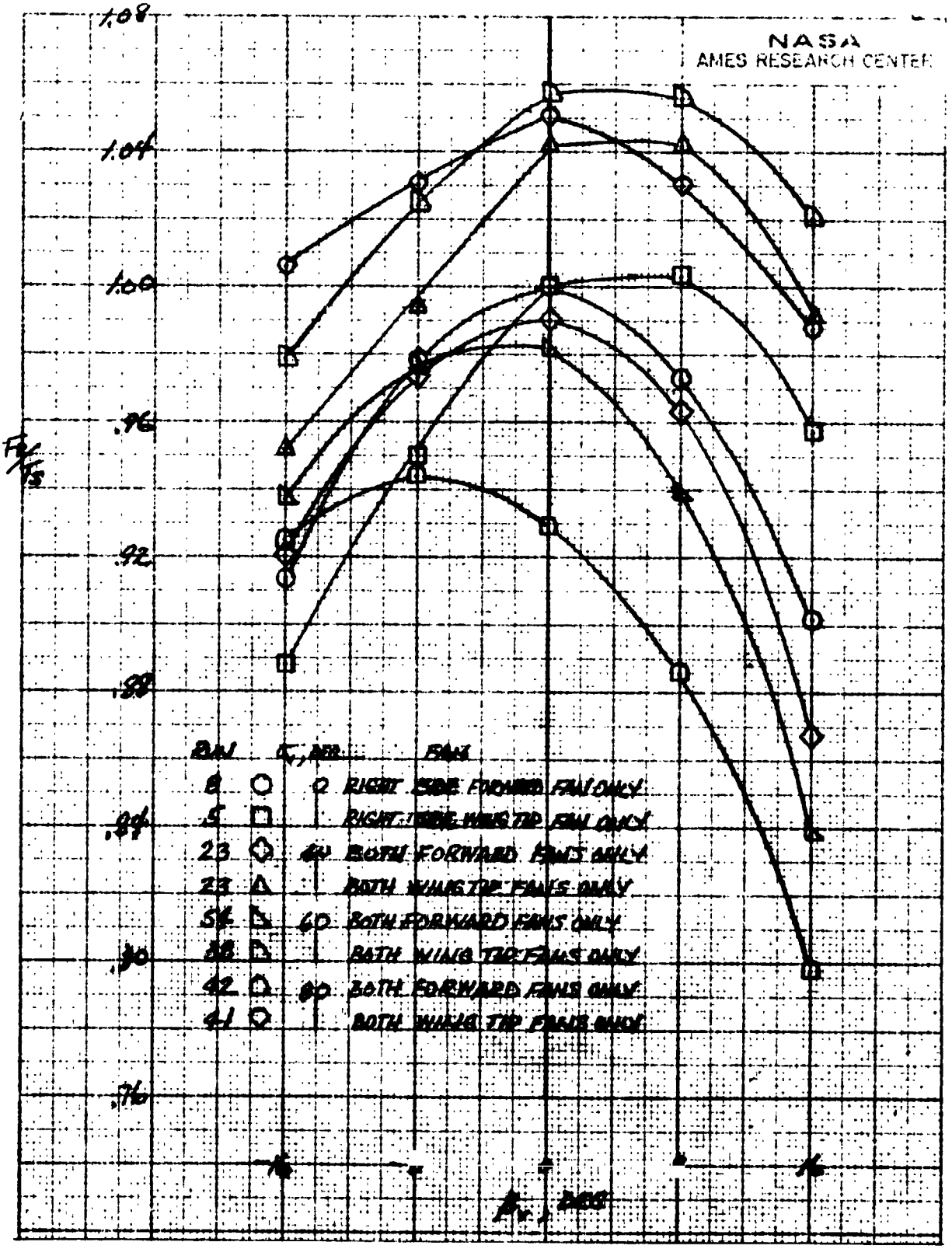

Figure 5.- Variation of static resultant fan thrust to maximum static fan-lift (σ_V = 0°, β_V = 0°) ratio with fan exit-lower-deflection angle; fan RPM = 3600, α = 0°.

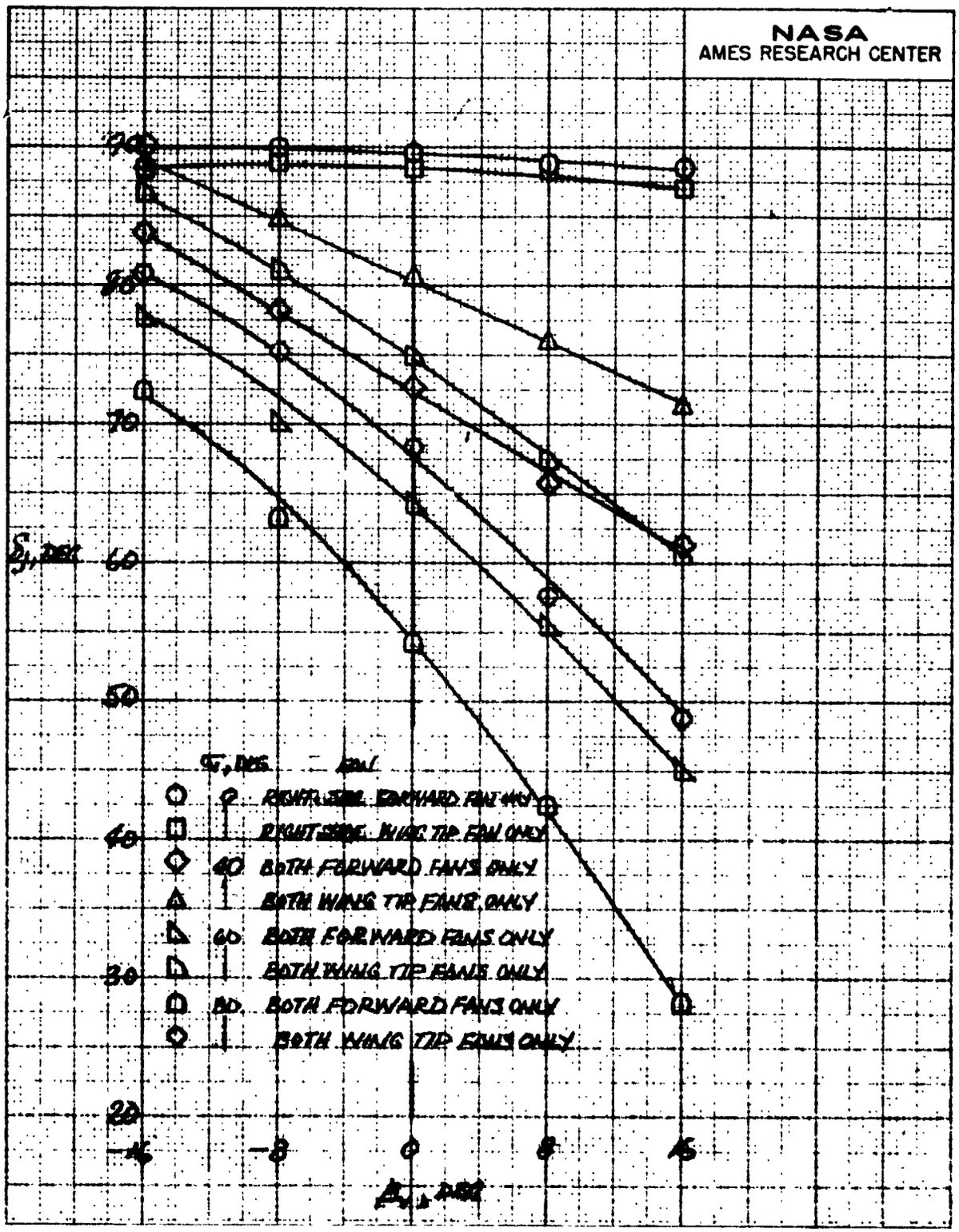

Figure 6.- Variation of fan efflux static turning angle with fan exit-lower deflection angle; fan RPM = 3600, $\alpha = 0°$.

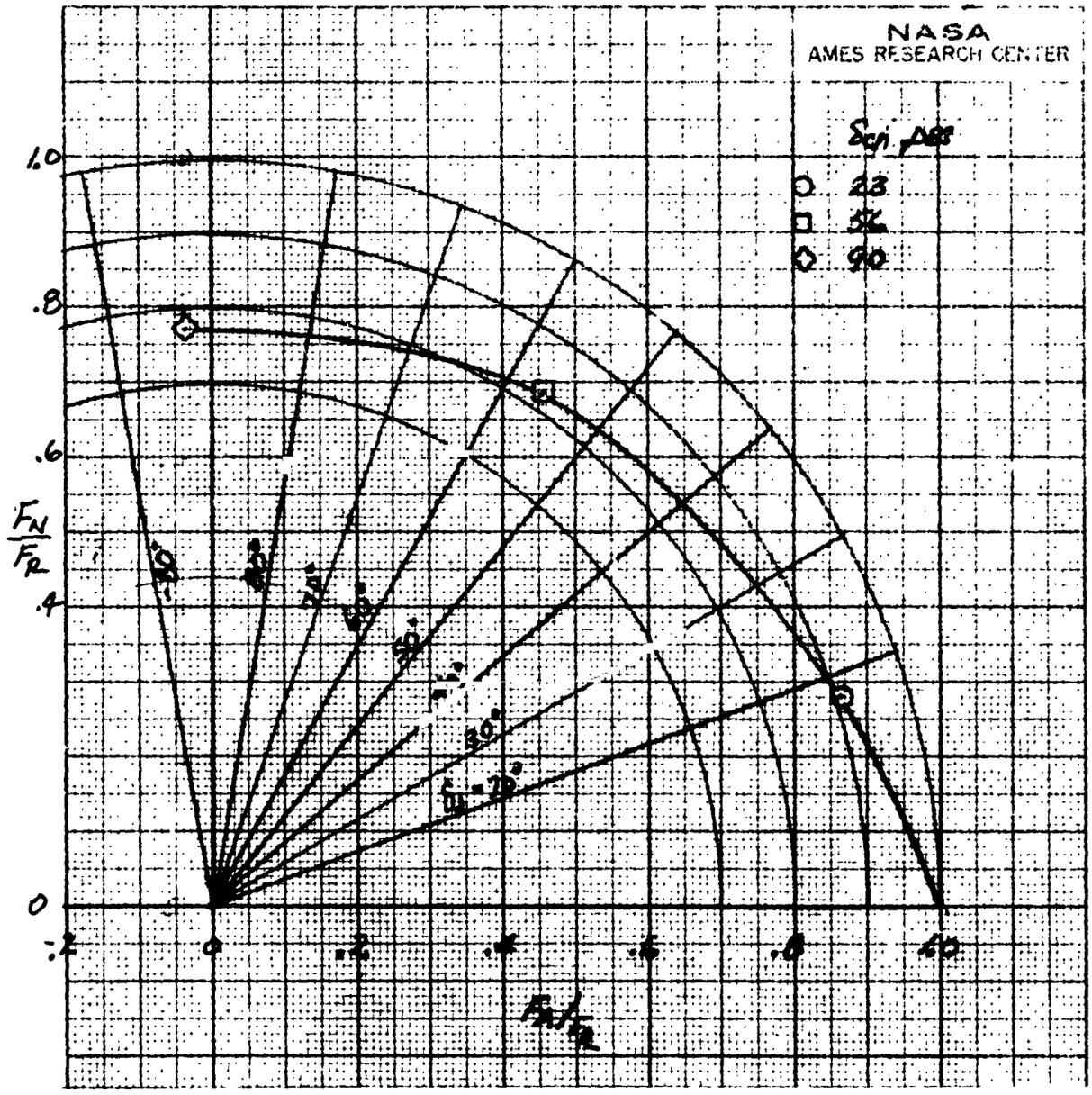

Figure 7.- Variation of static turning and static turning efficiency with lift/cruise fan exhaust duct angle.

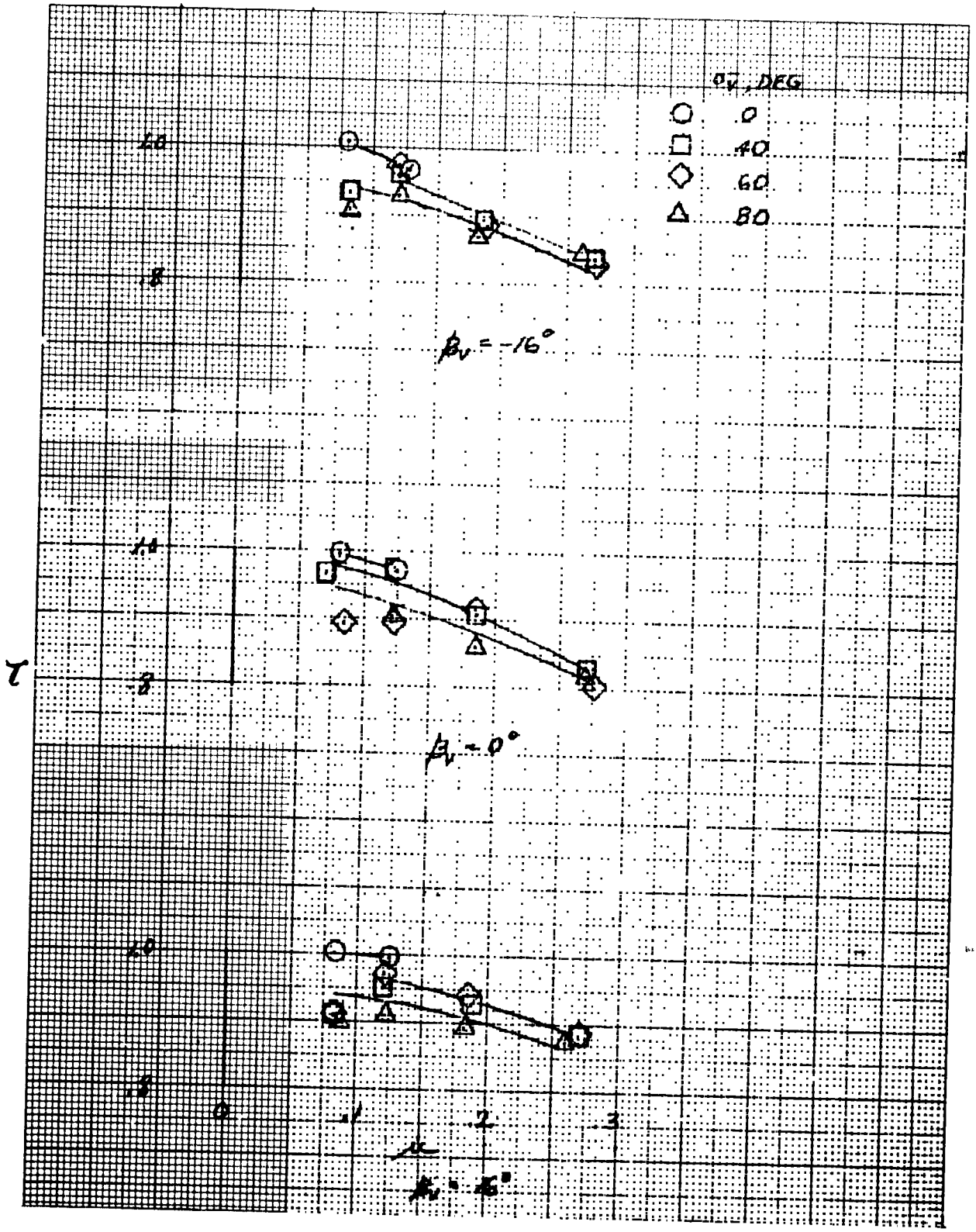

(a) Right forward fan.

Figure 8.- Variation of ideal thrust with forward speed to ideal static thrust ratio with fan-tip speed ratio.

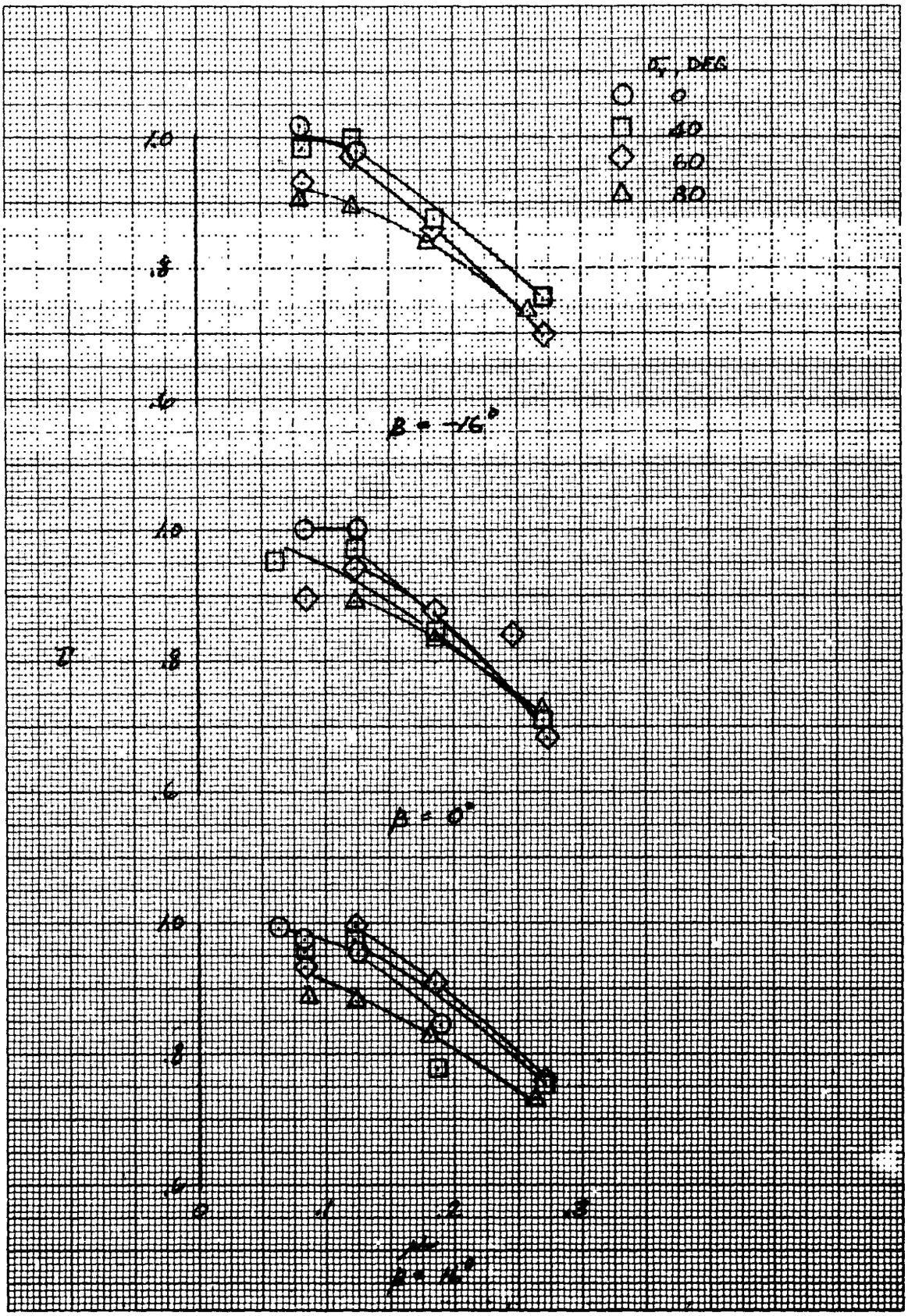

(b) Right wing tip fan.

Figure 8.- Continued.

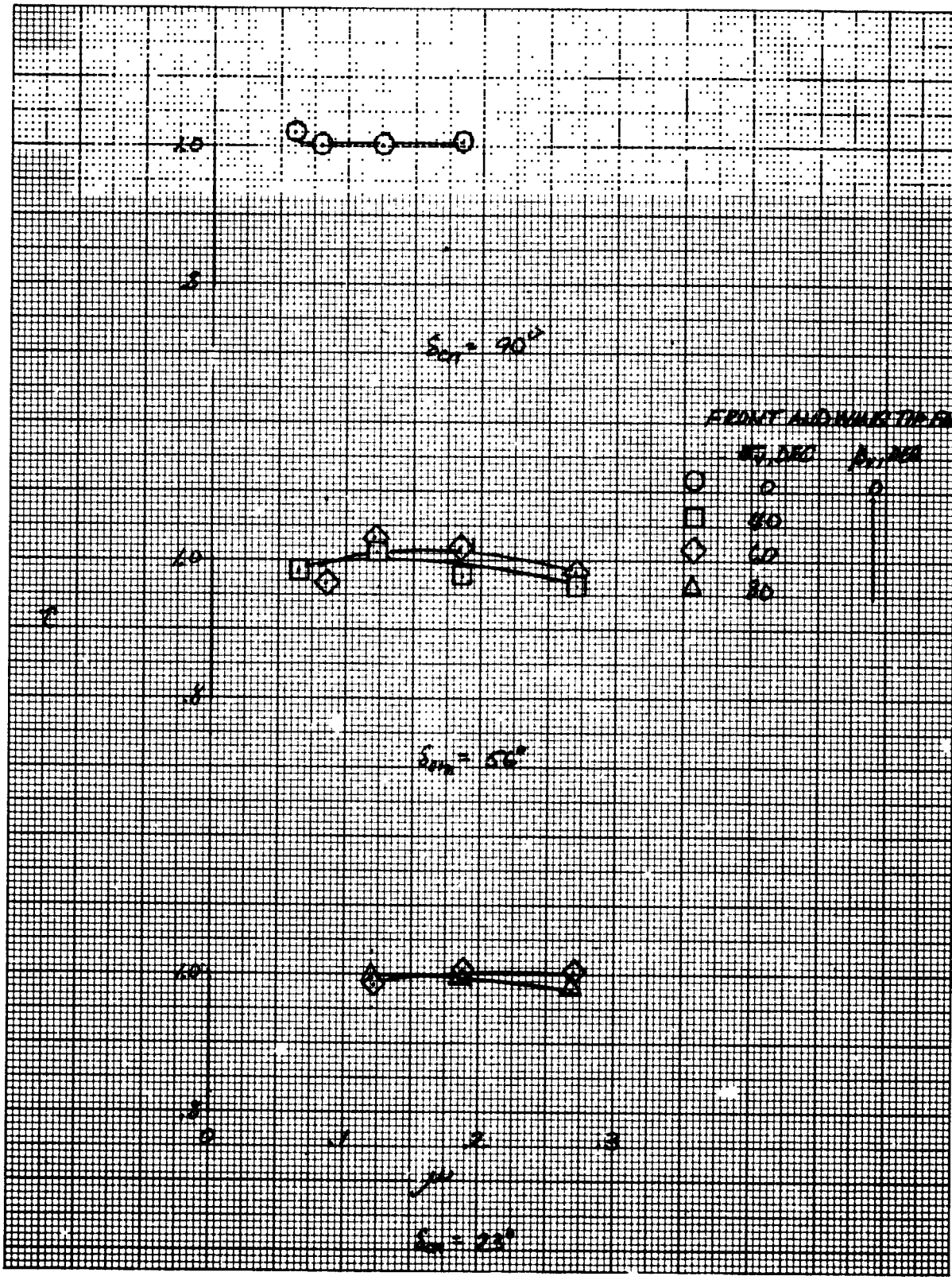

(c) Right lift/cruise fan.

Figure 8.- Concluded.

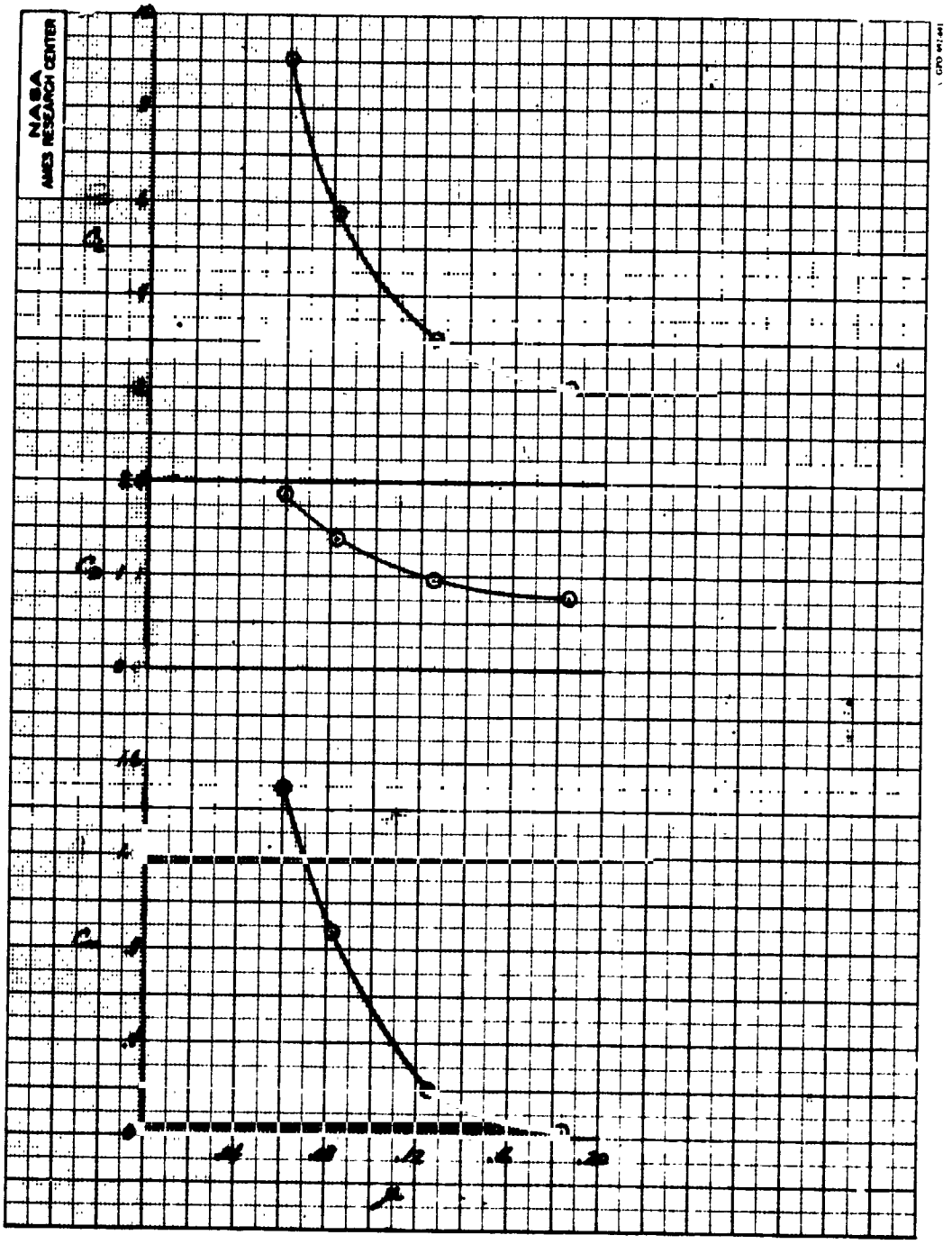

Figure 9.- The variation in longitudinal characteristics with tip-speed ratio; wing-tip lift fans only, $\beta_v = 0°$, forward lift fan inlets covered, $\delta_{cn} = 90°$, $\delta_f = 30°$, $\alpha_u = 0°$.

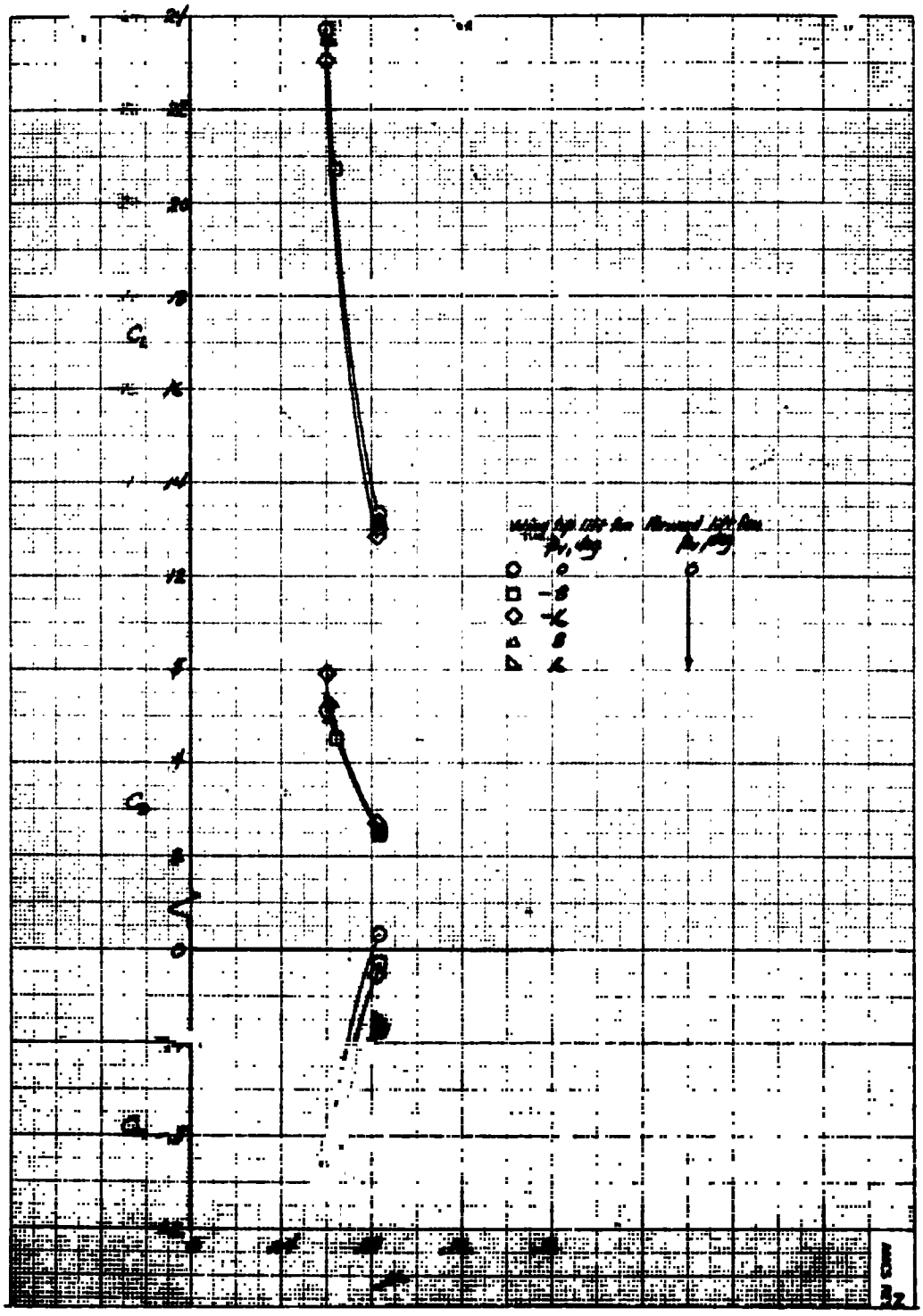

Figure 10.- The variation in longitudinal characteristics with tip speed ratio; all fans operating, $\sigma_v = 0°$, $\delta_{cn} = 90°$, $\delta_f = 30°$, $\alpha_u = 0°$.

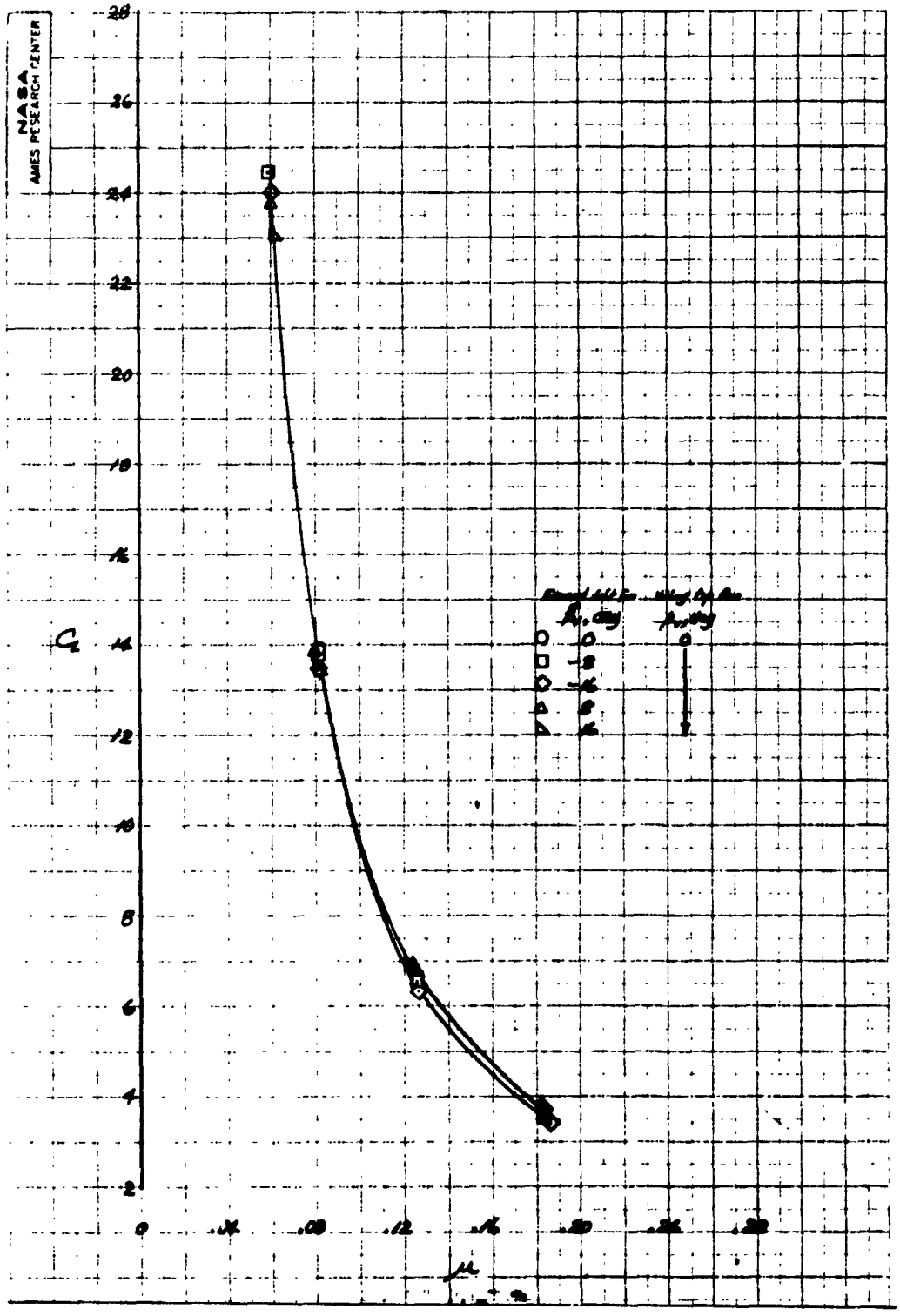

(a) C_L variation with μ.

Figure 11.- The variation in longitudinal characteristics with tip speed ratio; all fans operating, $\delta_{cn} = 90°$, $\delta_f = 30°$, $\alpha_u = 0°$.

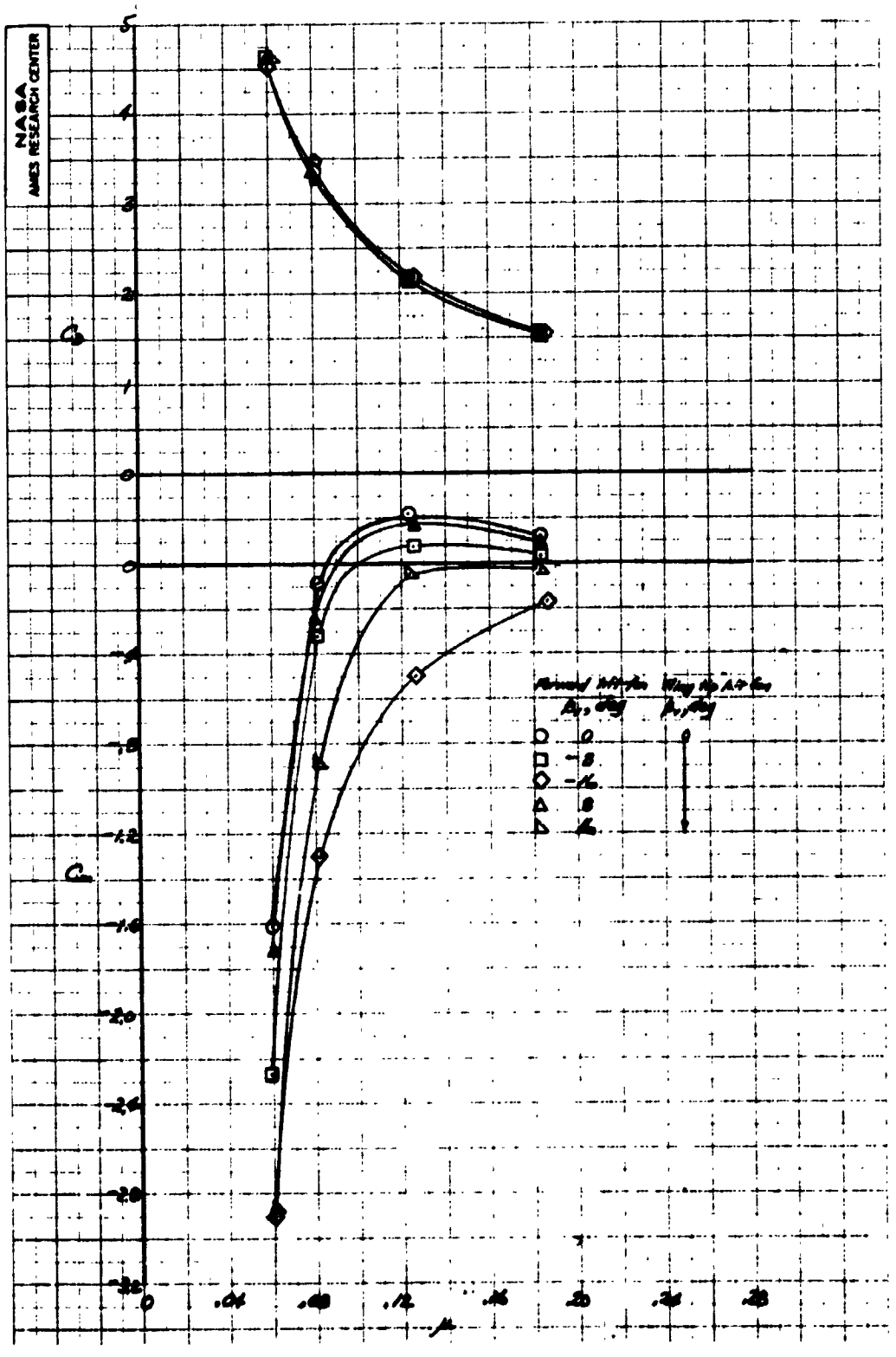

(b) C_D, C_m variation with μ.

Figure 11.- Concluded.

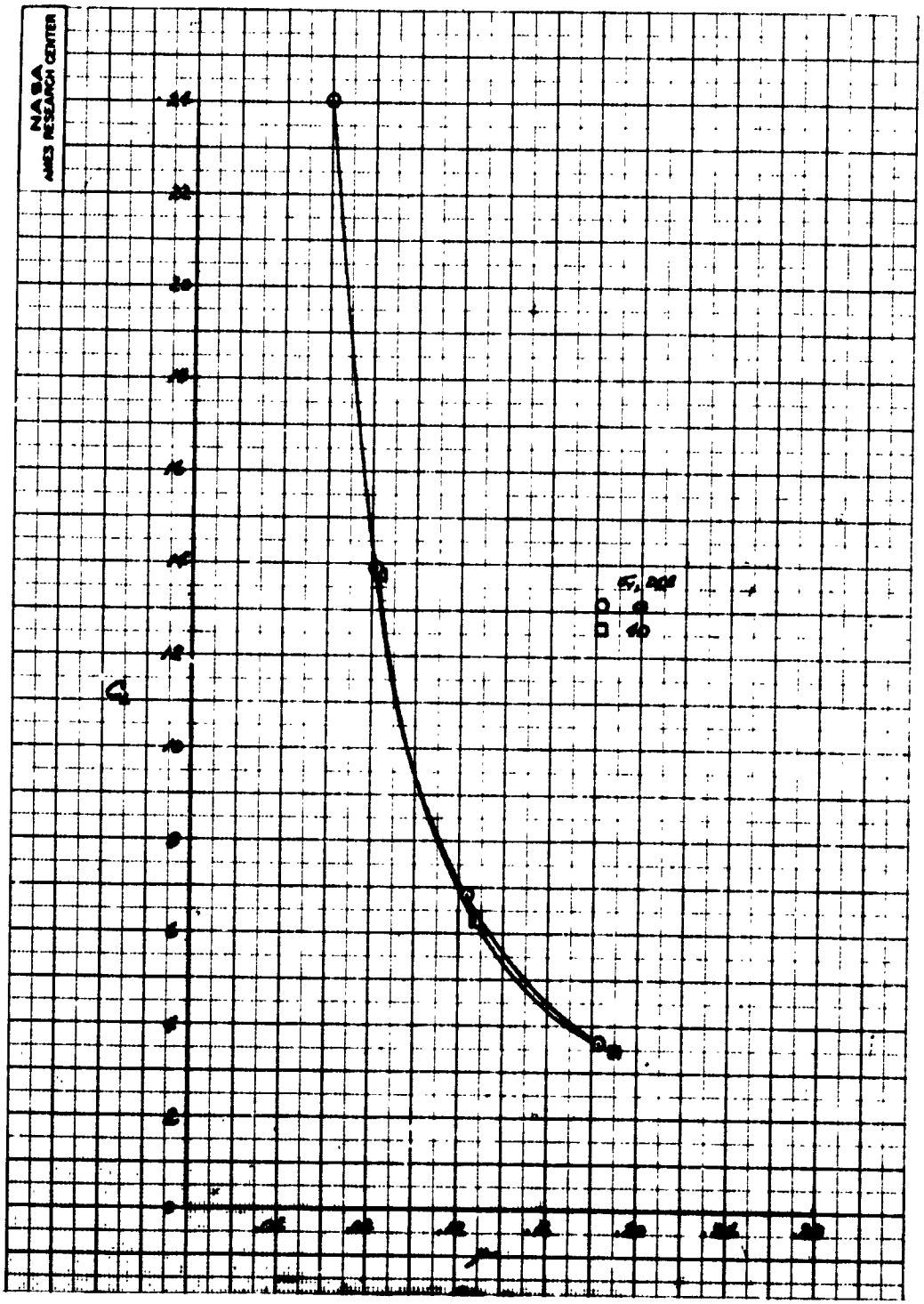

(a) C_L variation with μ.

Figure 12.- The variation in longitudinal characteristics with tip speed ratios; all fans operating, $\beta_v = 0°$, $\delta_{cn} = 90°$, $\delta_f = 30°$, $\alpha_u = 0°$.

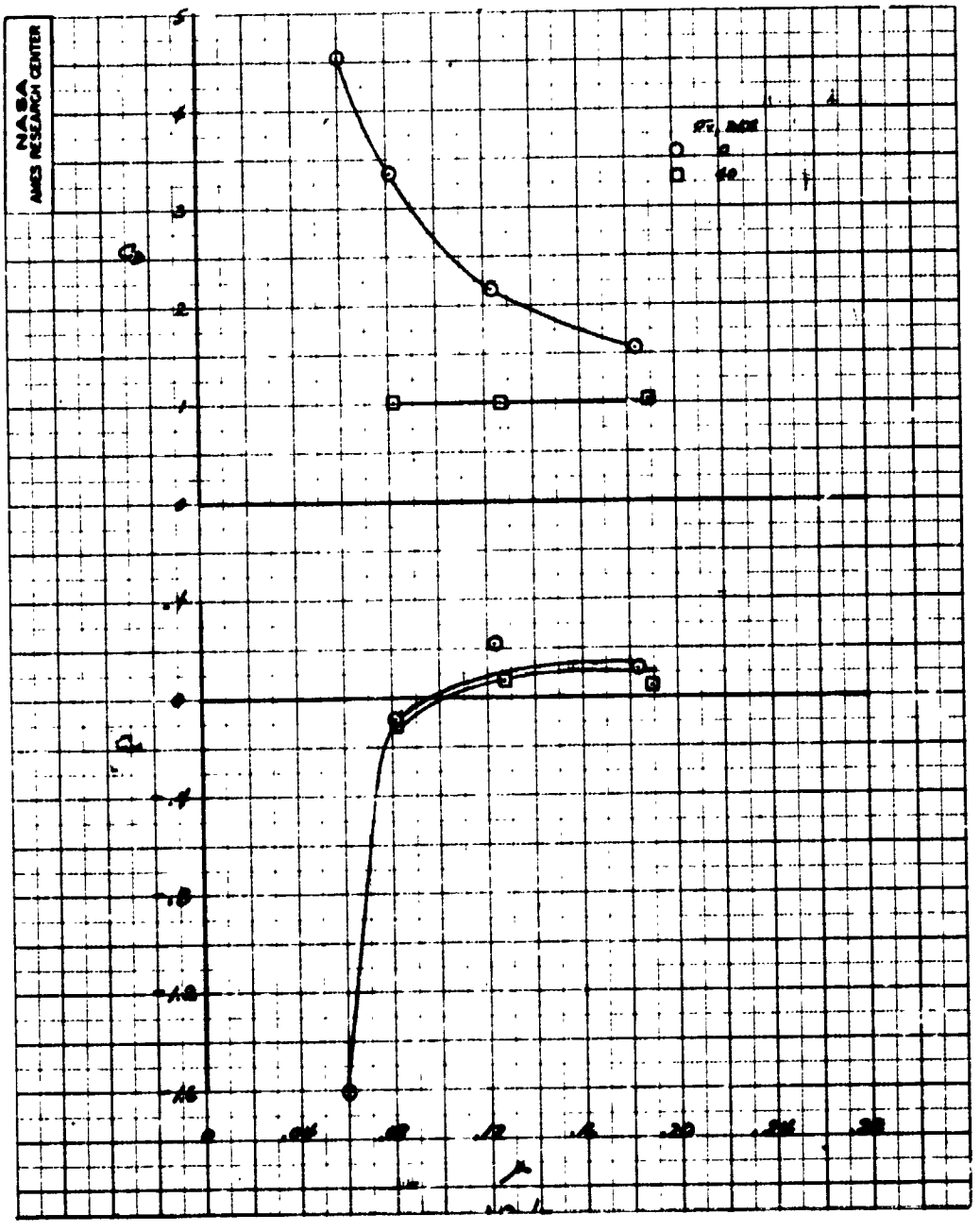

(b) C_D, C_m variation with μ.

Figure 12.- Concluded.

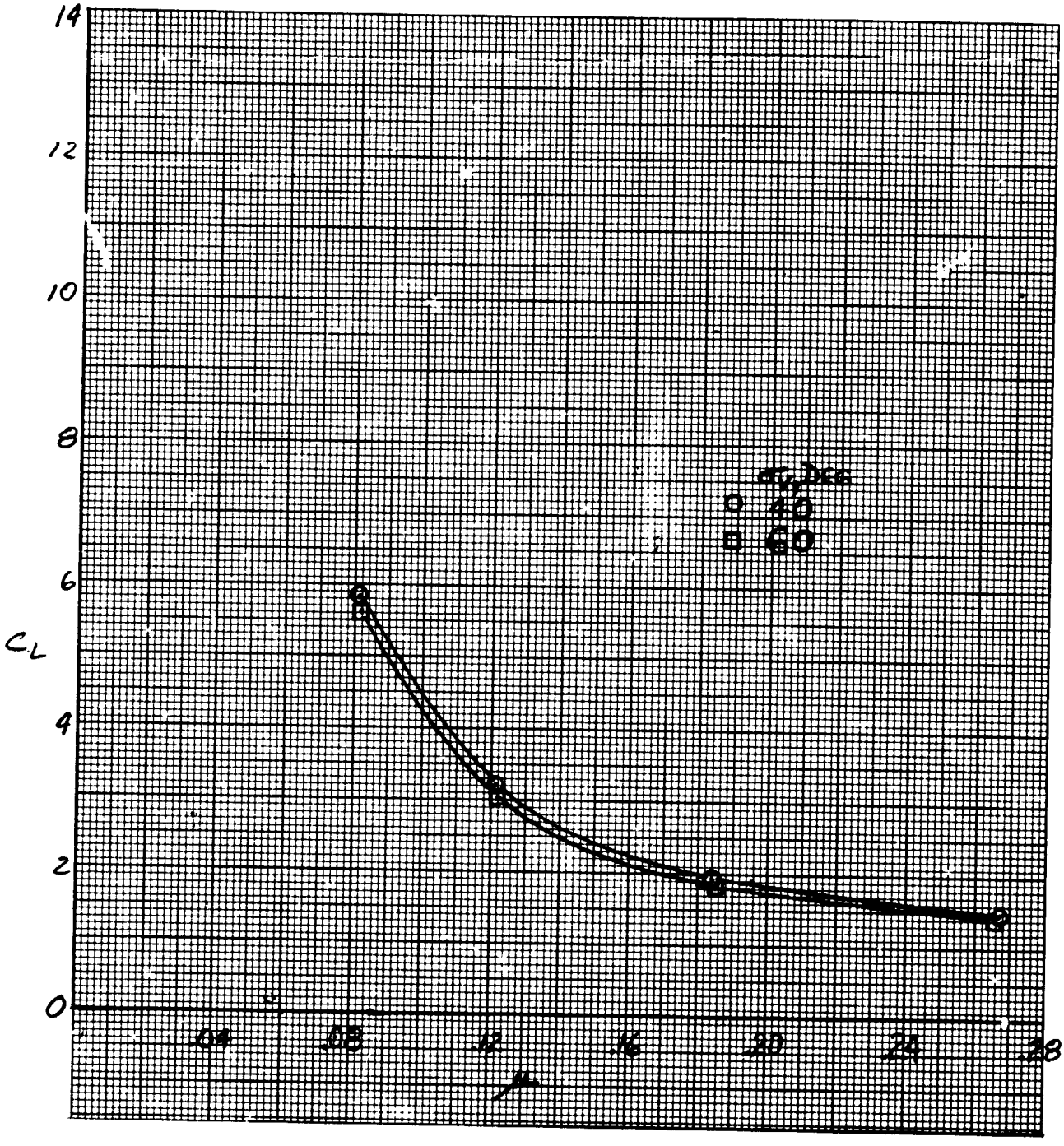

(a) C_L variation with μ.

Figure 13.- The variation in longitudinal characteristics with tip speed ratios; wing-tip lift fans operating only, $\beta_v = 0°$, $\delta_{cn} = 0$, $\delta_f = 30°$, $\alpha_u = 0°$.

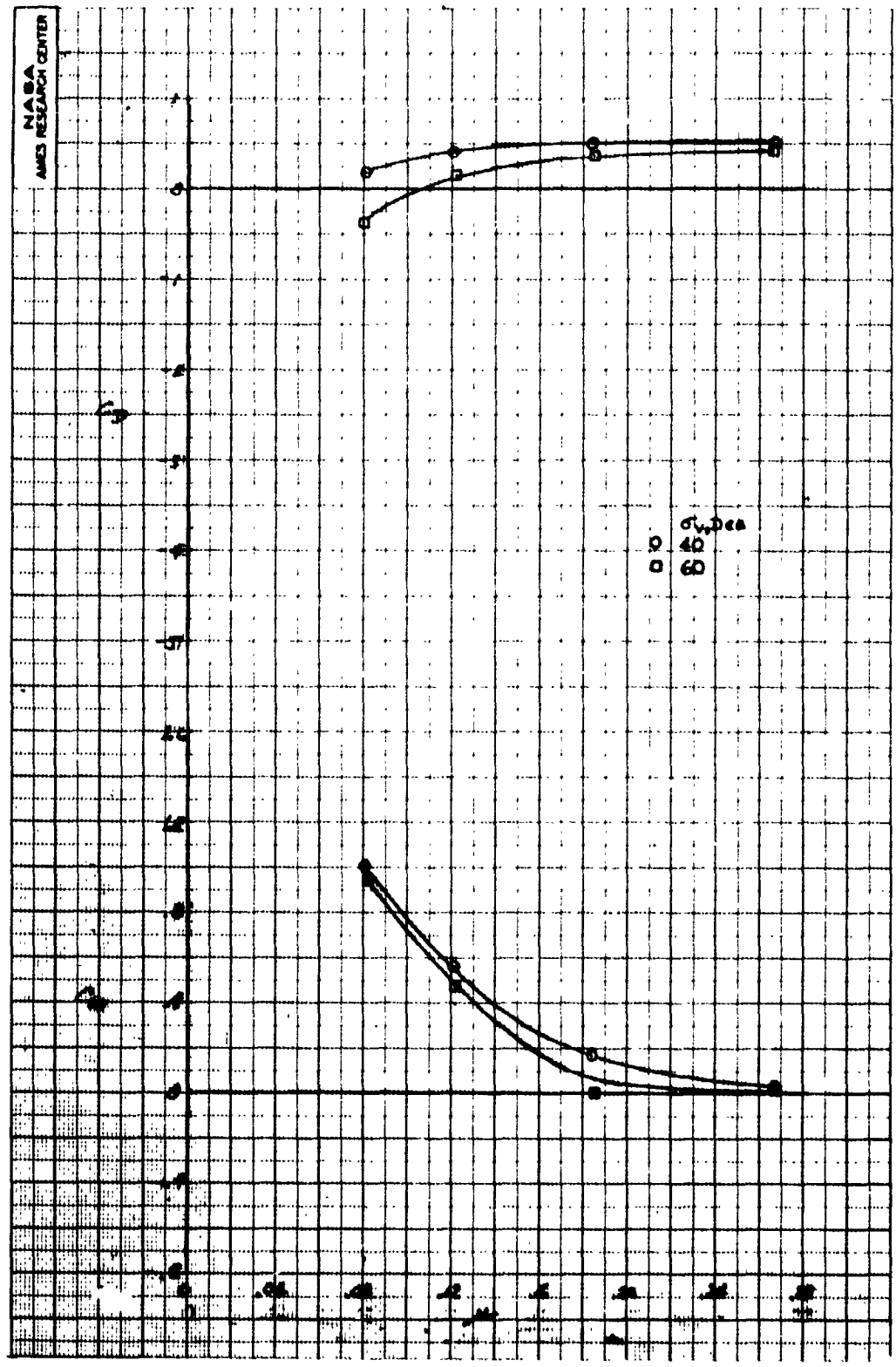

(b) C_D, C_m variation with μ.

Figure 13.- Concluded.

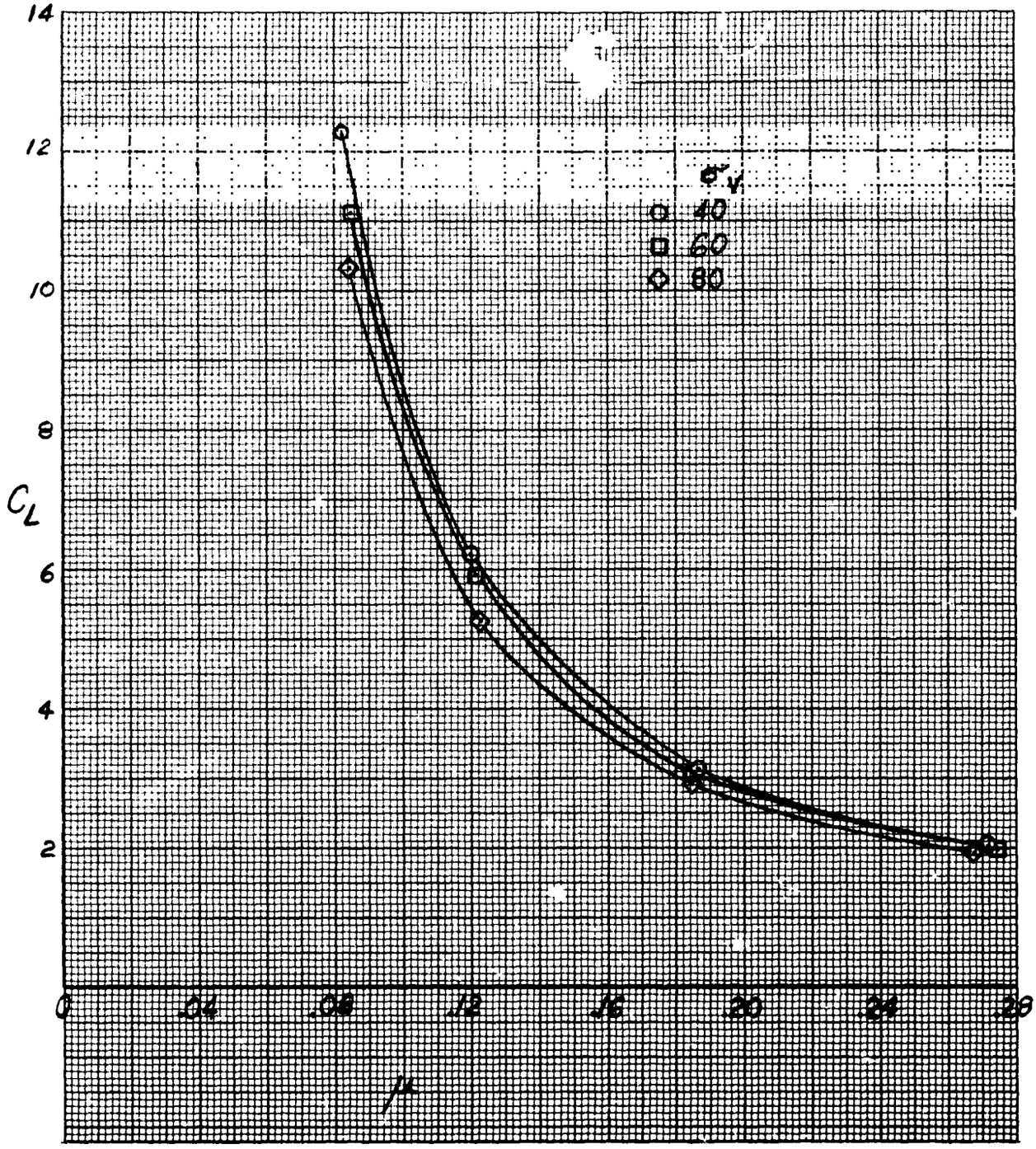

(a) C_L variation with μ, $\beta_v = 0°$.

Figure 14.- The variation in longitudinal characteristics with tip speed ratios; all fans operating, $\delta_{cn} = 56°$, $\delta_f = 30°$, $\alpha_u = 0°$.

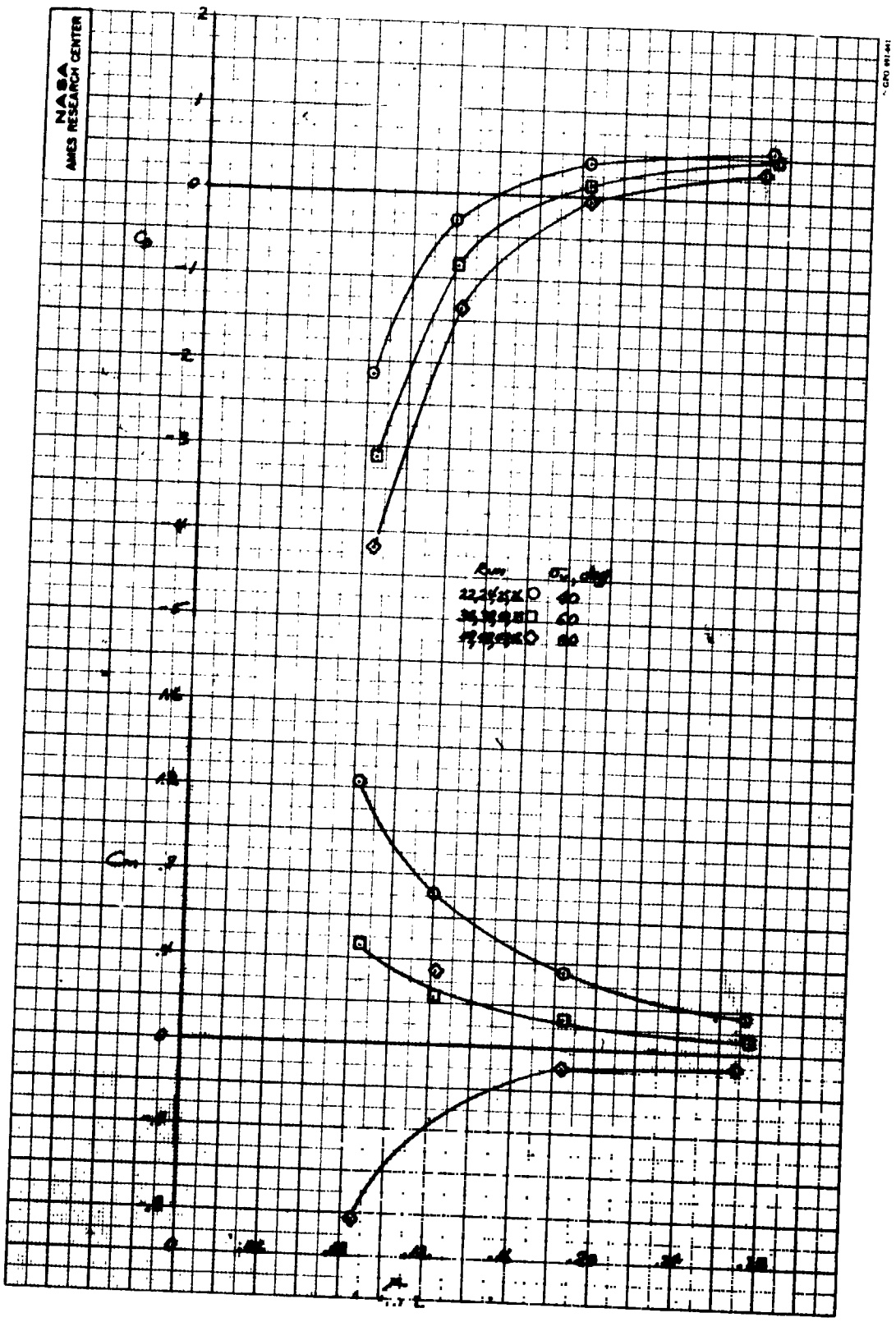

(b) C_D, C_m variation with μ, $\beta_v = 0°$.

Figure 14.- Continued.

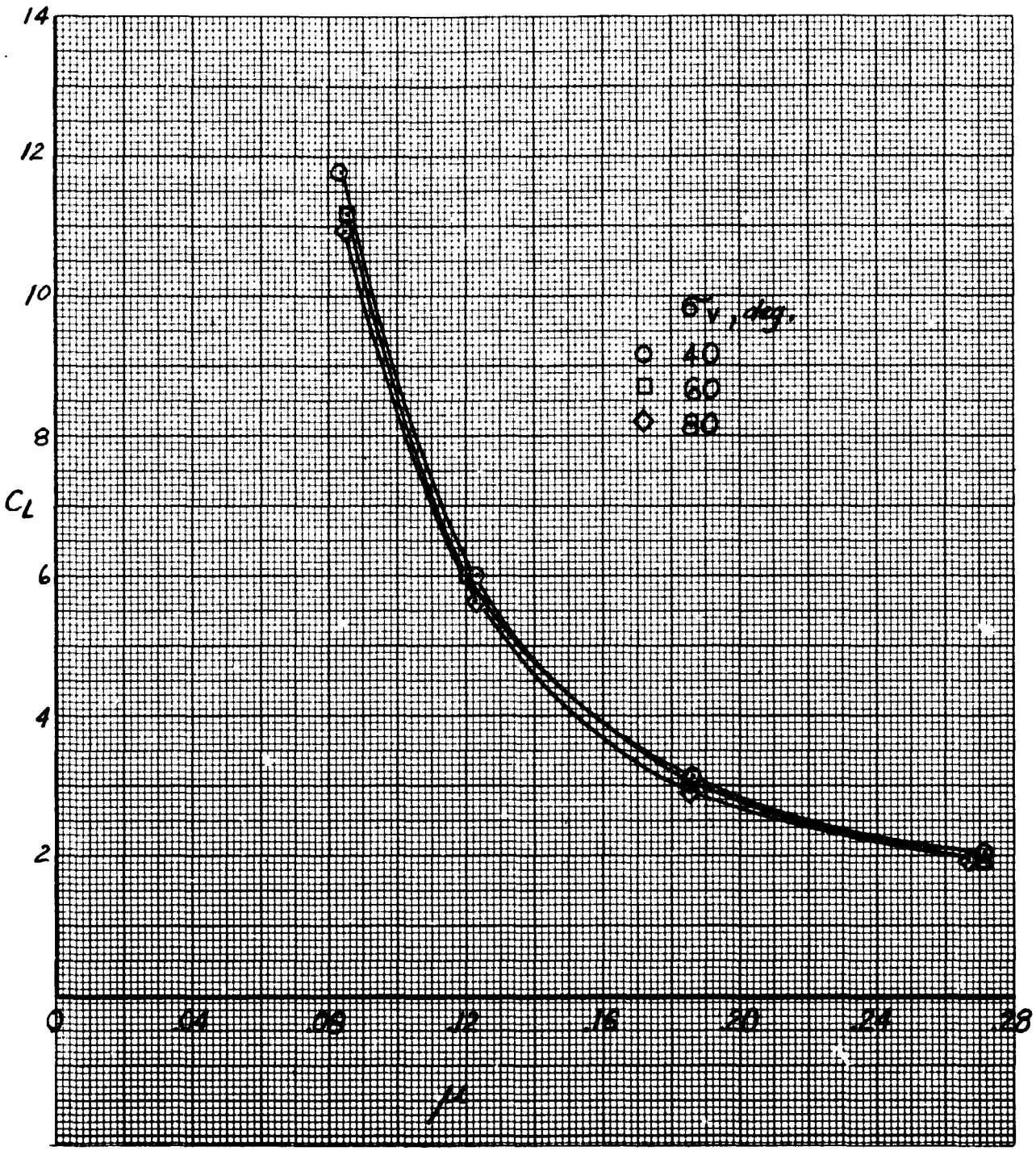

(c) C_L variation with μ, $\beta = -8°$.

Figure 14.- Continued.

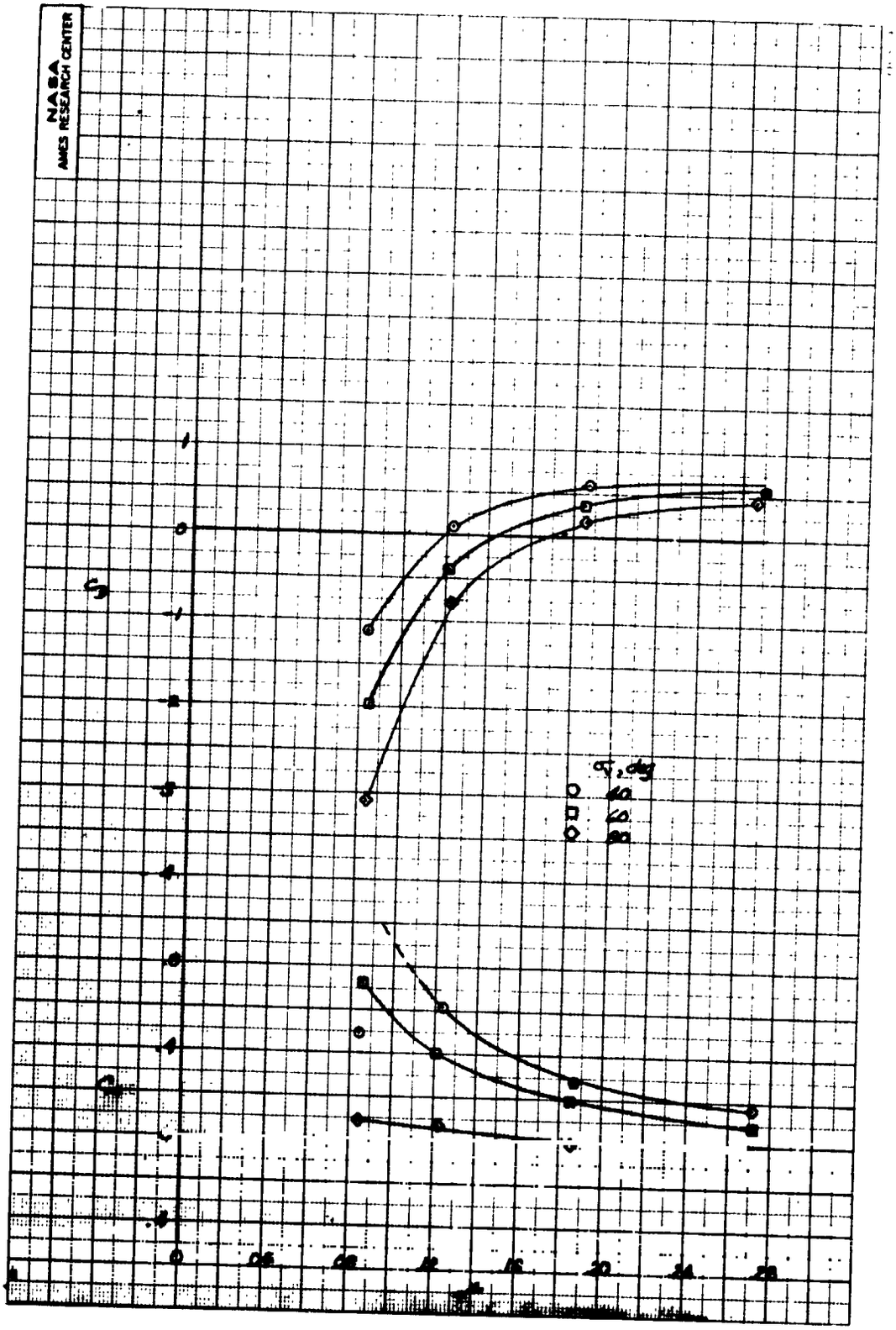

(d) C_D, C_m variation with μ, $\beta_v = -8°$.

Figure 14.- Continued.

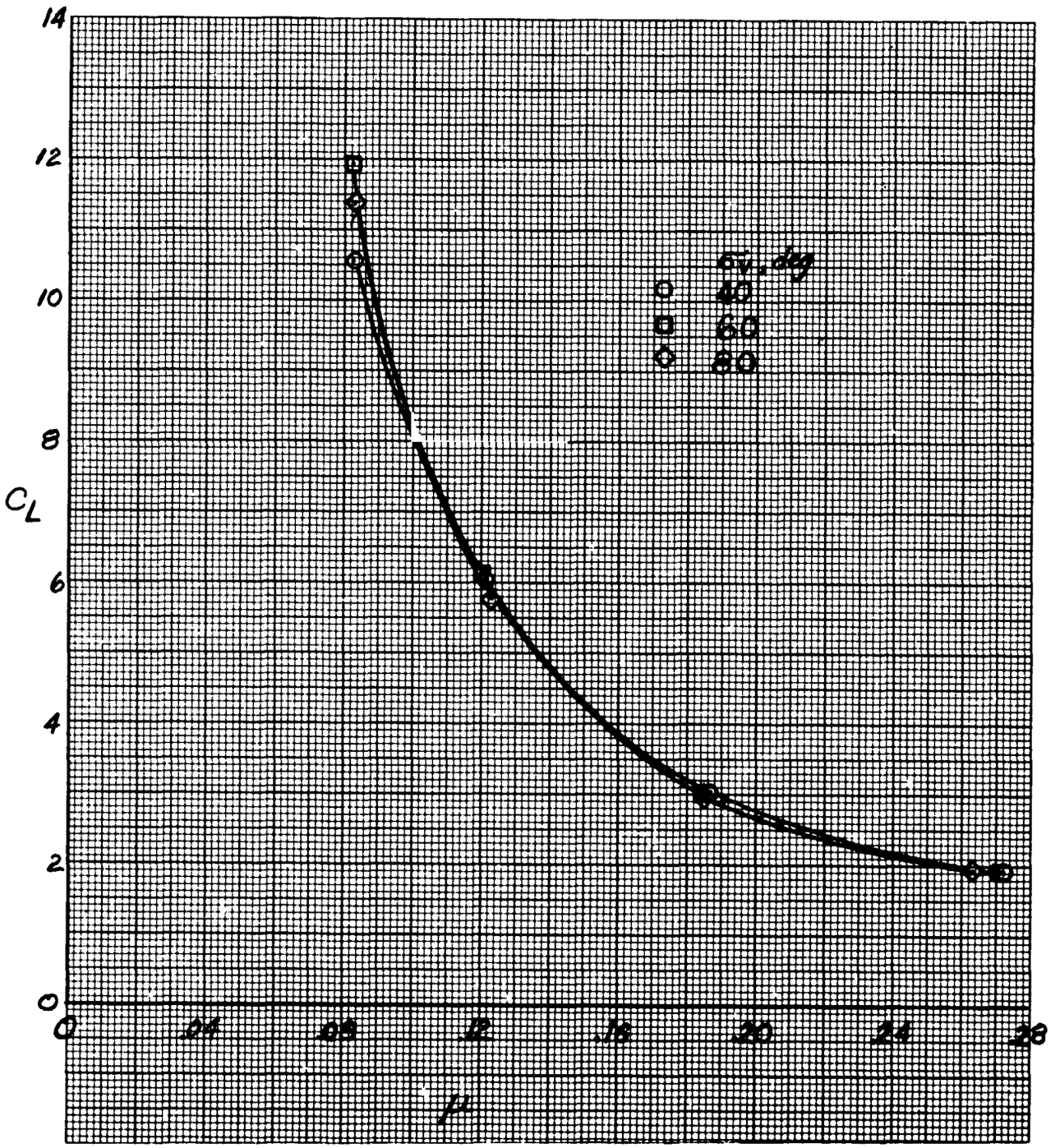

(e) C_L variation with μ, $\beta_v = -16°$.

Figure 14.- Continued.

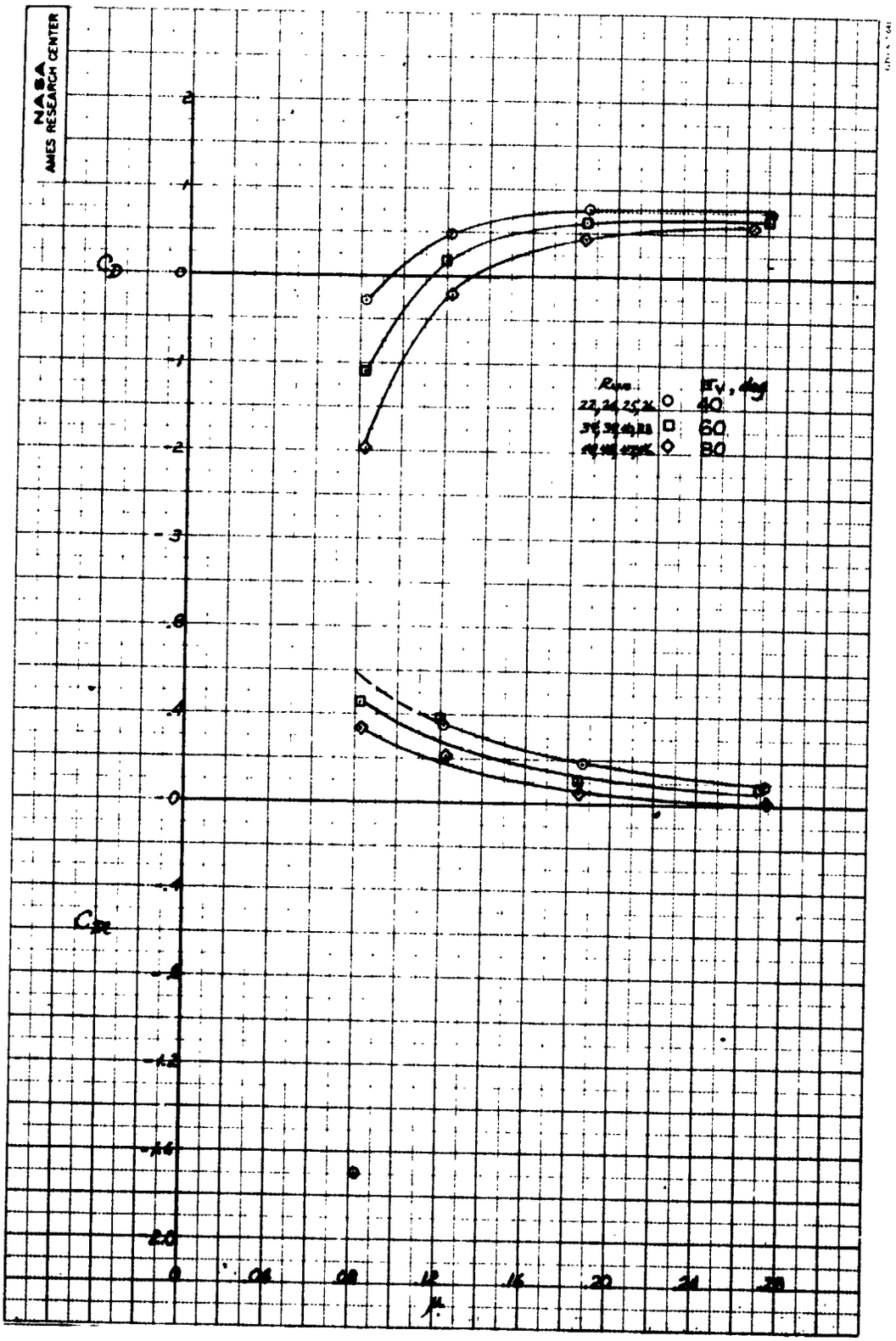

(f) C_D, C_m variation with μ, β_v = -16.°.

Figure 14.- Continued.

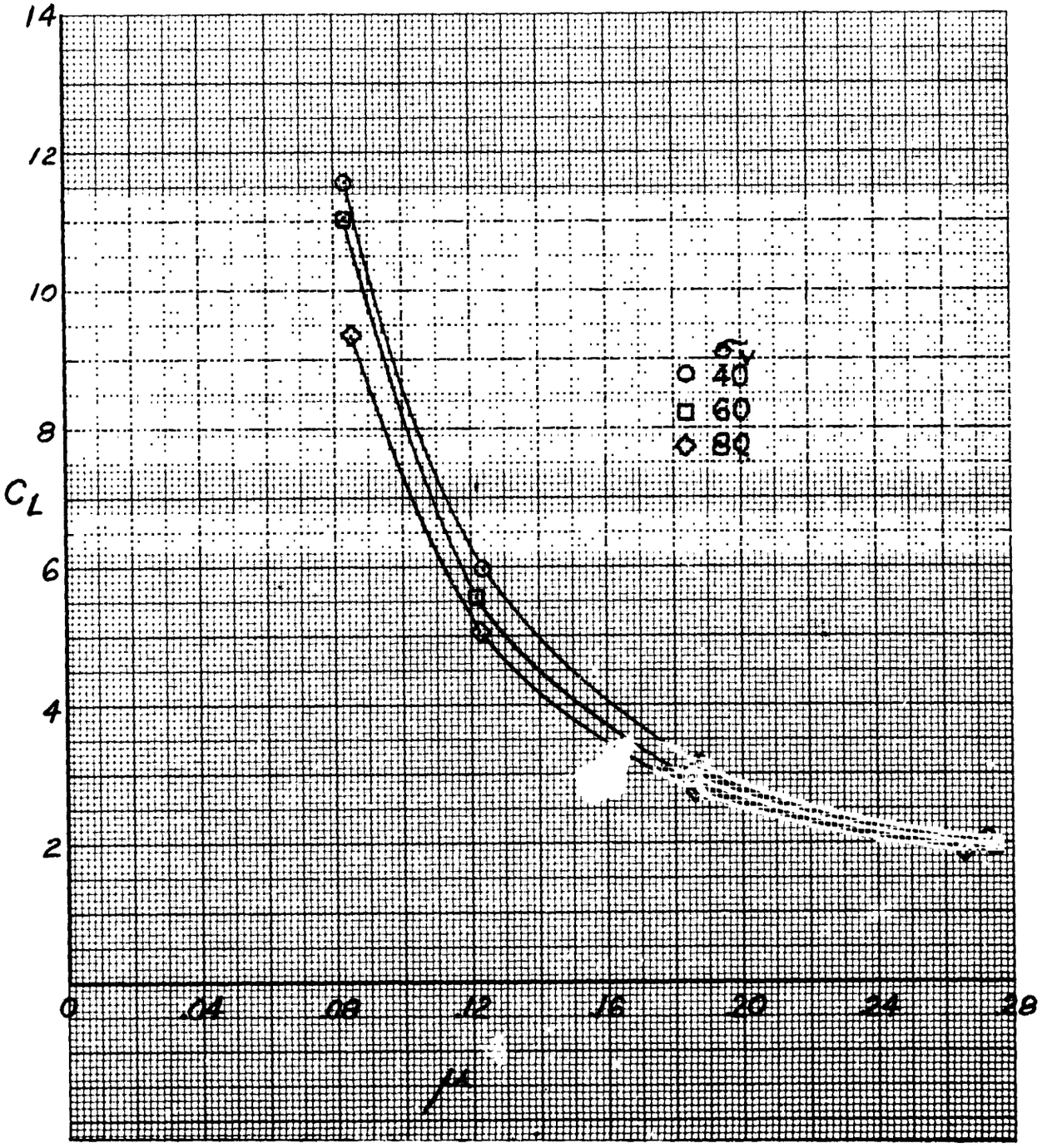

(g) C_L variation with μ, $\beta_v = 8°$.

Figure 14.- Continued

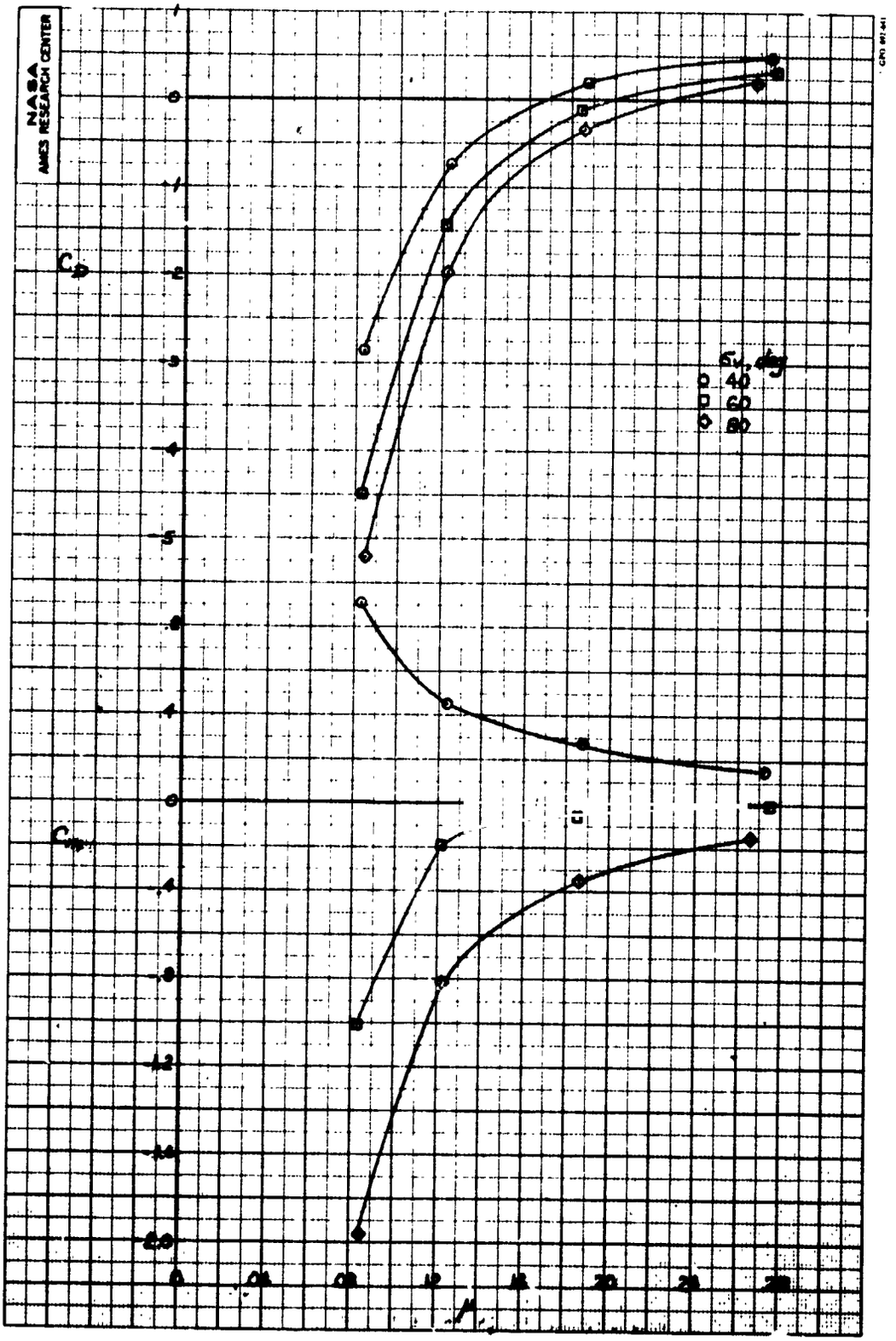

(h) C_D, C_m variation with μ, $\beta_v = 8°$.

Figure 14.- Continued.

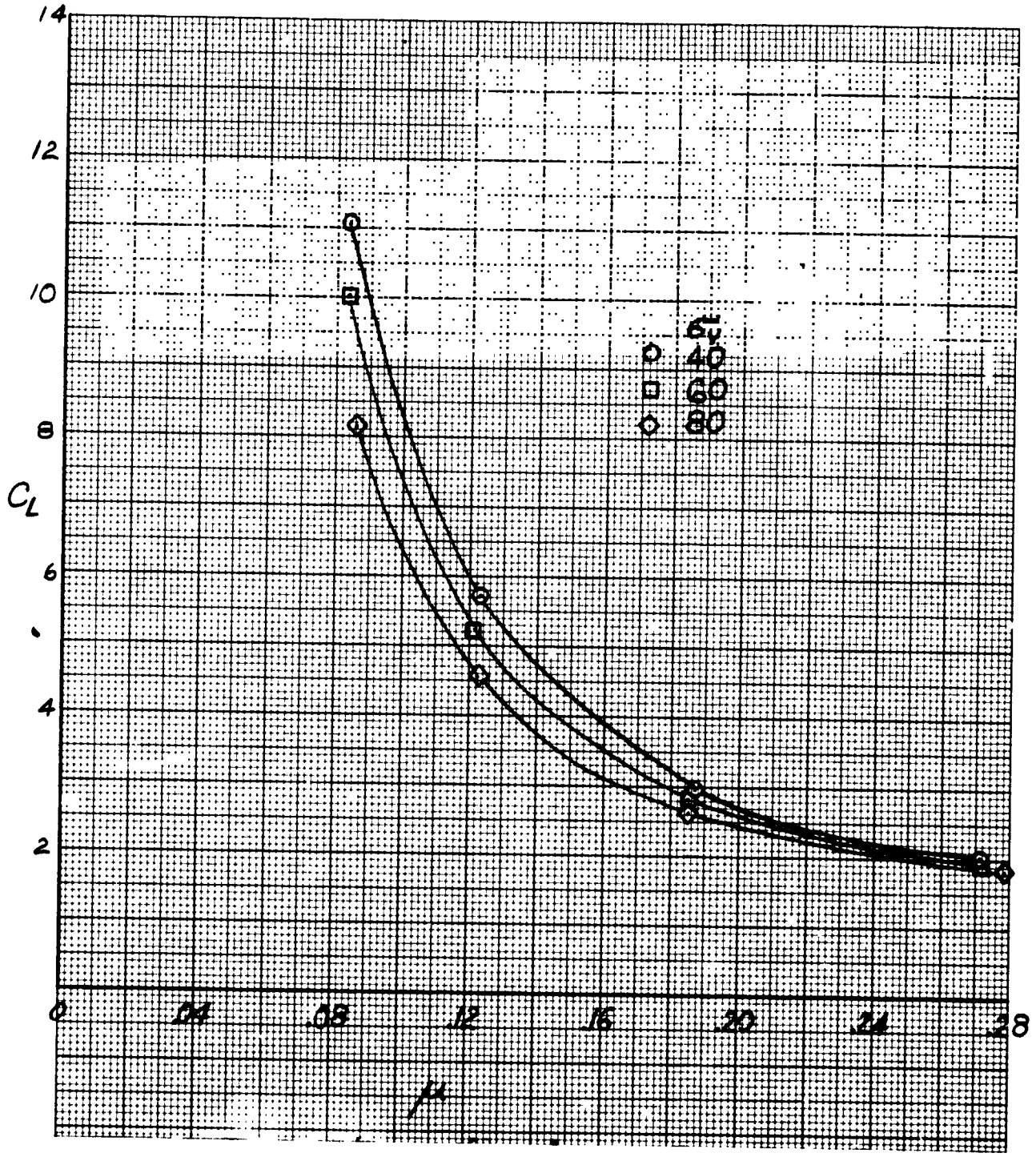

(i) C_L variation with μ, $\beta_v = 16°$.

Figure 14.- Continued.

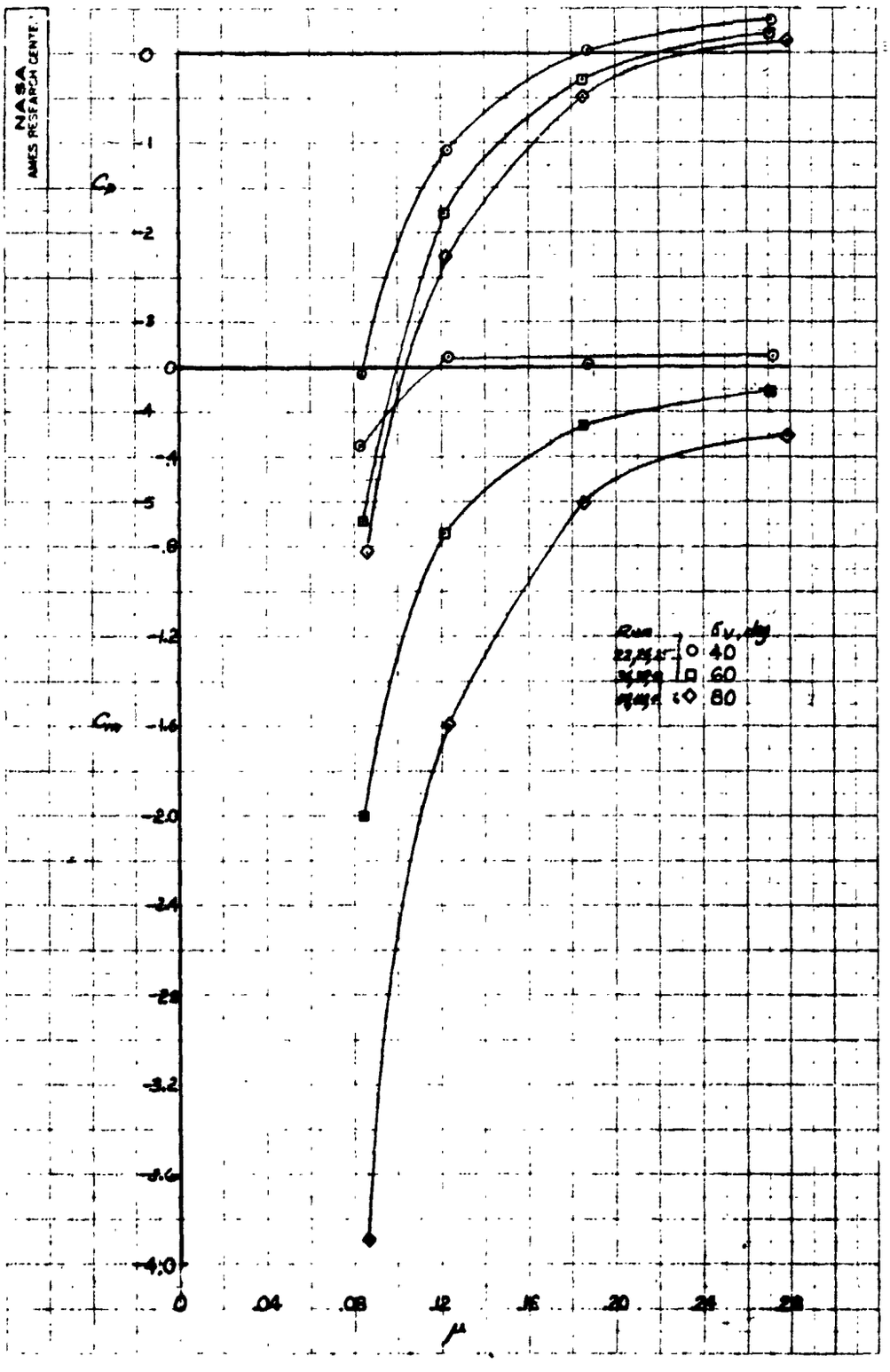

(j) C_D, C_m variation with μ, $\beta_v = 16°$.

Figure 14.- Concluded.

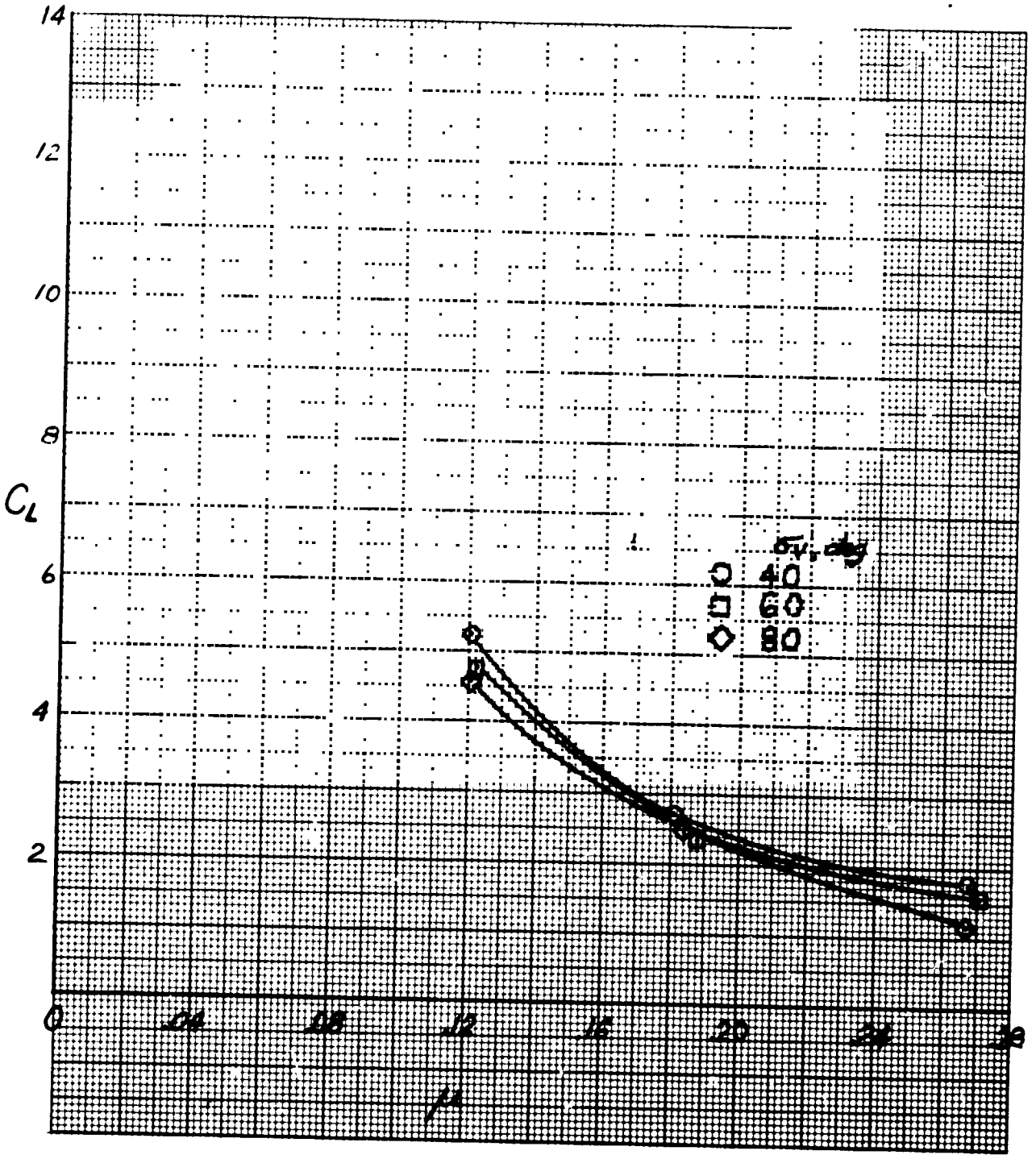

(a) C_L variation with μ.

Figure 15.- The variation in longitudinal characteristics with tip speed ratios; all fans operating, $\beta_v = 0°$, $\delta_{cn} = 23°$, $\delta_f = 30°$, $\alpha_u = 0°$.

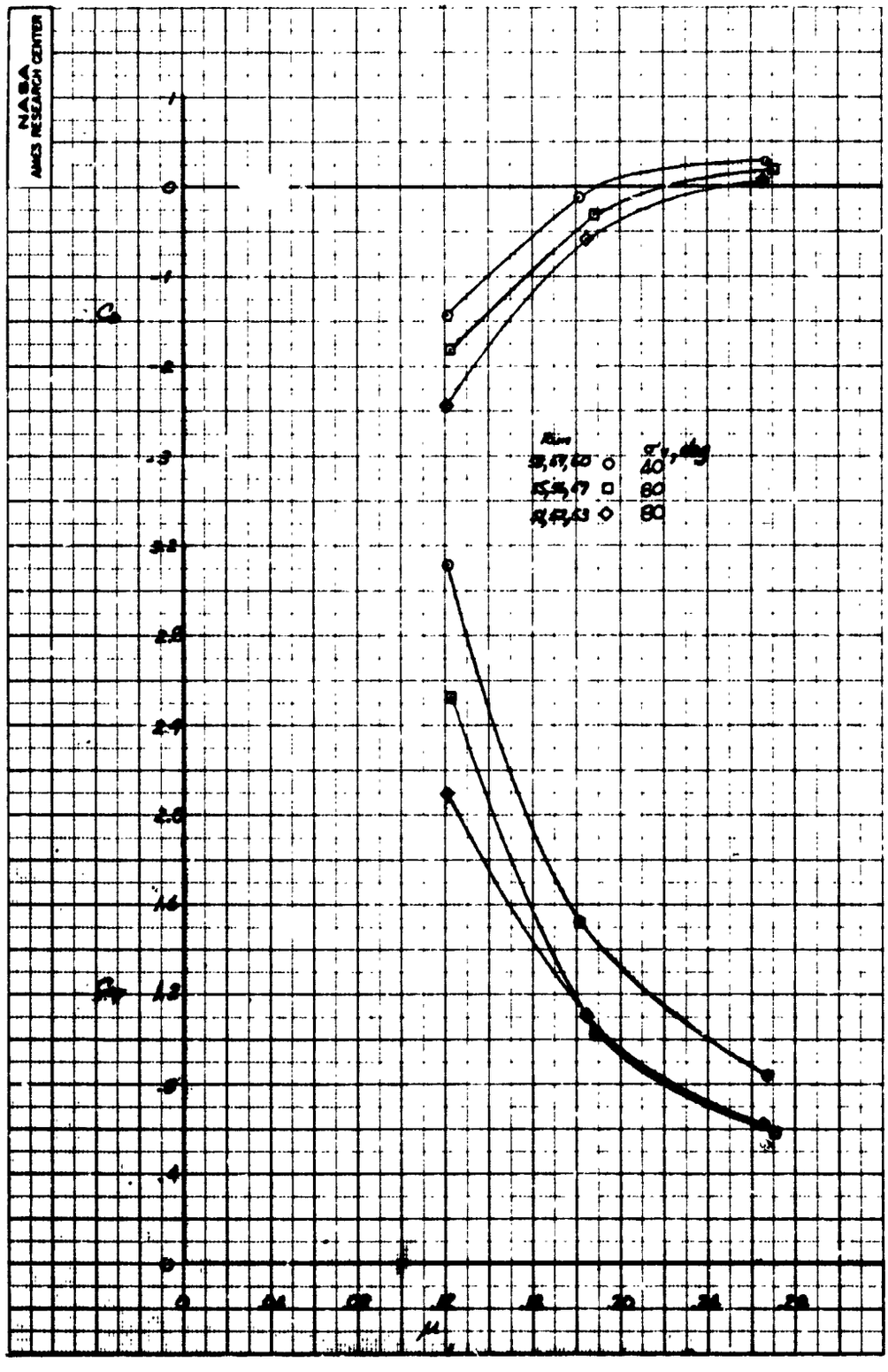

(b) C_D, C_m variation with μ.

Figure 15.- Concluded.

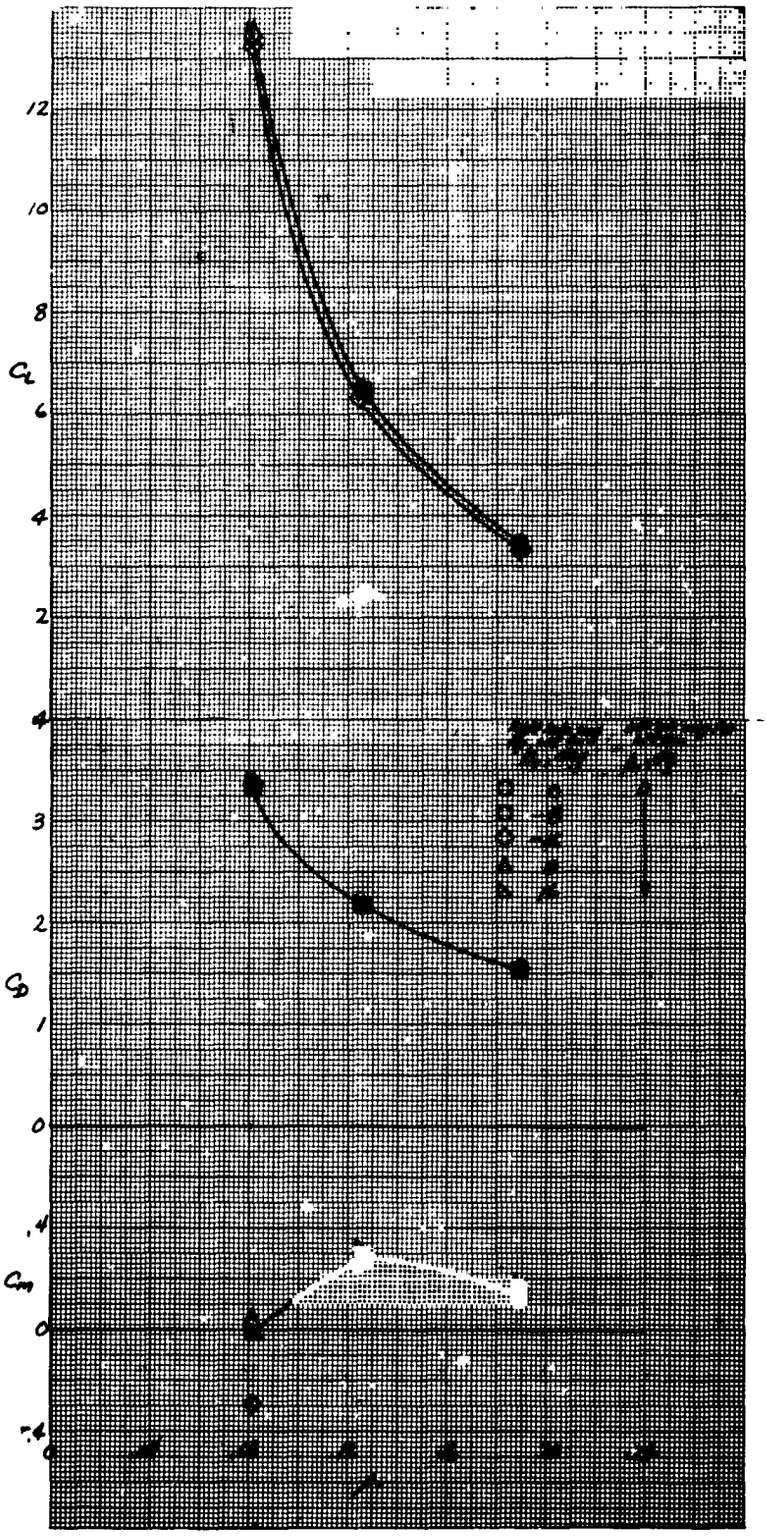

(a) C_L, C_D, C_m variation with μ.

Figure 16.- The variation in longitudinal and lateral characteristics with tip speed ratio; all fans operating, $\sigma_v = 0°$, forward lift fan $\beta_v = 0°$, $\delta_{cn} = 90°$, $\delta_f = 30°$, $\alpha_u = 0°$.

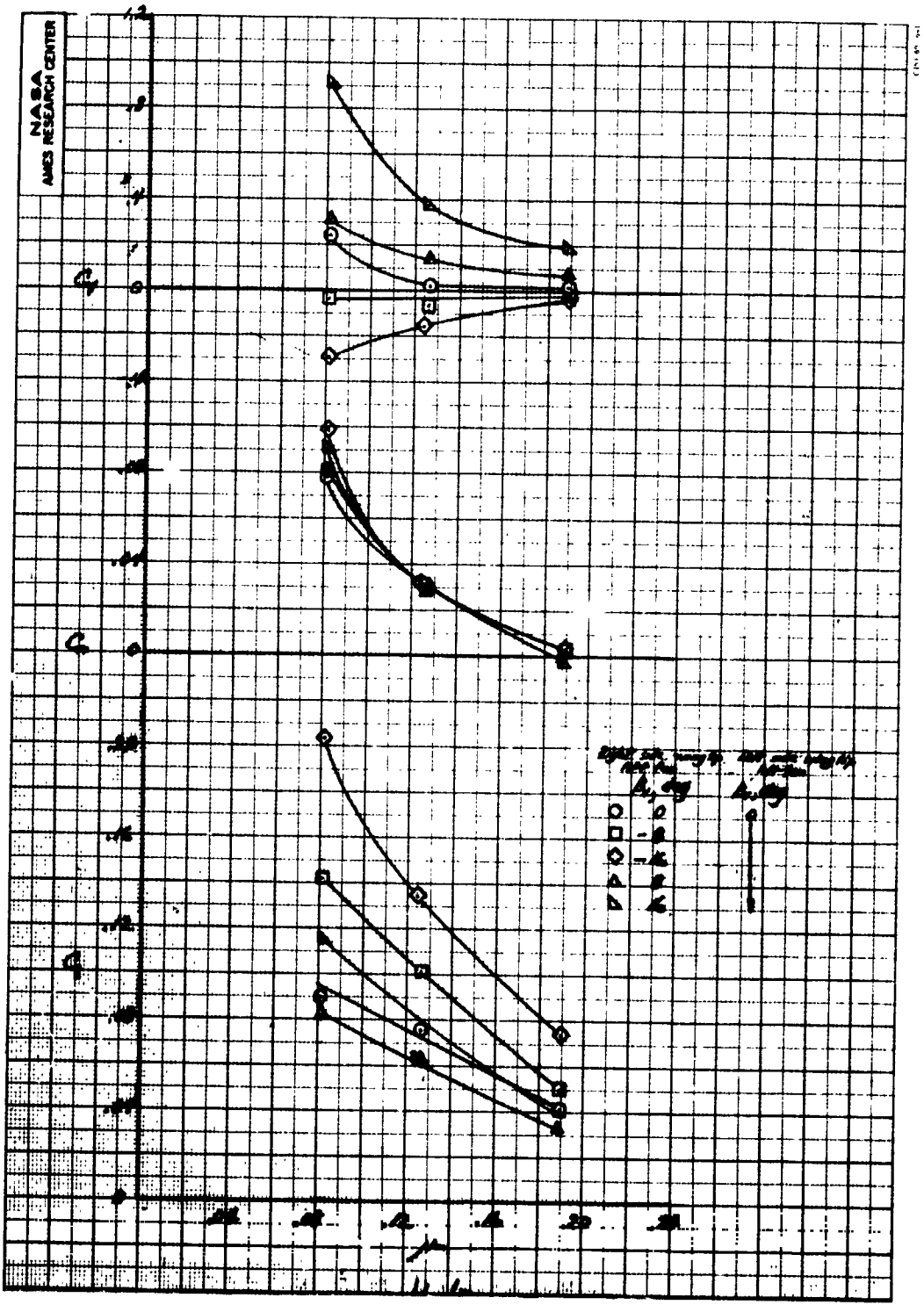

(b) C_y, C_n, C_l variation with μ.

Figure 16.- Concluded.

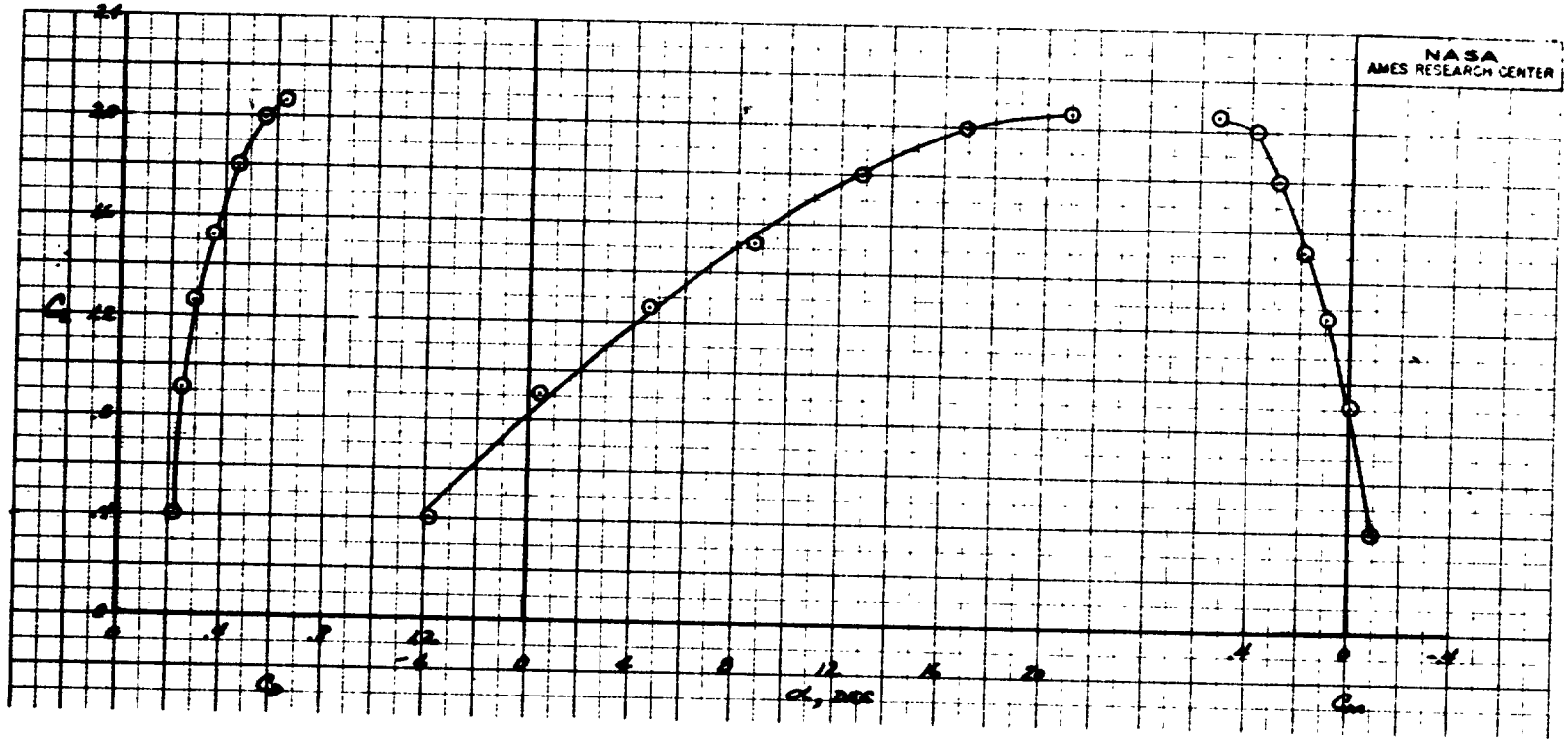

Figure 17.- Longitudinal characteristics of the model with power off; δ_{cn} = 23°, forward lift fan and wing-tip lift fan inlets covered, σ_v = 90°, β_v closed, δ_f = 30°, q = 594.19 N/m^2 (12.41 psf).

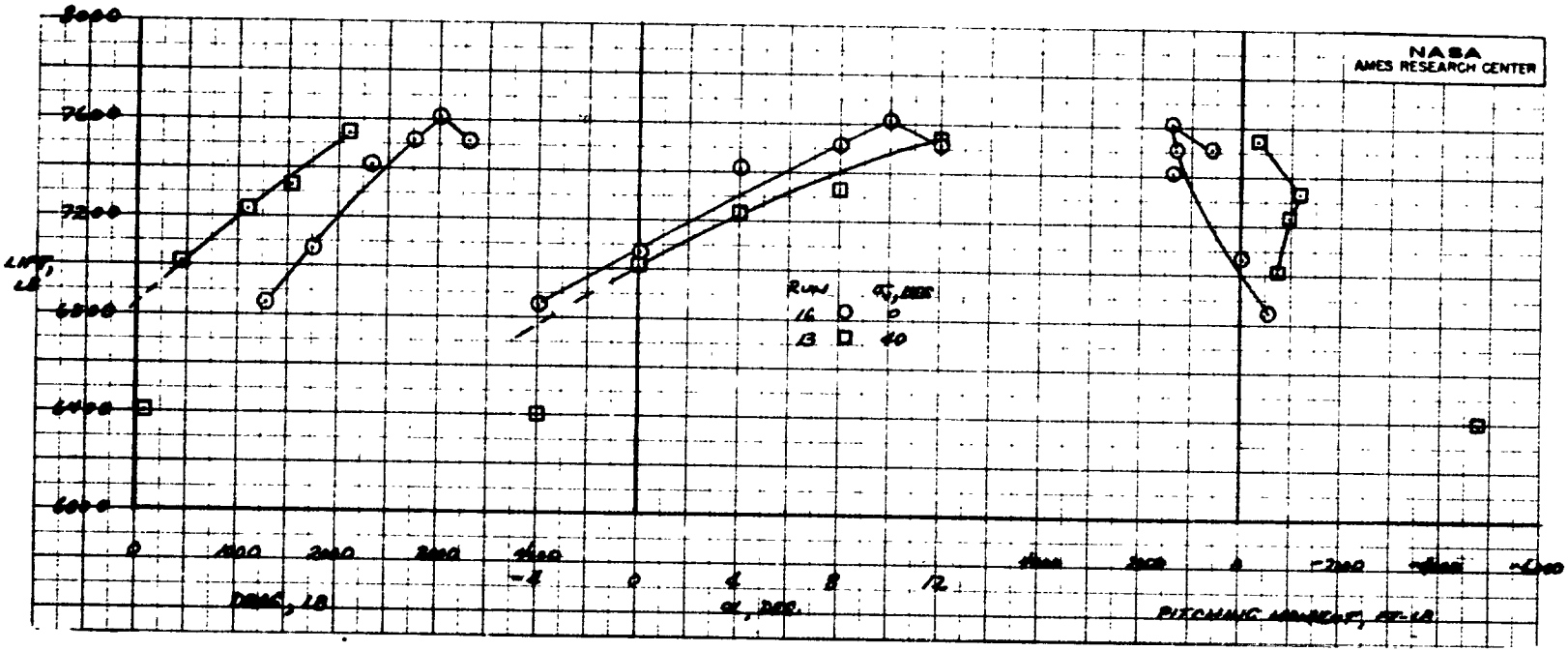

(a) $\mu = 0.08$.

Figure 18.- Longitudinal characteristics of the model with $\delta_{cn} = 90°$ at several tip speed ratios; $\beta_v = 0°$, $\delta_f = 30°$, horizontal tail off.

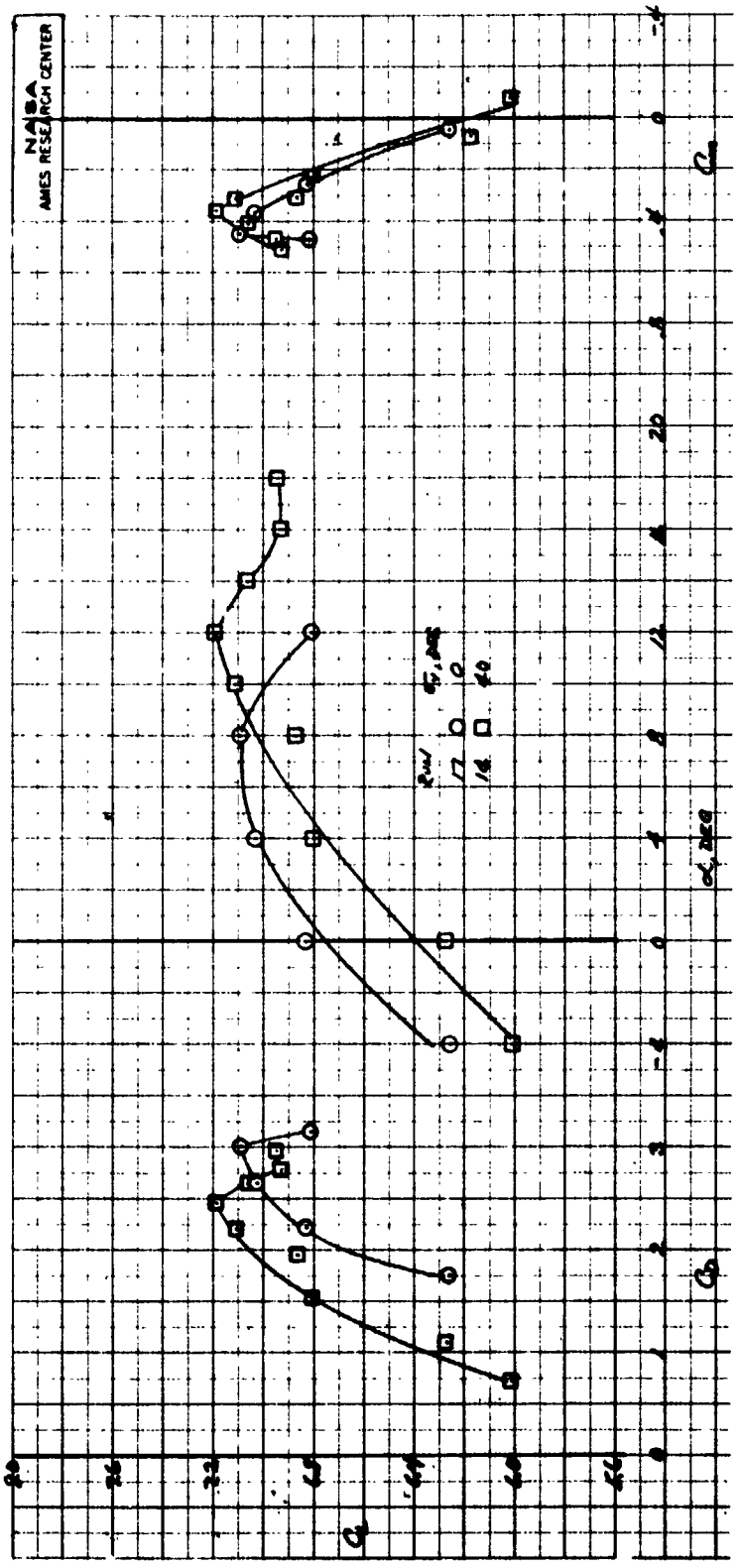

(b) $\mu = 0.12$.

Figure 18.- Continued.

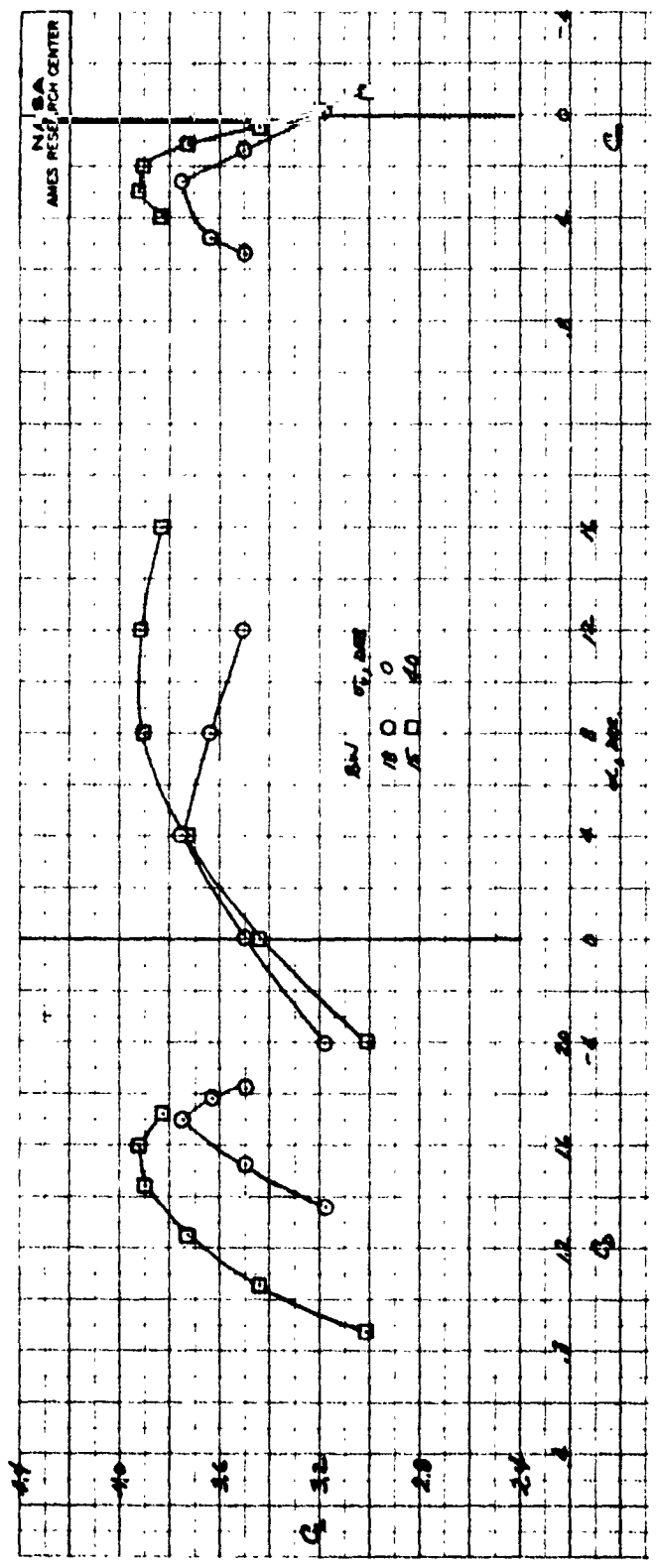

(c) $\mu = 0.18$.

Figure 18.- Concluded.

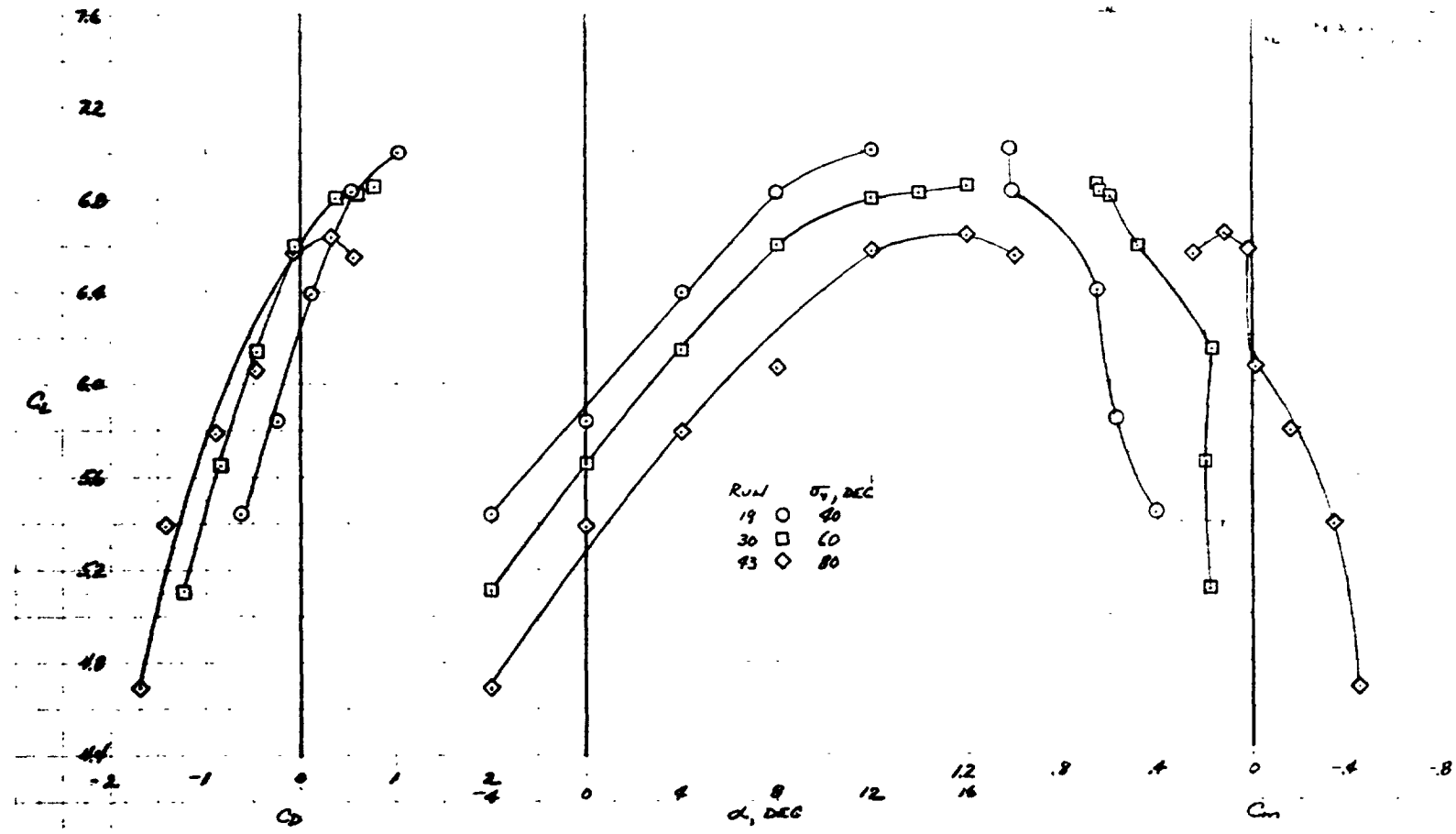

(a) μ = 0.12.

Figure 19.- Longitudinal characteristics of the model with δ_{cn} = 56° at several tip speed ratios; β_v = 0°, δ_f = 30°, horizontal tail off.

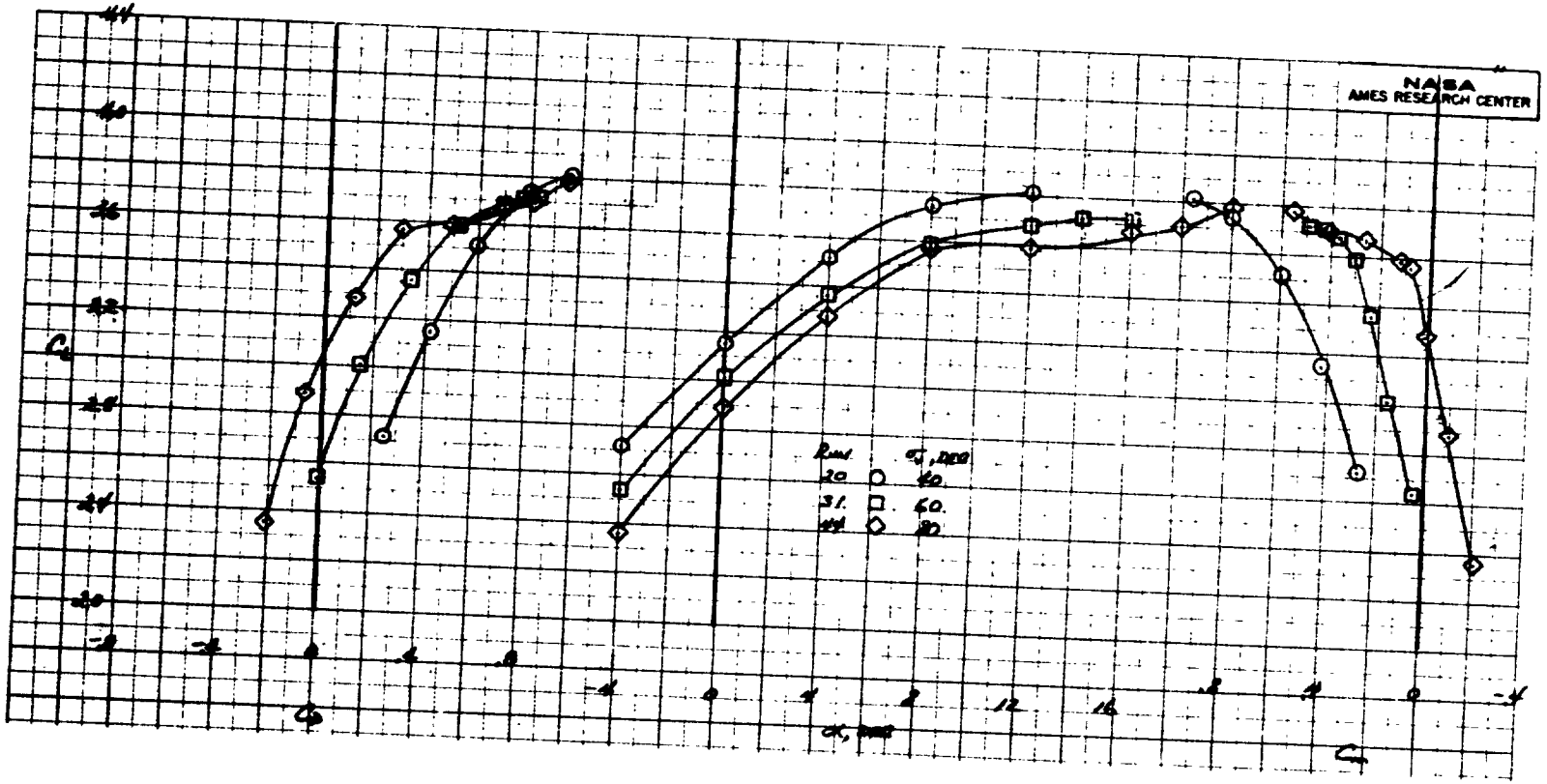

(b) $\mu = 0.18$.

Figure 19.- Continued.

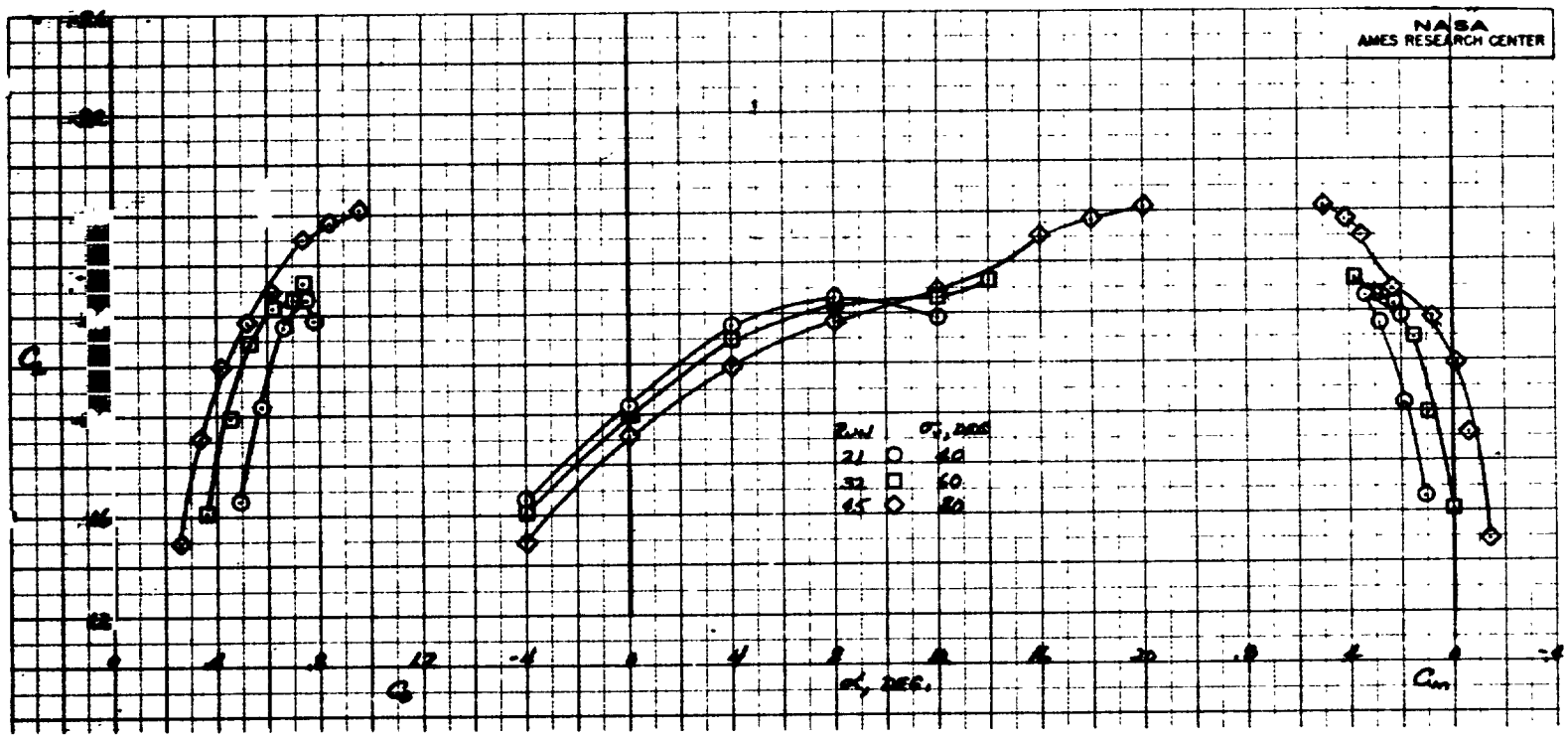

(c) μ = 0.26.

Figure 19.- Concluded.

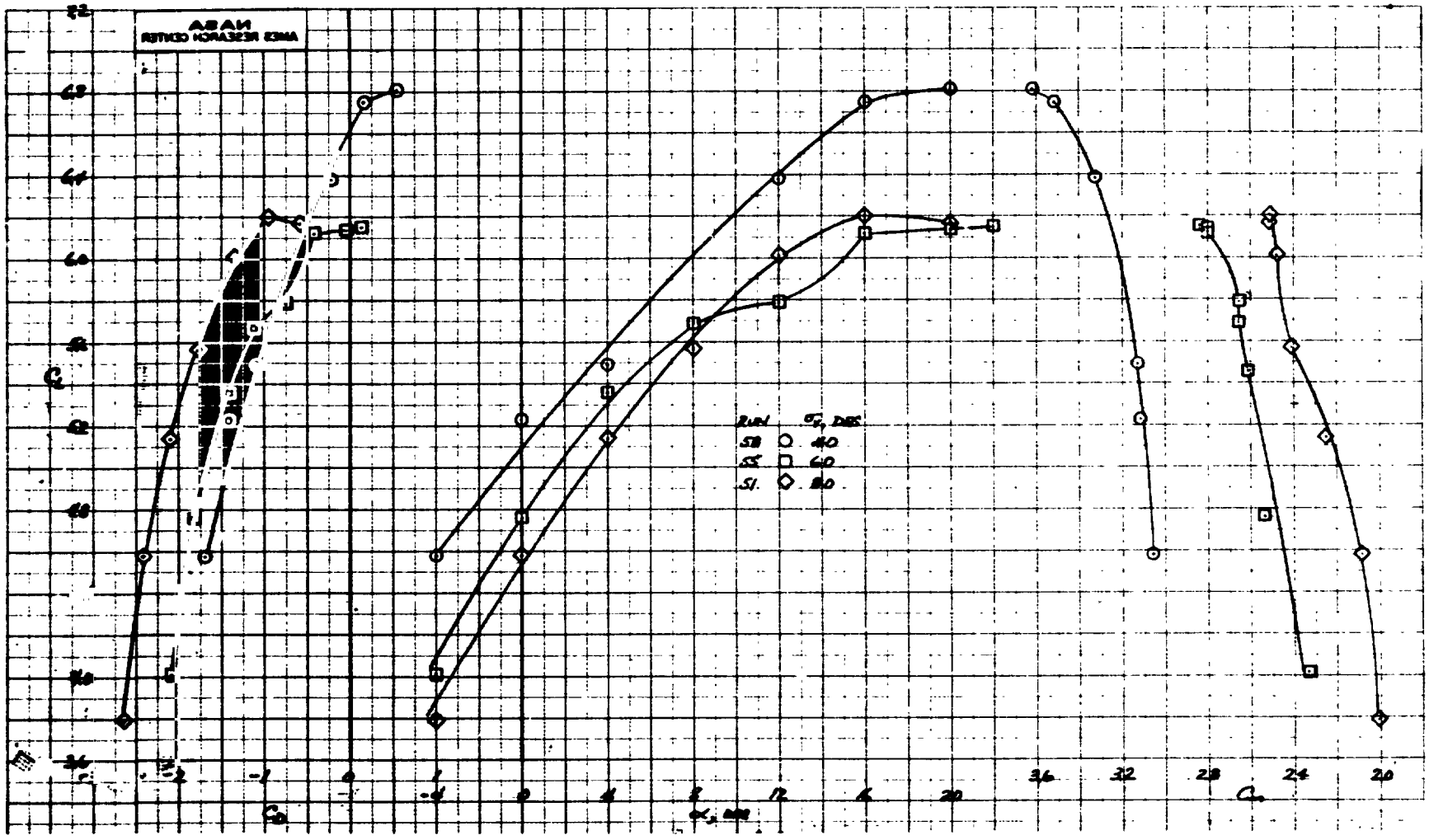

(a) $\mu = 0.12$.

Figure 20.- Longitudinal characteristics of the model with $\delta_{cn} = 23°$ at several tip speed ratios; $\beta_v = 0°$, $\delta_f = 30°$, horizontal tail off.

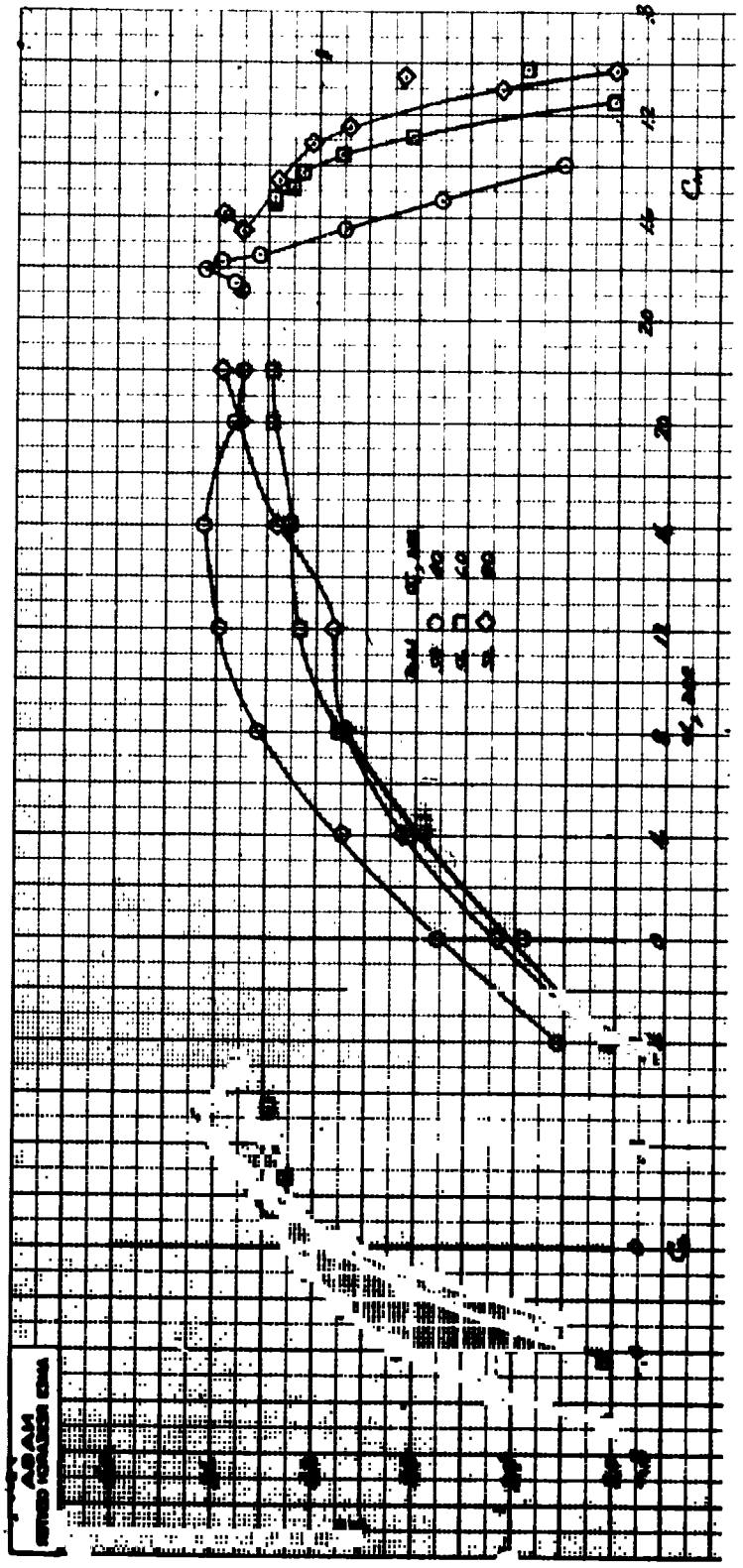

(b) $\mu = 0.18$.

Figure 20.- Continued.

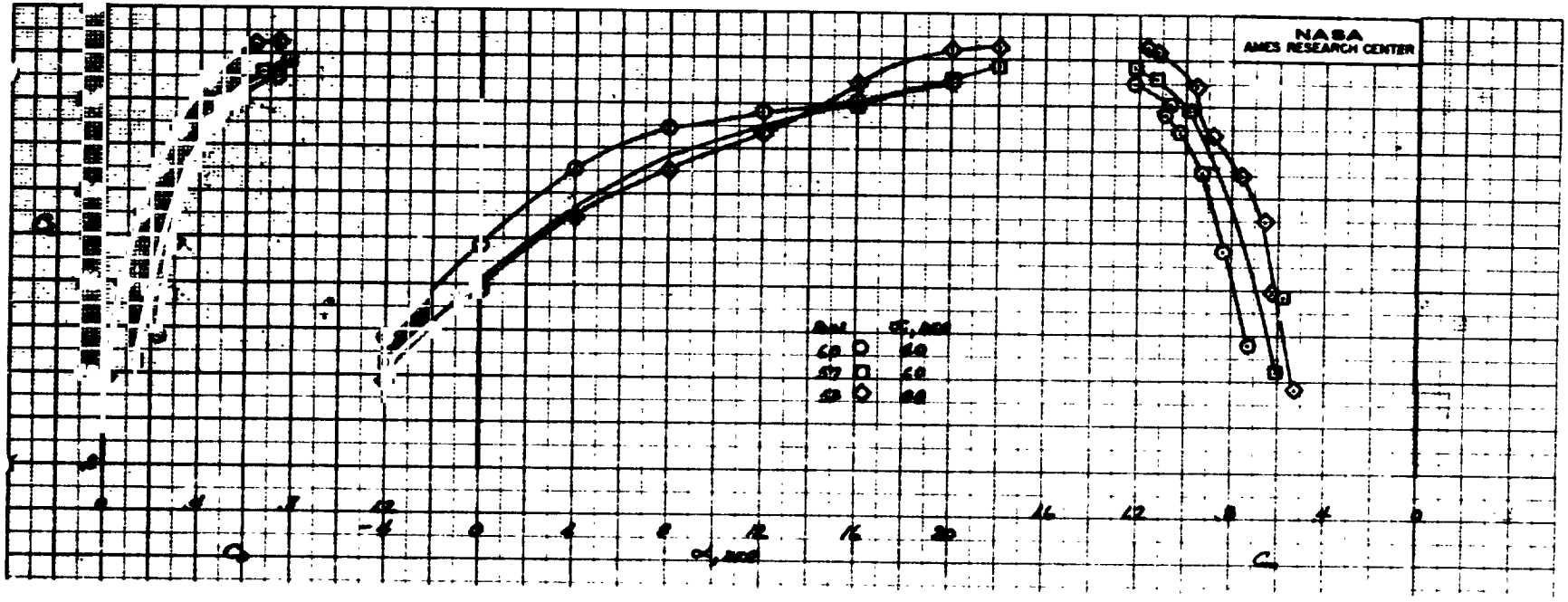

(c) $\mu = 0.26$.

Figure 20.- Concluded.

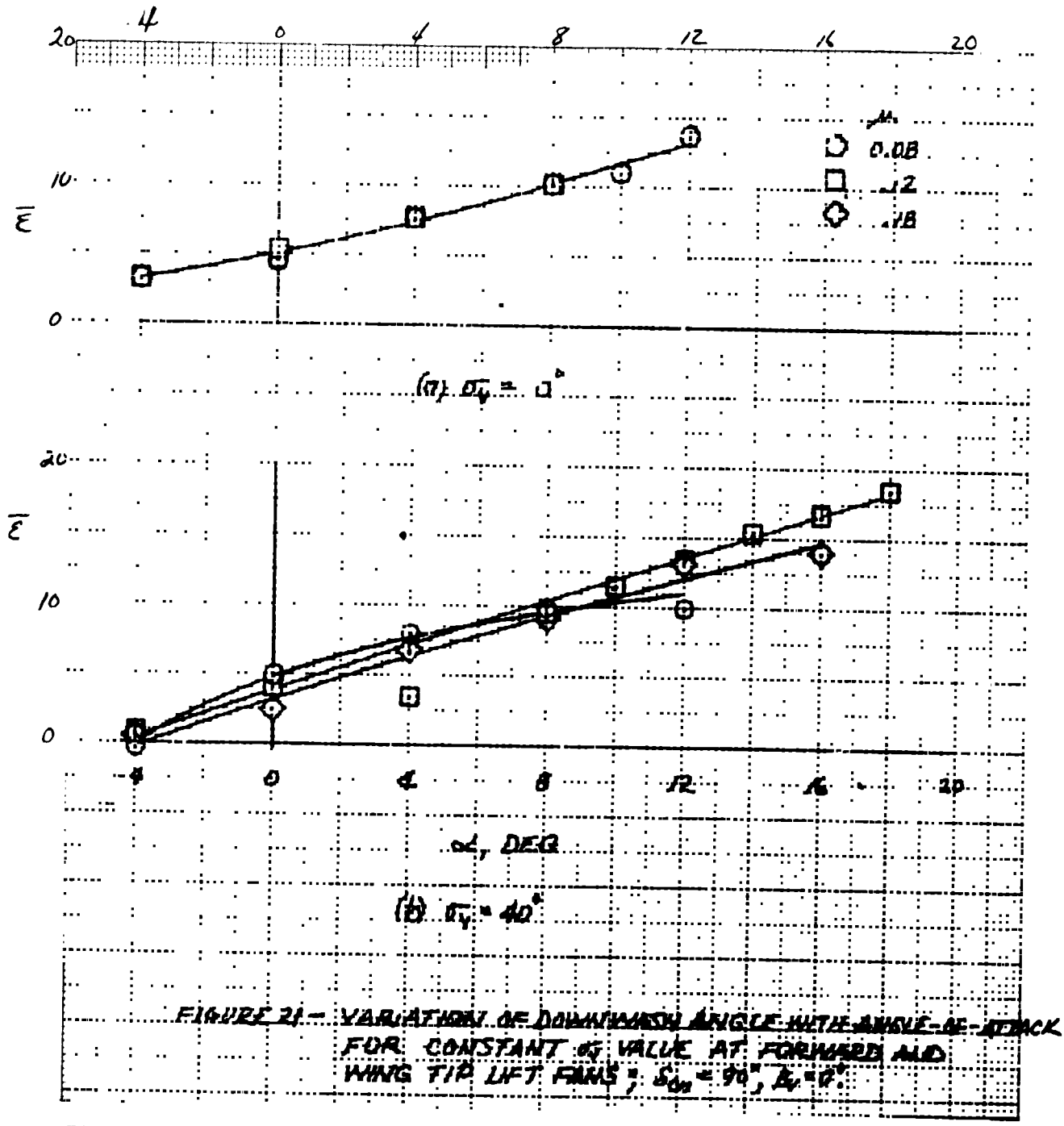

FIGURE 21 – VARIATION OF DOWNWASH ANGLE WITH ANGLE-OF-ATTACK FOR CONSTANT σ_v VALUE AT FORWARD AND WING TIP LIFT FANS; δ_{cn} = 90°, β_v = 0°.

Figure 21.- Variation of downwash angle with α for constant σ_v values at forward and wing-tip lift fans; δ_{cn} = 90°, β_v = 0°.

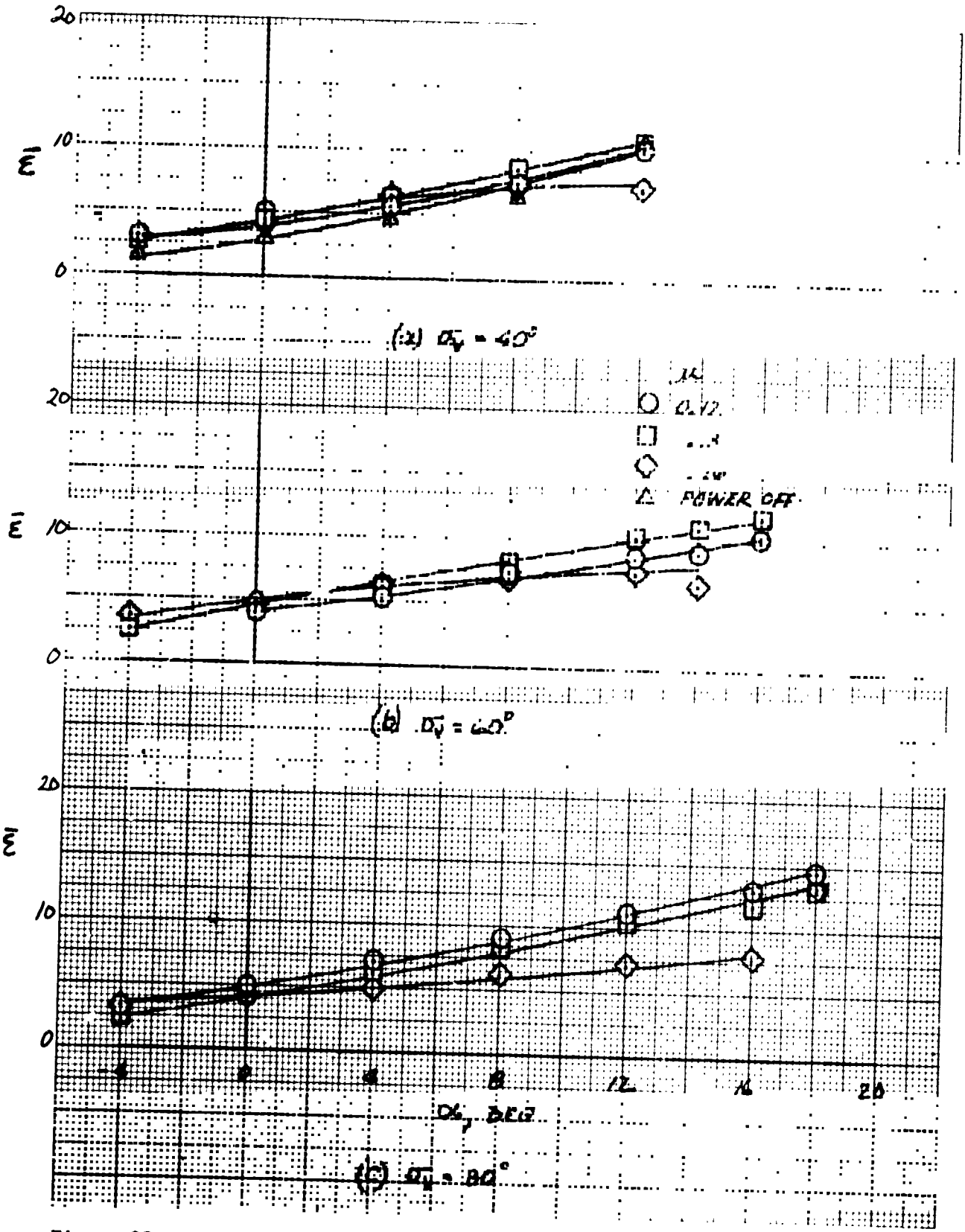

Figure 22.- Variation of downwash angle with α for constant σ_v value at forward and wing-tip lift fans; δ_{cn} = 56°, β_v = 0°.

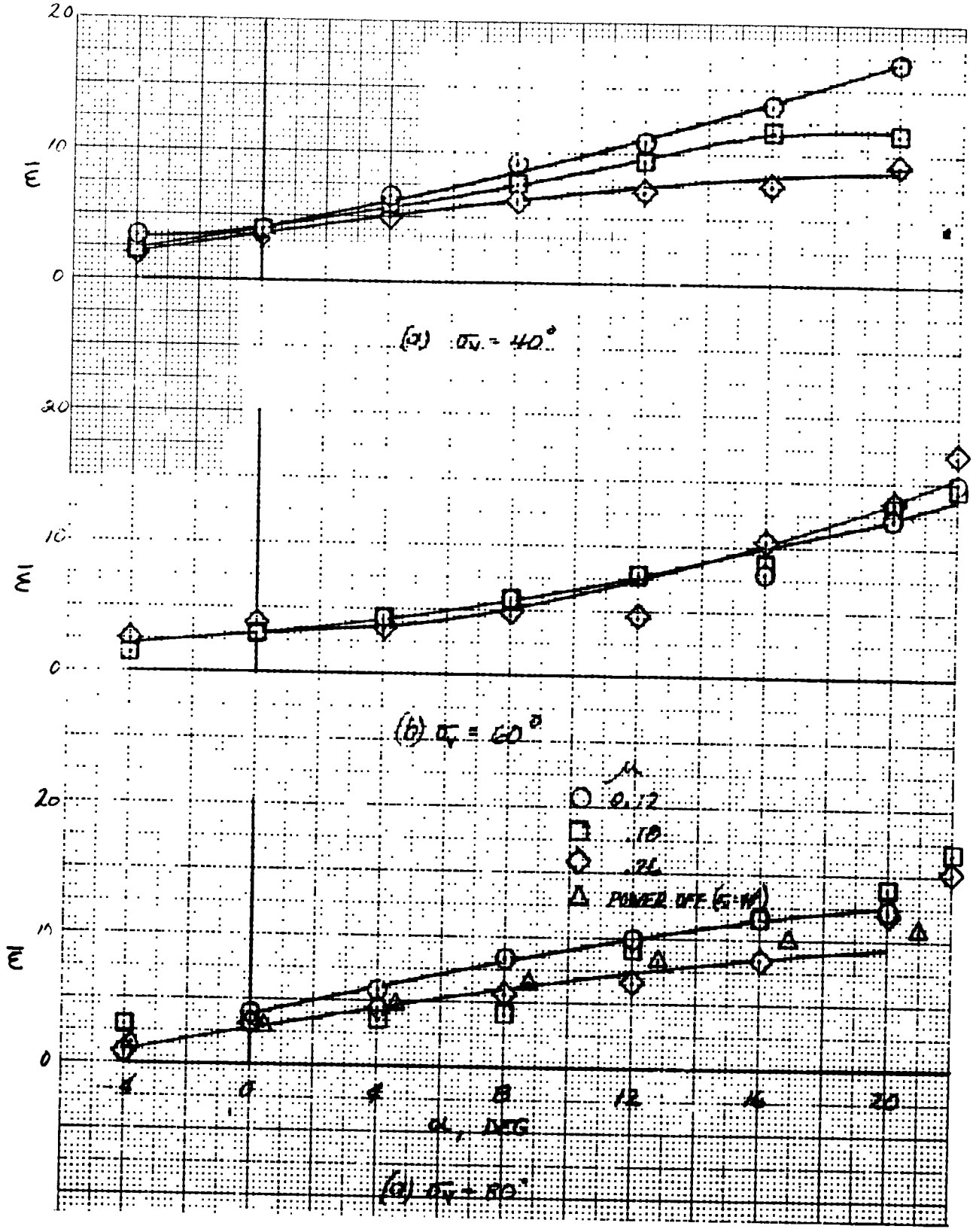

Figure 23.- Variation of downwash angle with α for constant σ_v value at forward and wing-tip lift fans; $\delta_{cn} = 23°$, $\beta_v = 0°$.

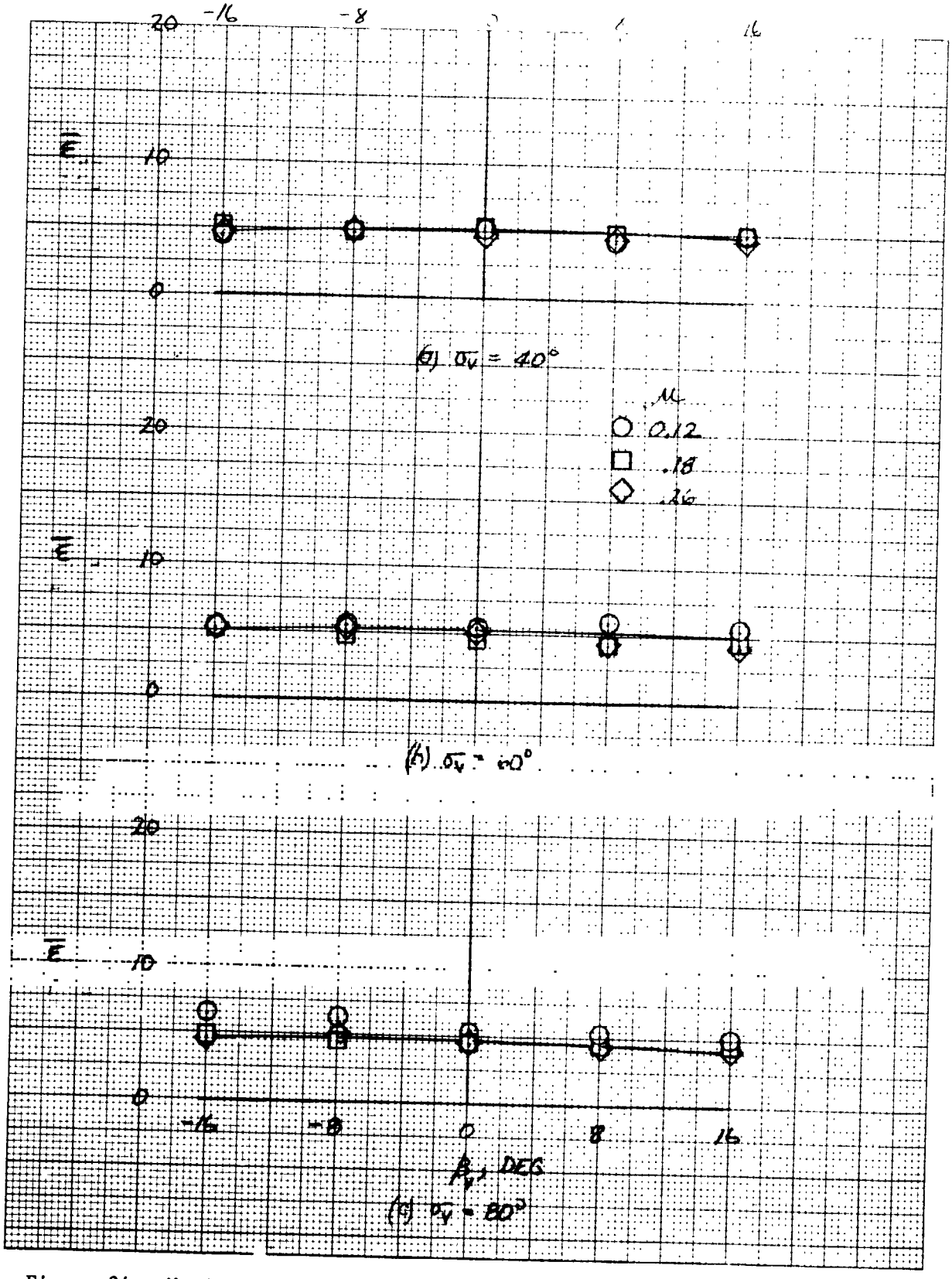

Figure 24.- Variation of downwash angle with β_v at several σ_v values; δ_{cn} = 56°, α_u = 0°.